

A New Equation of State Formulation for Argon Covering the Fluid Region for Temperatures From the Melting Line to 2300 K at Pressures up to 50 000 MPa

F. Aitken¹, N. Bonifaci, A. Denat and F. Volino

Univ. Grenoble Alpes, G2Elab, F-38000 Grenoble, France
CNRS, G2Elab, F-38000 Grenoble, France

Abstract

A new equation of state for argon has been developed in view to extend the range of validity of the equation of state previously proposed by Tegeler *et al.* and to obtain a better physical description of the experimental thermodynamic data for the whole fluid region (single-phase and coexistence states). As proposed by Tegeler *et al.*, this equation is also based on a functional form of the residual part of the reduced Helmholtz free energy. However in this work, the fundamental equation for the Helmholtz free energy has been derived from the measured quantities $C_V(\rho, T)$ and $P(\rho, T)$. An empirical description of the isochoric heat capacity $C_V(\rho, T)$ has been developed using mainly power laws with density dependent exponents and the thermodynamics properties (internal energy, entropy, free energy) are then obtained by combining integration of $C_V(\rho, T)$. The arbitrary functions introduced by the integration process have been deduced from a comparison between calculated and experimental pressure $P(\rho, T)$ data. The new formulation is valid for the whole fluid region from the melting line to 2300 K and for pressures up to 50 000 MPa. It also predicts existence of a maximum of the isochoric heat capacity C_V along isochors as experimentally observed in several other fluids.

The present approach contains much less coefficients and parameters than the model of Tegeler *et al.* and, in addition, eliminates the small oscillations on the thermodynamic quantities introduced by a polynomial description. This leads to a more physical description of the thermodynamic properties. However it does not describe accurately the properties in the vicinity of the critical point. Comparison of the model with data of L'Air Liquide also shows that our model is consistent with these data up to 1100 K and 100 MPa, thus extending the range of the NIST data.

Key words: argon, data evaluation, equation of state, fundamental equation, property tables, thermal and caloric properties, vapour–liquid coexistence curve.

¹ Author to whom correspondence should be addressed; Electronic mail: frederic.aitken@grenoble.cnrs.fr.

Contents

1. Introduction	6
2. The New Equation of State for the Isochoric Heat Capacity	8
3. Thermodynamic Properties Derived from the Isochoric Heat Capacity	16
3.1. Determination of the arbitrary functions for the Internal Energy and Entropy.....	20
3.2. Analytic expression of the ‘thermal equation of state’ for $T \geq T_{\text{div}}$	25
3.3. The liquid-vapour coexistence curve	26
3.4. Thermodynamic state inside the liquid-vapour coexistence curve for $T < T_{\text{div}}(\rho)$...	28
3.4.1. Expression for C_V inside the divergence curve	28
3.4.2. Choice of a reference state	29
4. Comparison of the New Equations of State with Experimental Data and the Equations of State of Tegeler <i>et al.</i>	35
4.1. Melting phase transition	35
4.1. Single Phase Region.....	36
4.1.1. Isochoric Heat Capacities.....	36
4.1.2. Thermal Properties	37
4.1.3. Isobaric Heat Capacities, Sound Velocities and Isothermal Throttling Coefficient	39
4.1.4. The “Ideal Curves”.....	40
4.1.5. Extrapolation to High Temperatures	41
4.2. Liquid-Vapour Phase Boundary.....	41
4.2.1. Isochoric Heat Capacities.....	41
4.2.2. Thermal Properties	43
4.2.3. The spinodal properties	44
5. The Uncertainty of the New Equation of State	48
6. Conclusions	48
7. References	49
Appendix 1 : Expression of the Regular Term of Pressure P_{reg}	50
Appendix 2 : Expression of the First and Second Derivatives of the Coefficients in C_V	54

List of Tables

Table 1. Coefficients and exponents of Eq. (6) to Eq. (12).....	14
Table 2. Characteristic values of densities of argon and there corresponding molar volumes.	15
Table 3. The ideal-gas part of the dimensionless Helmholtz free energy function and its derivatives.	19
Table 4. Coefficients and exponents for \hat{u}_0 and \tilde{s}_0	24
Table 5. Mathematical expressions of the dimensionless terms in the residual Helmholtz free energy for $T \geq T_{div}$	24
Table 6. Thermodynamic properties corresponding to $Z = 1$ (i.e. ideal curve) deduced from Eq. (46).....	27
Table 7. Mathematical expressions of the dimensionless terms for the non-extensive residual Helmholtz function and its partial derivatives with temperature.	32
Table 8. Mathematical expressions of the first partial derivatives with temperature of Z . All these derivatives are in K^{-1}	33
Table 9. Mathematical expressions of the first partial derivatives with density of Z for $T \geq T_{div}$. All these derivatives are in cm^3/g	34
Table 10. Characteristic values of the coexistence line calculated from the thermal equation of state and using the NIST values.	42
Table 11. Characteristic values of the coexistence line calculated from the Maxwell relations: Eq. (50) to (52).	42
Table 12 : Thermodynamic parameters of saturated argon.....	46

List of Symbols

Symbol description

c	Sound speed
C_P	Isobaric heat capacity
C_V	Isochoric heat capacity
F	Helmholtz free energy
G	Gibbs energy
H	Enthalpy
i, j, k	Serial numbers
M	Molar mass
\mathcal{N}_a	Avogadro number
P	Pressure
R_A	Specific gas constant
S	Entropy
T	Thermodynamic temperature
U	Internal energy
V	Specific volume ($V = 1/\rho$)
x	Dimensionless parameter ($x = T_{\text{div}}/T$)
y	Dimensionless parameter ($y = x^{-1} = T/T_{\text{div}}$)
Z	Compressibility factor

Greek

∂	Partial differential
δ_T	Isothermal throttling coefficient
ρ	Density
Γ	Incomplete gamma function

Superscripts

o	Ideal-gas property
$r, *$	Residual terms
\sim	Dimensionless quantity
\wedge	Dimensionless quantity using $\frac{3}{2}T_c$ instead of T for the adimensionnalisation

Subscripts

c	At the critical point
calc	Calculated
exp	Experimental
sat	Denotes states at saturation
sp	Denotes spinodal states
t	At the triple point
σ_l	Saturated liquid state
σ_v	Saturated vapour state
0	Terms that do not contribute to C_V

Physical Constants for Argon

M Molar mass

$$M = 39.948 \text{ g mol}^{-1}$$

R Universal gas constant

$$R = 8.314 \text{ 51 J mol}^{-1} \text{ K}^{-1}$$

R_A Specific gas constant

$$R_A = 0.208 \text{ 133 3 kJ kg}^{-1} \text{ K}^{-1}$$

T_c Critical temperature

$$T_c = 150.687 \text{ K}$$

P_c Critical pressure

$$P_c = 4.863 \text{ MPa}$$

ρ_c Critical density

$$\rho_c = 0.535 \text{ 599 g cm}^{-3}$$

T_t Triple-point temperature

$$T_t = 83.805 \text{ 8 K}$$

P_t Triple-point pressure

$$P_t = 68.891 \text{ kPa}$$

$\rho_{t,\text{Gaz}}$ Triple-point gaz density

$$\rho_{t,\text{Gaz}} = 0.004 \text{ 0546 g cm}^{-3}$$

$\rho_{t,\text{Liq}}$ Triple-point liquid density

$$\rho_{t,\text{Liq}} = 1.416 \text{ 80 g cm}^{-3}$$

$\rho_{t,\text{Sol}}$ Triple-point solid density

$$\rho_{t,\text{Sol}} = 1.623 \text{ 9 g cm}^{-3}$$

1. Introduction

Argon is a noble gas and, on earth, its isotopic composition is 99.6% ^{40}Ar , 0.34% ^{36}Ar and 0.06% ^{38}Ar . Argon is very stable and chemically inert under most conditions. Due to those properties and its low cost, argon is largely used in scientific and industrial applications. For instance in high-temperature industrial processes, an argon atmosphere can prevent material burning, material oxidation, material defects during growing of crystals, etc. Due to its molecular simplicity (monoatomic, quasi spherical geometry), argon is also considered as a reference fluid with well-known properties, e.g.: its triple point temperature (83.8058 K) is a defining fixed point in the International Temperature Scale of 1990. The widespread use of argon requires an accurate knowledge of its thermodynamic properties in the largest possible temperature and pressure ranges. Numerous empirical equations of state can be found in the literature, but most of them cover only small parts of the fluid region. The paper of Tegeler *et al.* (1999) contains a very detailed overview on the experimental thermodynamic data of argon as well as the most important equations of state which have been published before 1999. We will not go back over that here. In that paper, Tegeler *et al.* have also developed a new equation of state for argon which covers the largest part of the fluid region. In this study we shall systematically compare our new approach for the equations of state of argon with the wide-range equations of Tegeler *et al.*

The development of the equation of state generally starts by an empirical description of the Helmholtz free energy F with two independent variables, density ρ and temperature T . All thermodynamic properties of a pure substance can then be obtained by combining derivatives of $F(\rho, T)$. The dimensionless Helmholtz free energy $\tilde{a} = F/(R_s T)$ is commonly split into a part $\tilde{a}^o(\rho, T)$ which represents the properties of the ideal gas at given T and ρ , and a residual part $\tilde{a}^r(\rho, T)$ which takes into account the dense fluid behaviour. While statistical thermodynamics can predict the behaviour of fluids in the ideal-gas state with high accuracy, no physically founded equation is known which describes accurately the actual thermodynamic behaviour in the whole fluid region. Thus, an equation for the residual fluid behaviour, in this case for the residual part of the Helmholtz free energy \tilde{a}^r , has to be determined in an empirical way. However, as the Helmholtz free energy is not accessible to direct measurements, a suitable mathematical structure and some fitted coefficients have to be determined from properties for which experimental data are available. Hence all the physical properties are contained in the mathematical form given to the Helmholtz free energy.

In the wide-range equation of state for argon developed by Tegeler *et al.* (1999), the residual part of the Helmholtz free energy $\tilde{a}^r(\rho, T)$ contains polynomial terms, Gaussian terms and exponential terms which results in a total of 41 coefficients. This equation of state is valid for the fluid region delimited by

$$83.8058 \text{ K} < T < 700 \text{ K},$$

and

$$0 \text{ MPa} < P < 1000 \text{ MPa}.$$

The hundreds adjustable parameters of the equation of state of Tegeler *et al.* are determined by a sophisticated fitting technique which is a powerful mathematical tool and a practical way for representing data sets (by assigning weights to each of them subjectively). This technique provides an easily manipulable overall numerical representation of the data but it also allows completing the representation of measurable quantities in areas where no measurements have been made. However, passing in a set of data points does not mean that

the obtained variations have a physical meaning or that the physical ideas underlying mathematical representation are unique. For example, we can notice the following drawbacks of the equation of state of Tegeler *et al.*:

1. Extrapolation of the equation for the isochoric heat capacity in regions of high or low density and high temperature is non physical.
2. The extrapolation of polynomial developments does not generally give valid results; indeed, polynomial development is very sensitive (i.e. instable) with respect to the values of its coefficients and these coefficients cannot support to be truncated, even slightly. So all the coefficients n_i of Tegeler's *et al.* model have 14 decimals, thus the coefficient have no physical sense.
3. The model applies for the pure fluid phases and cannot in its actual form take into account particular properties inside the coexistence liquid-vapour region. Moreover, the model gives negative values of C_V on some isotherms inside the coexistence liquid-vapour region ($C_V < 0$ is never observed for classical thermodynamic systems). This implies for example some non-physical variations of the liquid spinodal curve.

The aim of this paper is no to increase the precision of the equation of state of Tegeler *et al.* in its own domain of validity but to develop a new equation of state based on different physical ideas that can fill the drawbacks previously expressed in order to obtain a more physical description of the experimental thermodynamic data of argon in a broader temperature and pressure ranges. In the classical approach, the ideal part of the free energy is generally determined from the well known properties of the ideal-gas heat capacities. We propose to extend this approach to the residual part therefore our new equation of state is based on an empirical description of the isochoric heat capacity $C_V(\rho, T)$. Then the thermodynamics properties (internal energy, entropy, free energy) are obtained by combining integration of functions involving $C_V(\rho, T)$. For instance, internal energy U can be deduced from: $U(\rho, T) = \int C_V(\rho, T) dT + U_0(\rho) + \text{constant}$, where $U_0(\rho)$ is an arbitrary function of density. In this way, possible data fluctuations are smoothed. However, an integration process introduces arbitrary functions (e.g. $U_0(\rho)$). These functions can be deduced from a comparison between calculated and experimental data. We chose pressure $P(\rho, T)$ which is the largest available data set-as shown latter.

This equation has also to be consistent with the results calculated from the theoretical model of Ronchi (1981). An important feature of the Ronchi model is to predict the appearance of a maximum on the isochoric heat capacity C_V along isochors. A maximum of C_V along isochors has experimentally been observed in several fluids as for example in water. Consequently, the extrapolation of C_V along isochors from a given model must show a maximum as predicted by the Ronchi model.

The Ronchi calculated data cover the largest available temperature range from 300 to 2300 K and the largest available pressure range from 9.9 to 47 058.9 MPa. It is important to notice that the calculated data of Ronchi are consistent with many experimental data which were used by Tegeler *et al.* (1999) but for which they assigned them to group 2-3. From the data of Ronchi, the highest available density is called $\rho_{\text{max, Ronc}}$ and its value is given in Table 2.

By construction, a part of the Ronchi and NIST data overlap, so we will first check the consistency of these two sets of data. On Fig. 1, we have plotted the relative error $(P_{\text{Ronchi}} - P_{\text{NIST}})/P_{\text{Ronchi}}$ as a function of T for their common range of density values. It is observed that the error is always less than 2.5%, so that the Ronchi data can be considered to be consistent with the NIST data.

2. The New Equation of State for the Isochoric Heat Capacity

As stated previously, our approach starts with the empirical description of a chosen thermodynamic quantity. We chose to describe an experimentally measured quantity, which is not the case for the Helmholtz free energy. The quantity which has the simplest mathematical and physical comprehensive variation is the isochoric heat capacity C_V as function of density ρ and temperature T . Starting with this quantity, we therefore lose the advantage of the description provided by the Helmholtz free energy from which all other thermodynamic quantities can be obtained by derivation but, it allows to introduce more easily new physical bases, in particular the non-extensivity, and we gain in simplicity. Indeed, the number of coefficients for the description of C_V is 11 and we will see in the next section that the number of coefficients for the description of the Helmholtz free energy is only **26** compared to **41** for the model of Tegeler *et al.* (1999).

After choosing the thermodynamic quantity to describe, we must find a mathematical structure for its representation. A virial like development is an easy and widespread approximation. The problem of polynomial terms is that they introduce very small oscillations that are not physical. To avoid such effects, we assumed that the description must not contain any form of polynomial expression. Thus, the description is made in terms of power laws and exponentials with density dependent exponents. We shall see that with such a description, we get among the parameters of the model a dozen of different characteristic densities instead of only ρ_c (which is consistent with the fact that argon does not follow the law of Corresponding States), therefore we have chosen to express all the equations of states in a dimensionless form according to the variables ρ and T which lead to simpler expressions than if we had considered the dimensionless variables ρ/ρ_c and T/T_c . In addition, the most suitable units for density and temperature have been chosen as g/cm^3 for ρ and Kelvin for T .

As for the Helmholtz free energy, the isochoric heat capacity is split into a part C_V^o which represents the properties of the ideal gas and a part C_V^r which takes into account the residual fluid behaviour at given T and ρ . We can remark here that the ideal part of the free energy is in fact determined from known properties of C_V^o in the classical approach. Since argon is monoatomic only the translational contribution to the ideal-gas heat capacity $C_{p,tr}^o = \frac{5}{2}R_A$ has to be taken into account, we deduce from the Mayer's law that $C_V^o = \frac{3}{2}R_A$. In dimensionless form, the isochoric heat capacity is written:

$$\tilde{c}_V(\rho, T) = \frac{C_V(\rho, T)}{R_A} = \tilde{c}_V^o + \tilde{c}_V^r(\rho, T) = \frac{3}{2} \left(1 + \frac{2}{3} \tilde{c}_V^r(\rho, T) \right) \quad (1)$$

To take into account all fluid domain including the liquid-vapour coexistence region and the region around the critical point, $\tilde{c}_V^r(\rho, T)$ must be split up into 3 terms such that $\tilde{c}_V^r(\rho, T) = \tilde{c}_{V,\text{reg}}^r + \tilde{c}_{V,\text{nonreg}}^r + \tilde{c}_{V,\text{crit}}^r$ with:

$$\left. \begin{aligned}
\tilde{c}_{V,\text{reg}}^r &= n_{\text{reg}}(\rho) \times \left\{ 1 - \exp\left(-\left(\lambda \frac{T}{T_c}\right)^{1-(m(\rho)-1)}\right) \right\} \times \left(\frac{T}{T_c}\right)^{m(\rho)-1} \\
\tilde{c}_{V,\text{nonreg}}^r &= n_{\text{nonreg}}(\rho) \times \exp\left(-\left(\frac{T_{\text{div}}(\rho)}{T}\right)^{-3/2}\right) \times \frac{1}{1 - \frac{T_{\text{div}}(\rho)}{T}} \\
\tilde{c}_{V,\text{crit}}^r &= n_{\text{crit}}(\rho) \times \left(\frac{T_{\text{div}}(\rho)}{T}\right)^{\varepsilon_{\text{crit}}(\rho)}
\end{aligned} \right\} \text{ for } T \geq T_{\text{div}} \quad (2)$$

where $\lambda = 6.8494$ and $n_{\text{reg}}(\rho)$, $m(\rho)$, $n_{\text{nonreg}}(\rho)$, $T_{\text{div}}(\rho)$, $n_{\text{crit}}(\rho)$, $\varepsilon_{\text{crit}}(\rho)$ are empirical functions determined from the best fitting of the NIST and Ronchi data. The Ronchi data (Ronchi, 1981) are calculated from his model. **It is important to note that relation (2) is valid only for temperatures $T \geq T_{\text{div}}(\rho)$, i.e. in particular for all states in the single phase region.** In this way, $T_{\text{div}}(\rho)$ defines an arbitrary divergence curve. We shall see in section 3.4 how this relation is transformed for $T < T_{\text{div}}(\rho)$ (i.e. for states inside the coexistence region).

It is very important to notice that with our approach, once chosen the mathematical form of the regular term, it is not possible to envisage any mathematical form for the two other residual terms. Indeed the two remaining terms must have a consistent mathematical form with that of the first one otherwise the amplitude terms n_i become erratic functions of density and are no more smooth functions. The mathematical forms are certainly not unique but there are strong constraints on these forms. This is a fundamental difference with the classical fitting approach of the free energy function where there is no mathematical constraint between the different terms.

The 3 terms of the residual part of C_V are now clarified.

- The first term $\tilde{c}_{V,\text{reg}}^r$ which is a simple power law, is called ‘regular’. It shows no singularity and can be calculated for temperature from T_t (triple point temperature) up to infinity. When $T \rightarrow 0$ K following isochors, this term can be approximated by:

$$\tilde{c}_{V,\text{reg}}^r(\rho, T \rightarrow 0\text{K}) \cong \frac{3}{2} n_{\text{reg}}(\rho) \times \lambda \frac{T}{T_c} \quad (3),$$

which tends towards zero as a linear law.

For $T \gg T_c/\lambda$, $\tilde{c}_{V,\text{reg}}^r$ reduces to:

$$\tilde{c}_{V,\text{reg}}^r(\rho, T \gg T_c/\lambda) \cong \frac{3}{2} n_{\text{reg}}(\rho) \times \left(\frac{T}{T_c}\right)^{m(\rho)-1} \quad (4)$$

The characteristic temperature $T_c/\lambda = 22.0$ K is not the Debye temperature of argon which is equal to 85 K. Our characteristic temperature here is much smaller and has been chosen in order to minimize the relative error of C_V on the saturated vapour pressure curve so that **the term containing $\lambda T / T_c$ becomes important only for temperatures smaller than the triple point temperature** (i.e. for $T \ll T_t$).

- The second term \tilde{c}_V^r ,_{nonreg} is called ‘non regular’, it presents an asymptote for $T = T_{\text{div}}(\rho)$ (i.e. C_V is infinite for this value of temperature). This term is only significant near the liquid-vapour coexistence region. We can also note that the divergence is weak.
- The third term \tilde{c}_V^r ,_{crit} is important only in a small region around the critical point. This term allows us to reproduce the very sharp evolution of C_V very close to the critical point. It can be understood as the macroscopic contribution of the critical fluctuations. This term plays the same mathematical role as the contribution of the four last terms in the second derivative with temperature of the residual free energy in the model of Tegeler *et al.* (1999).

We have pointed out that the regular term \tilde{c}_V^r ,_{reg} tends to zero when T tends to 0. We will show in section 3.4 that for $T < T_{\text{div}}$, the non-regular and critical terms have also a limit equal to zero when $T \rightarrow 0$ K. Hence, $\tilde{c}_V^r(\rho, T) \rightarrow 0$ if $T \rightarrow 0$; this result is in agreement with the third law of thermodynamics (i.e. assumption of Nernst-Planck). Since $\tilde{c}_V = \tilde{c}_V^0 + \tilde{c}_V^r$, this law imposes $\tilde{c}_V \rightarrow 0$ if $T \rightarrow 0$ and then $\tilde{c}_V^0 \rightarrow 0$ if $T \rightarrow 0$. To reach this result, \tilde{c}_V^0 is rewritten on the following form:

$$\tilde{c}_V^0(T) = \frac{3}{2} \left(1 - \exp\left(-\lambda_0 \frac{T}{T_c}\right) \right) \quad (5)$$

where $\lambda_0 = 18.2121$.

In the expression of $\tilde{c}_V^r(\rho, T)$, all coefficients depend on density ρ in the following way:

$$\begin{aligned} n_{\text{reg}}(\rho) = & \alpha_{\text{reg},1} \left(\frac{\rho}{\rho + \rho_{\text{t,Liq}}} \right)^{\epsilon_{\text{reg},1a}} \times \exp\left(-\left(\frac{\rho}{\rho_{\text{t,Gas}}}\right)^{\epsilon_{\text{reg},1b}}\right) \\ & + \alpha_{\text{reg},2} \left(\frac{\rho}{\rho_{\text{t,Liq}}} \right)^{\epsilon_{\text{reg},2a}} \left\{ 1 - \exp\left(-\left(\frac{\rho}{\rho_{\text{reg,Ronc}}}\right)^{-\epsilon_{\text{reg},2b}}\right) \right\} \end{aligned} \quad (6)$$

$$\begin{aligned} m(\rho) = & -\alpha_{m,1} + \alpha_{m,2} \times \exp\left(-\left(\frac{\rho}{\rho_{\text{t,Liq}}}\right)^{3/2}\right) + \alpha_{m,3} \left(\frac{\rho}{\rho_c}\right)^{3/2} \times \exp\left(-\frac{\rho}{\rho_c}\right) \\ & - \alpha_{m,4} \times \ln\left(\frac{\rho}{\rho_c}\right) + m_{\text{Ronc}}(\rho) \end{aligned} \quad (7)$$

$$m_{\text{Ronc}}(\rho) = \begin{cases} \left[\alpha_{m,1} + \alpha_{m,4} \ln\left(\frac{\rho}{\rho_c}\right) \right] \left(1 + \frac{\rho}{\rho_{\text{m,Ronc}}} \right)^{\epsilon_{m,5a}} \exp\left(-\exp\left(\left(\frac{\rho_{\text{m,Ronc}}}{\rho}\right)^{\epsilon_{m,5b}}\right)\right) & \text{for } \rho \geq \frac{M}{12.9} \text{ g/cm}^3 \\ 0 & \text{otherwise} \end{cases} \quad (8)$$

$$n_{\text{nonreg}}(\rho) = \begin{cases} \alpha_{\text{nonreg},1} \left(\frac{\rho}{\rho_{t,\text{Gas}}} \right)^{\varepsilon_{\text{nonreg},1a}} \exp \left(- \left(\frac{\rho_{t,\text{Liq}}}{\rho_{t,\text{Gas}}} \right)^{\varepsilon_{\text{nonreg},1b}} \left(\frac{\rho}{\rho_{t,\text{Liq}} - \rho} \right)^{\varepsilon_{\text{nonreg},1b}} \right) \\ \quad + \alpha_{\text{nonreg},2} \left(\frac{\rho}{\rho_{t,\text{Gas}}} \right)^{\varepsilon_{\text{nonreg},2a}} \exp \left(- \left(\frac{\rho_{t,\text{Liq}}}{\rho_{t,\text{Gas}}} \right)^{\varepsilon_{\text{nonreg},2b}} \left(\frac{\rho}{\rho_{t,\text{Liq}} - \rho} \right)^{\varepsilon_{\text{nonreg},2b}} \right) & \text{for } \rho \leq \rho_{t,\text{Liq}} \\ 0 & \text{otherwise} \end{cases} \quad (9)$$

$$T_{\text{div}}(\rho) = \alpha_{\text{div},1} \left(\frac{\rho}{\rho_c} \right)^{\varepsilon_{\text{div},1a}} \exp \left(- \left(\frac{\rho}{\rho_c} \right)^{\varepsilon_{\text{div},1b}} \right) + \alpha_{\text{div},2} \left(\frac{\rho}{\rho_{t,\text{Liq}}} \right)^{\varepsilon_{\text{div},2a}} \exp \left(- \left(\frac{\rho}{\rho_{t,\text{Liq}}} \right)^{\varepsilon_{\text{div},2b}} \right) \quad (10)$$

$$n_{\text{crit}}(\rho) = \alpha_{\text{crit},a} \left(\frac{\rho}{\rho_c} \right)^{\varepsilon_{\text{crit},a}} \exp \left(- \left(\alpha_{\text{crit},b} \frac{\rho - \rho_c}{\rho_c} \right)^2 \right)^{\varepsilon_{\text{crit},b}} \quad (11)$$

$$\varepsilon_{\text{crit}}(\rho) = \varepsilon_{\text{crit},c} + \varepsilon_{\text{crit},d} \exp \left(- \left(\varepsilon_{\text{crit},e} \frac{\rho - \rho_{\text{crit},a}}{\rho_{\text{crit},a}} \right)^2 \right) + \varepsilon_{\text{crit},f} \exp \left(- \left(\varepsilon_{\text{crit},g} \frac{\rho - \rho_{\text{crit},b}}{\rho_{\text{crit},b}} \right)^2 \right) \quad (12)$$

where ε_i are exponents and α_i characteristic coefficients. Table 1 lists the values of these parameters.

Now, some explanations will be given on the properties of these coefficients. Most of them involve the three characteristic densities of argon:

- the density $\rho_{t,\text{Liq}}$ of liquid at the triple point,
- the density $\rho_{t,\text{Gas}}$ of gas at the triple point,
- the critical density ρ_c .

Moreover, two other characteristic densities, $\rho_{\text{reg,Ronch}}$ and $\rho_{\text{m,Ronch}}$, have to be added in view to correctly fit the data of Ronchi at very high densities. All values of these characteristic densities are given in Table 2.

Obviously, other mathematical forms for the coefficients (6) to (12) could be used, but the proposed equations are the simplest ones we have found that lead to an accurate fitting of the whole data set. The most important argument in favour of these equations is that they give very nice straight lines if one plots the difference between the pressure data and the pressure values deduced from the nonzero contribution of C_V to the pressure via the derivative $\left(\frac{\partial C_V}{\partial V} \right)_T = T \left(\frac{\partial^2 P}{\partial T^2} \right)_V \neq 0$ as a function of temperature. This consequence will be detailed in section 3.1. This result clearly shows that the isochors curves $P(T)$ are not straight lines when C_V is a function of density.

The density dependence of the n_i coefficients are shown on Fig. 2. Each coefficient is equal to zero when $\rho \rightarrow 0$ and $\rho \rightarrow \infty$ and get through a maximum in-between (remark: the maximum of n_{reg} really occurs but outside the range of density shown on fig. 2).

The density dependence of exponent m is shown on Fig. 3. This coefficient is always strictly smaller than one and it tends to $-\infty$ when $\rho \rightarrow 0$ and $\rho \rightarrow \infty$. Then, there are two

density values for which $m = 0$. This means that, for the region where $T \gg T_c/\lambda$, $\tilde{c}_{V,\text{reg}}^r$ is always decreasing along isochors when the temperature is increasing.

The characteristic temperature T_{div} as a function of density defines a curve $T_{\text{div}}(\rho)$ which lies entirely inside the coexistence vapour-liquid region defined by $T_{\text{sat}}(\rho)$, see Fig. 4. For a first order phase transition the divergence of C_V must occur on the spinodal curve (i.e. loci of thermodynamic mechanical instability), corresponding to:

$$\left(\frac{\partial P}{\partial V}\right)_T = 0 \quad (13)$$

Because no experimental data of the spinodal curve can be found in all the density range from $\rho_{\text{t,Gas}}$ to $\rho_{\text{t,Liq}}$, T_{div} was only determined by fitting the data of C_V from NIST. If this set of data is enough accurate and consistent with the $P\rho T$ data set, we should be able to identify $T_{\text{div}}(\rho)$ as the spinodal temperature curve. We will discuss in more detailed the results obtained for the spinodal states in section 4.3.3.

From relation (2) it is also easy to see that the second thermodynamic instability (i.e. the thermal instability), defined by

$$C_V < 0 \quad (14)$$

will never occur in our approach contrary to the model of Tegeler *et al.* (1999).

Consequently, relation (2) being valid for $T > T_{\text{div}}$, this relation can be used into the coexistence vapour-liquid region by crossing $T_{\text{sat}}(\rho)$ till to approximately the spinodal curve. No trouble occurs as long as $T > T_{\text{div}}$, though the model is based on a pure fluid description. The fact that there is no discontinuity of C_V when crossing the coexistence curve (excepted at the critical point) is a characteristic of a first order transition. We shall see in section 3.4 how to treat the crossing of the divergence curve defined by $T_{\text{div}}(\rho)$. Finally, we can notice that $T_{\text{div}} = 0$ for $\rho = 0$ and $T_{\text{div}} \rightarrow 0$ when $\rho \rightarrow \infty$, hence, $T_{\text{div}}(\rho)$ shows the right density dependence which allows us to investigate the fluid properties from the gas phase up to the sublimation curve.

The flexibility of our method is illustrated now on the equation of state for the isochoric heat capacity. So if we want to represent for higher densities than $\rho_{\text{t,Liq}}$ the data from NIST instead of the data of Ronchi, it is only necessary to change the values of the couple $(\rho_{\text{reg,Ronch}}, \varepsilon_{\text{reg,2b}})$ and the mathematical form of the exponent function $m(\rho)$. In this case Eq. (7) must be replaced by the following function:

$$m_{\text{NIST}}(\rho) = \alpha_{m,1} - \alpha_{m,2} \times \ln\left(\frac{\rho}{\rho_{m,2}} + \frac{\rho_{m,2}}{\rho}\right) + \alpha_{m,3} \left(\frac{\rho}{\rho_{m,3}}\right)^{\varepsilon_{m,3a}} \times \exp\left(-\left(\frac{\rho}{\rho_{m,3}}\right)^{\varepsilon_{m,3b}}\right) + \alpha_{m,4} \times \exp\left(\left(\frac{\rho_{m,4b}}{\rho_{m,4a}}\right)^{2\varepsilon_{m,4}} \times \left(\frac{\rho_{m,4a}}{\rho-1}\right)^{2\varepsilon_{m,4}}\right) + m_{\text{Extrapol}}(\rho) \quad (7\text{bis})$$

with

$$m_{\text{Extrapol}}(\rho) = \frac{\rho_{\text{t,Liq}}}{\rho} \left[-\frac{\alpha_{m,5}}{\varepsilon_{m,5} - 1} \left(\frac{\rho}{\rho_{m,4a}} \right)^{\varepsilon_{m,5}} + \alpha_{m,6} \left(\frac{\rho}{\rho_{m,4a}} \right)^{\varepsilon_{m,6}} E_{\varepsilon_{m,6}} \left(\frac{\rho}{\rho_{m,6}} \right) \right]$$

where $E_n(z) = \int_1^{\infty} \frac{e^{-zt}}{t^n} dt$ represents the exponential integral function. The corresponding parameters have the following values:

- Coefficients: $\alpha_{m,1}=0.48962315$, $\alpha_{m,2}=0.24014465$, $\alpha_{m,3}=1.0932969$, $\alpha_{m,4}=0.08936644$,
 $\alpha_{m,5}=67.4598$, $\alpha_{m,6}=1331.29$.
- Exponents: $\varepsilon_{m,3a}=1.56671$, $\varepsilon_{m,3b}=0.930273$, $\varepsilon_{m,4}=4.785$, $\varepsilon_{m,5}=166.594$, $\varepsilon_{m,6}=5.93118$ and
 $\varepsilon_{\text{reg,2b}} = 5.248961$.
- Characteristic densities in g/cm^3 : $\rho_{m,2}=1.35802$, $\rho_{m,3}=0.449618$, $\rho_{m,4a}=3.30149$,
 $\rho_{m,4b}=4.05911$, $\rho_{m,6}=24.5967$ and the new value for $\rho_{\text{reg,Ronc}}$ is now equal to 2.22915.

We can immediately notice that this new function needs more parameters than for Eq. (7) but the global shape of the function $m_{\text{NIST}}(\rho)$ is very similar to that of Eq. (7) except that this new function has a strong oscillation around the density $\rho = 1.8 \text{ g/cm}^3$. This oscillation is needed for a good representation of the data but it is physically difficult to understand.

Table 1. Coefficients and exponents of Eq. (6) to Eq. (12).

i	ε_i	α_i
reg,1		11.23233957
reg,1a	1.1178177	
reg,1b	0.23513928	
reg,2		0.53278931
reg,2a	2.9322362	
reg,2b	15.5957	
m,1		0.07079238
m,2		0.33623345
m,3		1.3019754
m,4		-0.24008716
m,5a	14.4899	
m,5b	7.20862	
nonreg,1		0.089409
nonreg,1a	0.71915	
nonreg,1b	0.22569	
nonreg,2		0.015481
nonreg,2a	1.3401	
nonreg,2b	0.29485	
div,1		102.06515
div,1a	0.9218165	
div,1b	1.1328347	
div,2		120.40518
div,2a	0.12035802	
div,2b	4.424004	
crit,a	0.80803	701.52
crit,b	1.134	4.27385
crit,c	1.436786	
crit,d	123.1335	
crit,e	2.205614	
crit,f	26.32662	
crit,g	4.437711	

Table 2. Characteristic values of densities of argon and there corresponding molar volumes.

<i>i</i>	ρ_i (g/cm ³)	V_i (cm ³ /mole)
t,Gas	0.0040546	9852.51318
t,Liq	1.41680	28.1959
c	0.53559	74.5857
crit,a	0.51182	78.0502
crit,b	0.73085	54.6589
max,Ronc	3.35697	11.9
reg,Ronc	3.53159	11.3116
m,Ronc	3.67875	10.8591
u,1	6.61153	6.04217
u,2	3.99925	9.98884
u,3	3.90870	10.22026
s,1	1.50915	26.47047
s,4	1.18697	33.65528
sRonc,1	3.28898	12.146
sRonc,2	4.31602	9.25574

3. Thermodynamic Properties Derived from the Isochoric Heat Capacity

Since the Helmholtz free energy versus density and temperature is one of the four basic forms of an equation of state, we focus here on the process for deducing its expression. For this purpose we use the thermodynamic relation:

$$C_V = \left(\frac{\partial U}{\partial T} \right)_V = T \left(\frac{\partial S}{\partial T} \right)_V = -T \left(\frac{\partial^2 F}{\partial T^2} \right)_V \quad (15)$$

Consequently, F can be deduced from: (i) two successive integrations of C_V or, (ii) a single integration of C_V to calculate U and S and then use the thermodynamic relation:

$$F = U - TS \quad (16)$$

with $U(\rho, T) = \int C_V(\rho, T) dT + U_0(\rho) + \text{constant}$, $S(\rho, T) = \int \frac{C_V(\rho, T)}{T} dT + S_0(\rho) + \text{constant}$ and $C_V(\rho, T) = R_A (\tilde{c}_V^o(T) + \tilde{c}_V^r(\rho, T))$ (given by Eq. 1, 2 and 5).

We chose the second approach on account that the two integrations to find U and S induced the existence of two arbitrary functions, respectively $U_0(\rho)$ and $S_0(\rho)$, which are simpler to determine than directly finding the arbitrary function for F . The later simply writes $F_0(\rho, T) = U_0(\rho) - TS_0(\rho)$. We shall see in section 3.1 how the two arbitrary functions $U_0(\rho)$ and $S_0(\rho)$ can be determined.

There is no difficulty to find a primitive of $\tilde{c}_V^o(T)$ for U or S . For the residual part of C_V (Eq. 2), there is also no difficulty to find a primitive of $\tilde{c}_{V,\text{reg}}^r$ and $\tilde{c}_{V,\text{crit}}^r$. However, for $\tilde{c}_{V,\text{reg}}^r$ when $T \gg T_c/\lambda$, two expressions can be obtained for the primitive of U depending on whether the value of $m(\rho)$ is zero or not, that is to say a power law if $m \neq 0$ and a logarithmic law if $m = 0$. We can see on Fig. 3 that there are two values of ρ for which $m = 0$, namely for $\rho_{\text{low}} = 0.11726382 \text{ g/cm}^3$ and $\rho_{\text{high}} = 3.29510771 \text{ g/cm}^3$. To obtain a single expression uniformly valid, we write the primitive as follows:

$$\int \tilde{c}_{V,\text{reg}}^r(T \gg T_c/\lambda) dT = \frac{3}{2} n_{\text{reg}}(\rho) T_c \frac{(T/T_c)^{m(\rho)} - 1}{m(\rho)} \quad (17)$$

By using the Hospital's rule, we can easily verify that: $\lim_{m \rightarrow 0} \frac{(T/T_c)^{m(\rho)} - 1}{m(\rho)} = \ln \left(\frac{T}{T_c} \right)$,

which corresponds to the right expression for the primitive when $m = 0$.

The same problem occurs for the primitive of S , but this time the expression depends whether $m = 1$ or not. For argon, the value $m = 1$ is never reached, but to maintain a general expression, we proceed in the same manner to determine the expression for the primitive of S .

For the integration of C_V , the only term for which it may be difficult to find a primitive is $\tilde{c}_{V,\text{nonreg}}^r$ (see Eq. 2). We could integrate it numerically but a reference state must be chosen; this will be done in section 3.4. To find a primitive it is also possible to perform a series expansion of the term $(1-x)^{-1}$ with $x = T_{\text{div}}/T$. Hence $\tilde{c}_{V,\text{nonreg}}^r$ can be written in the following form:

$$\tilde{c}_{V,\text{nonreg}}^r(\rho, x) = \frac{3}{2} n_{\text{nonreg}}(\rho) \sum_{k=0}^{\infty} \exp(-x^{-3/2}) x^k, \quad k \in \mathbb{N} \quad (18)$$

A primitive for each term of the series can be obtained. For a practical calculation the series expansion must be truncated. The convergence is slower as x approaches the unit value, and as a result the number of terms that must be considered increases. We give below an empirical formula to calculate the required number of terms so that the residual error due to truncation is less than 0.1% (except for $x > 0.99$ since the function weakly diverges as $T \rightarrow T_{\text{div}}$)

$$k_{\text{max}}(x) = 1 + \left\lfloor 400 \frac{\exp[\exp(-8.52 \times |1-x|) - 1]}{1 + 16.6 \times |1-x|} \right\rfloor \quad (19)$$

Finally the equations for U and S can be written in standard dimensionless form (i.e. an ideal gas part and a residual one) as:

$$\tilde{u}(\rho, T) = \frac{U(\rho, T)}{R_A T} = \frac{3}{2} \left[1 + \frac{T_c}{\lambda_0 T} \exp\left(-\frac{\lambda_0 T}{T_c}\right) \right] + \tilde{u}^*(\rho, T) + \tilde{u}_0(\rho) \quad (20)$$

with

$$\begin{aligned} \tilde{u}^*(\rho, T) = & \frac{3}{2} n_{\text{reg}}(\rho) \frac{T_c}{T} \left\{ \frac{\left(\frac{T}{T_c}\right)^{m(\rho)} - 1}{m(\rho)} + \frac{\lambda^{-m(\rho)}}{2 - m(\rho)} \Gamma\left(\frac{m(\rho)}{2 - m(\rho)}, \left(\frac{\lambda T}{T_c}\right)^{2 - m(\rho)}\right) \right\} \\ & - n_{\text{nonreg}}(\rho) \frac{T_{\text{div}}(\rho)}{T} \sum_{k=0}^{\infty} \Gamma\left(-\frac{2}{3}(k-1), \left(\frac{T_{\text{div}}(\rho)}{T}\right)^{-3/2}\right) + \frac{3}{2} n_{\text{crit}}(\rho) \frac{(T_{\text{div}}(\rho)/T)^{\varepsilon_{\text{crit}}(\rho)}}{1 - \varepsilon_{\text{crit}}(\rho)} \end{aligned} \quad (21)$$

and

$$\tilde{s}(\rho, T) = \frac{S(\rho, T)}{R_A} = \frac{3}{2} \left[\ln(T) - \text{Ei}\left(-\frac{\lambda_0 T}{T_c}\right) \right] + \tilde{s}^*(\rho, T) + \tilde{s}_0(\rho) \quad (22)$$

with

$$\begin{aligned} \tilde{s}^*(\rho, T) = & \frac{3}{2} n_{\text{reg}}(\rho) \left\{ \frac{\left(\frac{T}{T_c}\right)^{m(\rho)-1} - 1}{m(\rho)-1} + \frac{\lambda^{1-m(\rho)}}{2 - m(\rho)} \Gamma\left(\frac{m(\rho)-1}{2 - m(\rho)}, \left(\frac{\lambda T}{T_c}\right)^{2 - m(\rho)}\right) \right\} \\ & - n_{\text{nonreg}}(\rho) \sum_{k=0}^{\infty} \Gamma\left(-\frac{2}{3}k, \left(\frac{T_{\text{div}}(\rho)}{T}\right)^{-3/2}\right) - \frac{3}{2} n_{\text{crit}}(\rho) \varepsilon_{\text{crit}}(\rho)^{-1} \left(\frac{T_{\text{div}}(\rho)}{T}\right)^{\varepsilon_{\text{crit}}(\rho)} \end{aligned} \quad (23)$$

where $\Gamma(a, z) = \int_z^\infty t^{a-1} \exp(-t) dt$ represents the incomplete gamma function and $\text{Ei}(z) = \int_{-z}^\infty \frac{\exp(-t)}{t} dt$ represents the exponential integral function.

In the ideal gas limit, the relations for the internal energy and entropy must be written respectively as:

$$U^\circ(T) = \frac{3}{2} R_A T + U_0^\circ \quad (24)$$

$$S^\circ(\rho, T) = \frac{3}{2} R_A \ln(T) - R_A \ln(\rho) + S_0^\circ \quad (25)$$

where U_0° and S_0° are arbitrary constants. These formulas can be rewritten as follows (using Eq. (5) for \tilde{c}_v°):

$$U^\circ(T) = \frac{3}{2} R_A T \left[1 + \frac{T_c}{\lambda_0 T} \exp\left(-\frac{\lambda_0 T}{T_c}\right) \right] + U_0^\circ \quad (26)$$

$$S^\circ(\rho, T) = \frac{3}{2} R_A \left[\ln(T) - \text{Ei}\left(-\frac{\lambda_0 T}{T_c}\right) \right] - R_A \ln(\rho) + S_0^\circ \quad (27)$$

We can now use these expressions to rearrange Eq. (20) and Eq. (22) in order to extract the residual part for the internal energy (i.e. $\tilde{u}(\rho, T)$ minus the ideal gas part) and for the entropy:

$$\tilde{u}^r(\rho, T) = \tilde{u}^*(\rho, T) + \tilde{u}_0(\rho) - \zeta_0 \frac{T_c}{T} \quad \text{with} \quad \zeta_0 = \frac{U_0^\circ}{R_A T_c} \quad (28)$$

$$\tilde{s}^r(\rho, T) = \tilde{s}^*(\rho, T) + \tilde{s}_0(\rho) + \ln(\rho) - \omega_0 \quad \text{with} \quad \omega_0 = \frac{S_0^\circ}{R_A} \quad (29)$$

where ζ_0 and ω_0 are two arbitrary constants. In view to fit NIST data, the constant values must be such that: $\zeta_0 = -0.00070133$ and $\omega_0 = 2.71428$.

Table 3. The ideal-gas part of the dimensionless Helmholtz free energy function and its derivatives.

$$\tilde{a}^\circ = \frac{3}{2} \left[1 - \ln(T) + \frac{T_c}{\lambda_0 T} \exp\left(-\frac{\lambda_0 T}{T_c}\right) + \text{Ei}\left(-\frac{\lambda_0 T}{T_c}\right) \right] + \ln(\rho) + \zeta_0 \frac{T_c}{T} - \omega_0$$

$$T_c \left(\frac{\partial \tilde{a}^\circ}{\partial T} \right)_\rho = -\frac{T_c}{T} \left[\frac{3}{2} \left(1 + \frac{T_c}{\lambda_0 T} \exp\left(-\frac{\lambda_0 T}{T_c}\right) \right) + \zeta_0 \frac{T_c}{T} \right]$$

$$T_c^2 \left(\frac{\partial^2 \tilde{a}^\circ}{\partial T^2} \right)_\rho = \frac{3}{2} \left(\frac{T_c}{T} \right)^2 \left(1 + \frac{4}{3} \frac{T_c}{T} \zeta_0 \right) + \frac{3}{2} \left(\frac{T_c}{T} \right)^2 \left(1 + 2 \frac{T_c}{\lambda_0 T} \right) \exp\left(-\frac{\lambda_0 T}{T_c}\right)$$

$$\rho_c \left(\frac{\partial \tilde{a}^\circ}{\partial \rho} \right)_T = \frac{\rho_c}{\rho}$$

$$\rho_c^2 \left(\frac{\partial^2 \tilde{a}^\circ}{\partial \rho^2} \right)_T = -\left(\frac{\rho_c}{\rho} \right)^2$$

$$\left(\frac{\partial^2 \tilde{a}^\circ}{\partial \rho \partial T} \right) = 0$$

3.1. Determination of the arbitrary functions for the Internal Energy and Entropy

The two arbitrary functions $U_0(\rho)$ and $S_0(\rho)$ can be determined in two different ways. One way is to make the difference between previously published data of U (or S) with our calculated U (or S) values and then finding a function ($U_0(\rho)$ or $S_0(\rho)$) which best fits this difference. However, this way could be problematic as U and S are not measured quantities and depend on a chosen reference state. Another way is to use a new experimentally measured quantity namely pressure P , and by using the relation:

$$P = -\left(\frac{\partial F}{\partial V}\right)_T = \rho^2 \left(\frac{\partial F}{\partial \rho}\right)_T \quad (30)$$

Along isochors, from relations (15) and (16) we obtain $F = \int C_V dT + U_0 - T \left(\int \frac{C_V}{T} dT + S_0 \right)$ and its derivative in relation to V (or ρ) gives: $P - P_{C_V} = U'_0 - TS'_0$, with $P_{C_V} = \frac{\partial}{\partial V} \left(- \int C_V dT + T \int \frac{C_V}{T} dT \right)$ and $U'_0 = \frac{\partial}{\partial V} (U_0)$ and $S'_0 = \frac{\partial}{\partial V} (S_0)$. Here P_{C_V} is calculated from C_V values given by Eq. (1). For a given isochor of density ρ , the difference $P - P_{C_V}$ must be a straight line (of slope S'_0 and ordinate at origin U'_0) if the C_V values are well predicted by Eq. (1). This is effectively observed on Fig. 5 which displays $P - P_{C_V}$ versus T on different isochors. The best and simplest functions that represent $U'_0(\rho)$ and $S'_0(\rho)$ are:

$$\begin{aligned} \hat{u}'_0(\rho) = \frac{U'_0(\rho)}{\frac{3}{2} R_A T_c} = \frac{\alpha_{u,0}}{\rho_{t,Liq}} - \frac{1}{\rho} \left(\frac{\rho_{t,Liq}}{\rho} \right) & \left[\alpha_{u,1} \exp\left(-\frac{\rho_{u,1}}{\rho}\right) - \alpha_{u,2} \left(\frac{\rho_{u,2}}{\rho_{t,Liq}} \right)^{\epsilon_{u,2}} \left(\frac{\rho}{\rho_{u,2} - \rho} \right)^{\epsilon_{u,2}} + \alpha_{u,3} \left(\frac{\rho_{u,3}}{\rho_{t,Liq}} \right)^{\epsilon_{u,3}} \left(\frac{\rho}{\rho_{u,3} - \rho} \right)^{\epsilon_{u,3}} \right. \\ & \left. + \alpha_{u,4} \left(\frac{\rho}{\rho_{t,Liq}} \right)^{\epsilon_{u,4}} - \alpha_{u,5} \left(\frac{\rho}{\rho_{t,Liq}} \right)^3 \exp\left(-\left(\frac{\rho_{u,1}}{\rho}\right)^2\right) + \alpha_{u,6} \left(\frac{\rho}{\rho + \rho_c} \right)^{\epsilon_{u,6}} \right] \end{aligned} \quad (31)$$

and

$$\begin{aligned} \tilde{s}'_0(\rho) = \frac{S'_0(\rho)}{R_A} = -\frac{1}{\rho} & \left[1 + \alpha_{s,1} \left(\frac{\rho}{\rho_{t,Liq}} \right)^{\epsilon_{s,1}-1} \left(\frac{\rho_{s,1}}{\rho + \rho_{s,1}} \right)^{\epsilon_{s,1}} - \alpha_{s,2} \left(\frac{\rho}{\rho_{t,Liq}} \right)^{\epsilon_{s,2}-1} \ln\left(\frac{\rho}{\rho_{t,Liq}}\right) + \alpha_{s,3} \left(\frac{\rho}{\rho_{t,Liq}} \right)^{\epsilon_{s,3}-1} \ln\left(\frac{\rho}{\rho_{t,Liq}}\right) \right. \\ & \left. + \alpha_{s,4} \left(\frac{\rho}{\rho_{t,Liq}} \right)^{\epsilon_{s,4}-1} \exp\left(-\frac{\rho}{\rho_{s,4}}\right) + \alpha_{s,5} \left(\frac{\rho}{\rho_{t,Liq}} \right) \exp\left(-\left(\frac{\rho}{\rho_{s,1}}\right)^{\epsilon_{s,5}}\right) + \alpha_{s,6} \left(\frac{\rho}{\rho_{t,Liq}} \right) \exp\left(-\left(\frac{\rho - \rho_{s,4}}{\rho_c}\right)^2\right) \right] \\ & + \tilde{s}'_{0,Ronc}(\rho) \end{aligned} \quad (32)$$

with

$$\tilde{s}'_{0,Ronc}(\rho) = \frac{1}{\rho_{sRonc,1}} \left[\alpha_{sRonc,1} \left(\frac{\rho}{\rho_{sRonc,1}} \right)^{\epsilon_{sRonc,1}} - \alpha_{sRonc,2} \left(\frac{\rho}{\rho_{sRonc,1}} \right) \exp\left(-\frac{\rho_{sRonc,2}}{\rho}\right) \right] \times \left[1 - \exp\left(-\left(\frac{\rho}{\rho_c}\right)^2\right) \right] \quad (33)$$

Before continuing, it is worth noting that $\lim_{\rho \rightarrow 0} \frac{\rho U'_0(\rho)}{\frac{3}{2} R_A T_c} = 0$ and $\lim_{\rho \rightarrow 0} \frac{\rho S'_0(\rho)}{R_A} = -1$.

A primitive of expressions (31) and (32) leads to the functions $U_0(\rho)$ and $S_0(\rho)$ such that:

$$\begin{aligned} \hat{u}_0(\rho) = \frac{U_0(\rho)}{\frac{3}{2} R_A T_c} = & \alpha_{u,0} \frac{\rho}{\rho_{t,Liq}} - \frac{\alpha_{u,1}}{\varepsilon_{u,1} - 1} \left(\frac{\rho_{t,Liq}}{\rho_{u,1}} \right) \exp\left(-\frac{\rho_{u,1}}{\rho}\right) + \frac{\alpha_{u,2}}{\varepsilon_{u,2} - 1} \left(\frac{\rho_{u,2}}{\rho_{t,Liq}} \right)^{\varepsilon_{u,2}-1} \left(\frac{\rho}{\rho_{u,2} - \rho} \right)^{\varepsilon_{u,2}-1} \\ & - \frac{\alpha_{u,3}}{\varepsilon_{u,3} - 1} \left(\frac{\rho_{u,3}}{\rho_{t,Liq}} \right)^{\varepsilon_{u,3}-1} \left(\frac{\rho}{\rho_{u,3} - \rho} \right)^{\varepsilon_{u,3}-1} - \frac{\alpha_{u,4}}{\varepsilon_{u,4} - 1} \left(\frac{\rho}{\rho_{t,Liq}} \right)^{\varepsilon_{u,4}-1} \\ & + \frac{1}{2} \alpha_{u,5} \left(\frac{\rho}{\rho_{t,Liq}} \right)^2 \left[\exp\left(-\left(\frac{\rho_{u,1}}{\rho}\right)^2\right) - \left(\frac{\rho_{u,1}}{\rho}\right)^2 \Gamma\left(0, \left(\frac{\rho_{u,1}}{\rho}\right)^2\right) \right] \\ & - \frac{\alpha_{u,6}}{\varepsilon_{u,6} - 1} \left(\frac{\rho_{t,Liq}}{\rho_c} \right) \left(\frac{\rho}{\rho + \rho_c} \right)^{\varepsilon_{u,6}-1} \end{aligned} \quad (34)$$

and

$$\begin{aligned} \tilde{s}_0(\rho) = \frac{S_0(\rho)}{R_A} = & -\ln\left(\frac{\rho}{\rho_{t,Liq}}\right) - \frac{\alpha_{s,1}}{\varepsilon_{s,1} - 1} \left(\frac{\rho}{\rho_{t,Liq}} \right)^{\varepsilon_{s,1}-1} \left(\frac{\rho_{s,1}}{\rho + \rho_{s,1}} \right)^{\varepsilon_{s,1}-1} \\ & + \frac{\alpha_{s,2}}{(\varepsilon_{s,2} - 1)^2} \left(\frac{\rho}{\rho_{t,Liq}} \right)^{\varepsilon_{s,2}-1} \left[-1 + (\varepsilon_{s,2} - 1) \ln\left(\frac{\rho}{\rho_{t,Liq}}\right) \right] \\ & - \frac{\alpha_{s,3}}{(\varepsilon_{s,3} - 1)^2} \left(\frac{\rho}{\rho_{t,Liq}} \right)^{\varepsilon_{s,3}-1} \left[-1 + (\varepsilon_{s,3} - 1) \ln\left(\frac{\rho}{\rho_{t,Liq}}\right) \right] - \alpha_{s,4} \left(\frac{\rho}{\rho_{t,Liq}} \right)^{\varepsilon_{s,4}-1} E_{2-\varepsilon_{s,4}}\left(\frac{\rho}{\rho_{s,4}}\right) \\ & + \frac{\alpha_{s,5}}{\varepsilon_{s,5}} \left(\frac{\rho}{\rho_{t,Liq}} \right) E_{\frac{\varepsilon_{s,4}-1}{\varepsilon_{s,4}}}\left(\left(\frac{\rho}{\rho_{s,1}}\right)^{\varepsilon_{s,5}}\right) - \frac{\sqrt{\pi}}{2} \alpha_{s,6} \left(\frac{\rho_c}{\rho_{t,Liq}} \right) \operatorname{erf}\left(\frac{\rho - \rho_{s,4}}{\rho_c}\right) + \tilde{s}_{0,Ronc}(\rho) \end{aligned} \quad (35)$$

with

$$\begin{aligned} \tilde{s}_{0,Ronc}(\rho) = & \frac{\alpha_{sRonc,1}}{2(\varepsilon_{sRonc,1} + 1)} \left(\frac{\rho}{\rho_{sRonc,1}} \right)^{1+\varepsilon_{sRonc,1}} \left[2 + (1 + \varepsilon_{sRonc,1}) E_{\frac{1-\varepsilon_{sRonc,1}}{2}}\left(\left(\frac{\rho}{\rho_c}\right)^2\right) \right] \\ & - \frac{\alpha_{sRonc,2}}{\rho_{sRonc,1}} \int_0^\rho \left(\frac{t}{\rho_{sRonc,1}} \right) \exp\left(-\frac{\rho_{sRonc,2}}{t}\right) \left(1 - \exp\left(-\left(\frac{t}{\rho_c}\right)^2\right) \right) dt \end{aligned} \quad (36)$$

where $E_n(z) = \int_1^\infty \frac{e^{-zt}}{t^n} dt$ represents the exponential integral function and $\operatorname{erf}(x)$ represents the error function.

The coefficient and exponent values appearing in these equations are given in Table 4. The density dependence of the terms \tilde{u}_0 and \tilde{s}_0 are shown on Fig. 6.

It is important to remember that the two above primitives depend on an arbitrary constant α_{u_0} and α_{s_0} respectively. Moreover, we must be careful that the dimensionless form for internal energy is such that:

$$\tilde{u}_0(\rho) = \frac{T_c}{T} \left[\frac{3}{2} \hat{u}_0(\rho) + \alpha_{u_0} \right] \quad (37)$$

and for the entropy:

$$\tilde{s}_0^*(\rho) = \tilde{s}_0(\rho) + \ln(\rho) \quad (38)$$

From Eq. (20) and (22) and relations (34) to (38), the expression for the Helmholtz free energy can be easily deduced. In dimensionless form, this one writes:

$$\tilde{a}(\rho, T) = \frac{F}{R_A T} = \frac{U}{R_A T} - \frac{S}{R_A} = \tilde{u}(\rho, T) - \tilde{s}(\rho, T) = \tilde{a}^o(\rho, T) + \tilde{a}^r(\rho, T) \quad (39)$$

where $\tilde{a}^o(\rho, T)$ is given in Table 3 and

$$\tilde{a}^r(\rho, T) = \underbrace{\tilde{a}_{\text{reg}}^r(\rho, T) + \tilde{a}_{\text{nonreg}}^r(\rho, T) + \tilde{a}_{\text{crit}}^r(\rho, T)}_{\tilde{u}^* - \tilde{s}^*} + \tilde{a}_0^r(\rho, T) \quad (40)$$

with

$$\tilde{a}_0^r(\rho, T) = \tilde{u}_0(\rho, T) - [\tilde{s}_0^*(\rho) - \omega_0] - \zeta_0 \frac{T_c}{T} = \frac{T_c}{T} \left[\frac{3}{2} \hat{u}_0(\rho) + \alpha_{u_0} - \zeta_0 \right] - [\tilde{s}_0^*(\rho) + \alpha_{s_0} - \omega_0] \quad (41)$$

The two constants α_{u_0} and α_{s_0} can be chosen such that $\alpha_{u_0} = \zeta_0$ and $\alpha_{s_0} = \omega_0$. It follows that:

$$\tilde{a}_0^r(\rho, T) = \frac{3}{2} \frac{T_c}{T} \hat{u}_0(\rho) - \tilde{s}_0^*(\rho) \quad (42)$$

and

$$\tilde{u}^r(\rho, T) = \tilde{u}^*(\rho, T) + \frac{3}{2} \frac{T_c}{T} \hat{u}_0(\rho) \quad (43)$$

$$\tilde{s}^r(\rho, T) = \tilde{s}^*(\rho, T) + \tilde{s}_0^*(\rho) \quad (44)$$

We can remark that if we want to represent for higher densities than $\rho_{t,\text{Liq}}$ the data from NIST instead of the data of Ronchi, it is only necessary to change the mathematical form of eq. (31), (32) and (33). For example, we just indicate that the new function for $\hat{u}'_0(\rho)$ can be written with the same mathematical terms as in eq. (31) but without the two last terms and with different values of the parameters. So we can understand that the global shape of the new functions $\hat{u}'_0(\rho)$ and $\tilde{s}'_0(\rho)$ will have very similar variations. This remark shows also that the

two data sets discussed above for high densities can be represented by only small variations of the shape of the two derivative functions $\hat{u}'(\rho)$ and $\tilde{s}'(\rho)$. But once these two functions are determined all the thermodynamic equations of state are known.

Table 4. Coefficients and exponents for \hat{u}_0 and \tilde{s}_0 .

i	ε_i	α_i
u,0		16.86969325
u,1		71.08169282
u,2	2.57795090	12.16671437
u,3	2.01916041	22.41395798
u,4	12.94678106	0.13352634
u,5		16612.44198645
u,6	1.78738624	0.04855950
s,1	2.23951150	11.75732913
s,2	3.18259094	9.91697667
s,3	2.71140252	12.27973100
s,4	1.55994791	0.04075918
s,5	21.47158258	0.31499626
s,6		0.46391511
sRonc,1	62.32164244	57.01690712
sRonc,2		187.65045674

Table 5. Mathematical expressions of the dimensionless terms in the residual Helmholtz free energy for $T \geq T_{\text{div}}$.

$$\begin{aligned}
 \tilde{a}_{\text{reg}}^r &= \frac{3}{2} n_{\text{reg}} \frac{T_c}{T} \left\{ \frac{\left(\frac{T}{T_c}\right)^m - 1}{m} + \frac{\lambda^{-m}}{2-m} \Gamma\left(\frac{m}{2-m}, \left(\frac{\lambda T}{T_c}\right)^{2-m}\right) \right\} \\
 &\quad - \frac{3}{2} n_{\text{reg}} \left\{ \frac{\left(\frac{T}{T_c}\right)^{m-1} - 1}{m-1} + \frac{\lambda^{1-m}}{2-m} \Gamma\left(\frac{m-1}{2-m}, \left(\frac{\lambda T}{T_c}\right)^{2-m}\right) \right\} \\
 \tilde{a}_{\text{nonreg}}^r &= n_{\text{nonreg}} \sum_{k=0}^{\infty} \left\{ \Gamma\left(-\frac{2}{3}k, \left(\frac{T_{\text{div}}}{T}\right)^{-3/2}\right) - \frac{T_{\text{div}}}{T} \Gamma\left(-\frac{2}{3}(k-1), \left(\frac{T_{\text{div}}}{T}\right)^{-3/2}\right) \right\} \\
 \tilde{a}_{\text{crit}}^r &= \frac{3}{2} n_{\text{crit}} \frac{(T_{\text{div}}/T)^{\varepsilon_{\text{crit}}}}{(1-\varepsilon_{\text{crit}})\varepsilon_{\text{crit}}} \\
 \tilde{a}_0^r &= \frac{3}{2} \frac{T_c}{T} \hat{u}_0(\rho) - \{\tilde{s}_0(\rho) + \ln(\rho)\}
 \end{aligned}$$

3.2. Analytic expression of the ‘thermal equation of state’ for $T \geq T_{\text{div}}$

The thermal state equation $P = P(\rho, T)$ which is a fundamental equation to calculate the basic thermal properties of argon, can easily be established using Eq. (30) and Eq. (39) for free energy. The free energy is made up of four terms coming from the residual Helmholtz free energy and a term that represents the behaviour of the ideal gas:

$$P(\rho, T) = P_{\text{reg}}(\rho, T) + P_{\text{nonreg}}(\rho, T) + P_{\text{crit}}(\rho, T) + P_0(\rho, T) + \rho R_A T \quad (45)$$

or in dimensionless form

$$Z = \frac{P}{\rho R_A T} = \underbrace{\frac{P_{\text{reg}}(\rho, T)}{\rho R_A T}}_{Z_{\text{reg}}} + \underbrace{\frac{P_{\text{nonreg}}(\rho, T)}{\rho R_A T}}_{Z_{\text{nonreg}}} + \underbrace{\frac{P_{\text{crit}}(\rho, T)}{\rho R_A T}}_{Z_{\text{crit}}} + \underbrace{\frac{P_0(\rho, T)}{\rho R_A T}}_{Z_0} + 1 \quad (46)$$

with

$$Z_{\text{reg}} = \rho \left(\frac{\partial \tilde{a}_{\text{reg}}^r}{\partial \rho} \right)_T$$

$$Z_{\text{nonreg}} = \rho \left(\frac{\partial \tilde{a}_{\text{nonreg}}^r}{\partial \rho} \right)_T = -\rho n'_{\text{nonreg}}(\rho) \sum_{k=0}^{\infty} \left[x \Gamma \left(-\frac{2}{3}(k-1), x^{-3/2} \right) - \Gamma \left(-\frac{2}{3}k, x^{-3/2} \right) \right]$$

$$- n_{\text{nonreg}}(\rho) \frac{\rho T'_{\text{div}}(\rho)}{T} \sum_{k=0}^{\infty} \Gamma \left(-\frac{2}{3}(k-1), x^{-3/2} \right) \quad (47)$$

$$Z_0 = \rho \left(\frac{\partial \tilde{a}_0^r}{\partial \rho} \right)_T + 1 = \rho \left[\frac{3}{2} \frac{T_c}{T} \hat{u}'_0(\rho) - \tilde{s}'_0(\rho) \right] \quad (48)$$

$$Z_{\text{crit}} = \rho \left(\frac{\partial \tilde{a}_{\text{crit}}^r}{\partial \rho} \right)_T = \frac{3}{2} \rho n'_{\text{crit}}(\rho) \frac{(T_{\text{div}}(\rho)/T)^{\varepsilon_{\text{crit}}(\rho)}}{\varepsilon_{\text{crit}}(\rho)(1 - \varepsilon_{\text{crit}}(\rho))}$$

$$+ \frac{3}{2} \rho n_{\text{crit}}(\rho) \left\{ \frac{2\varepsilon_{\text{crit}}(\rho) - 1}{\varepsilon_{\text{crit}}(\rho)^2 (\varepsilon_{\text{crit}}(\rho) - 1)^2} \varepsilon'_{\text{crit}}(\rho) \left(\frac{T_{\text{div}}(\rho)}{T} \right)^{\varepsilon_{\text{crit}}(\rho)} \right.$$

$$\left. - \frac{(T_{\text{div}}(\rho)/T)^{\varepsilon_{\text{crit}}(\rho)}}{\varepsilon_{\text{crit}}(\rho)(\varepsilon_{\text{crit}}(\rho) - 1)} \left[\varepsilon'_{\text{crit}}(\rho) \ln \left(\frac{T_{\text{div}}(\rho)}{T} \right) + \varepsilon_{\text{crit}}(\rho) \frac{T'_{\text{div}}(\rho)}{T_{\text{div}}(\rho)} \right] \right\} \quad (49)$$

We recall that $x = T_{\text{div}}/T$ in the expression of Z_{nonreg} . $Z_{\text{reg}}(\rho, T)$ displaying too many terms, its expression is given in Appendix 1. The expressions of the first derivatives of coefficients (6) to (12) are listed in Appendix 2. From the expression of these factors, it is easy to see that $Z_{\text{reg}} = Z_{\text{nonreg}} = Z_{\text{crit}} = 0$ and $Z_0 = 1$ for $\rho \rightarrow 0$ and, therefore, $Z \rightarrow 1$ for any temperature when density tends to zero. In a certain range of temperature, isotherms intersect the line $Z = 1$ for ρ values that are not identically zero. As thermodynamic quantities

corresponding to $Z = 1$ are physically important and not easy to find in the literature, they are listed in Table 6.

3.3. The liquid-vapour coexistence curve

At a given temperature T , vapour pressure and densities of the coexisting phases can be determined by simultaneous resolution of the equations:

$$\frac{P_{\text{sat}}}{\rho_{\text{ol}} R_A T} = 1 + \rho_{\text{ol}} \left(\frac{\partial \tilde{a}_{\text{ol}}^r}{\partial \rho_{\text{ol}}} \right)_T = Z(\rho_{\text{ol}}, T) \quad (50)$$

$$\frac{P_{\text{sat}}}{\rho_{\text{ov}} R_A T} = 1 + \rho_{\text{ov}} \left(\frac{\partial \tilde{a}_{\text{ov}}^r}{\partial \rho_{\text{ov}}} \right)_T = Z(\rho_{\text{ov}}, T) \quad (51)$$

$$\frac{P_{\text{sat}}}{R_A T} \left(\frac{1}{\rho_{\text{ov}}} - \frac{1}{\rho_{\text{ol}}} \right) - \ln \left(\frac{\rho_{\text{ol}}}{\rho_{\text{ov}}} \right) = \tilde{a}^r(\rho_{\text{ol}}, T) - \tilde{a}^r(\rho_{\text{ov}}, T) \quad (52)$$

These equations represent the phase equilibrium conditions, i.e., the equality of pressure, temperature and specific Gibbs energy (Maxwell criterion) in the coexisting phases. The calculated values on the liquid-vapour coexistence curve (vapour pressure, saturated liquid density, saturated vapour density, etc.) are given in Table 12.

Table 6. Thermodynamic properties corresponding to $Z = 1$ (i.e. ideal curve) deduced from Eq. (46).

T/T_c	P/P_c	ρ/ρ_c	C_V/R_A	C_P/R_A	$c/\sqrt{R_A T}$
0.56408	5.3565	2.7491	2.7545	5.1425	7.1030
0.62500	5.7641	2.6699	2.6239	5.0445	6.5008
0.69444	6.1935	2.5819	2.4987	4.9633	5.9013
0.76389	6.5850	2.4956	2.3942	4.9091	5.3765
0.83333	6.9372	2.4100	2.3054	4.8869	4.9093
0.90278	7.2480	2.3242	2.2290	4.8871	4.4926
0.97222	7.5154	2.2379	2.1626	4.8993	4.1212
1.0417	7.7380	2.1505	2.1044	4.9136	3.7909
1.1111	7.9149	2.0622	2.0532	4.9213	3.4978
1.1806	8.0462	1.9731	2.0078	4.9165	3.2384
1.2500	8.1324	1.8835	1.9673	4.8967	3.0090
1.3194	8.1744	1.7935	1.9309	4.8621	2.8062
1.3889	8.1729	1.7036	1.8979	4.8148	2.6267
1.4583	8.1284	1.6136	1.8676	4.7565	2.4674
1.5278	8.0406	1.5236	1.8395	4.6881	2.3258
1.5972	7.9091	1.4335	1.8133	4.6093	2.1994
1.6667	7.7330	1.3432	1.7887	4.5188	2.0865
1.7361	7.5118	1.2526	1.7653	4.4151	1.9854
1.8056	7.2453	1.1617	1.7429	4.2976	1.8947
1.8750	6.9343	1.0707	1.7214	4.1672	1.8133
1.9444	6.5801	0.97968	1.7005	4.0261	1.7402
2.0139	6.1845	0.88903	1.6803	3.8775	1.6743
2.0833	5.7492	0.79890	1.6605	3.7247	1.6150
2.1528	5.2754	0.70942	1.6412	3.5712	1.5617
2.2222	4.7635	0.62056	1.6223	3.4196	1.5137
2.2917	4.2127	0.53218	1.6038	3.2719	1.4707
2.3611	3.6210	0.44397	1.5857	3.1294	1.4322
2.4306	2.9847	0.35551	1.5682	2.9927	1.3977
2.5000	2.2996	0.26630	1.5511	2.8616	1.3667
2.5500	1.7737	0.20137	1.5389	2.7700	1.3462
2.6000	1.2211	0.13596	1.5266	2.6803	1.3270
2.6500	0.66245	0.072369	1.5144	2.5944	1.3095
2.6900	0.29167	0.031390	1.5061	2.5396	1.2987
2.7100	0.14787	0.015796	1.5029	2.5193	1.2947
2.7125	0.11575	0.012354	1.5022	2.5149	1.2939

3.4. Thermodynamic state inside the liquid-vapour coexistence curve for $T < T_{\text{div}}(\rho)$

The thermodynamic properties of argon have been calculated from the isochoric heat capacity equation $C_V(\rho, T)$. However, the equation being only valid for $T \geq T_{\text{div}}$, a new equation, valid for $T < T_{\text{div}}$ (i.e. inside the coexistence liquid-vapour region), has to be established. This requires solving three mathematical problems.

- First, an expression of $C_V(\rho, T)$ for $T < T_{\text{div}}(\rho)$ has to be found.
- Secondly, to integrate C_V it is required to remove the artificial divergence introduced with the term $\tilde{c}_{V, \text{nonreg}}^r$ in order to have a finite value of C_V for $T = T_{\text{div}}(\rho)$.
- Finally, also for the integration of C_V , a reference state must be chosen.

The procedure used to develop the modified equation is now presented. It will be shown that this new formulation leads to a better description of the two-phase thermodynamic properties than the polynomial approach.

3.4.1. Expression for C_V inside the divergence curve

The two terms in $C_V(\rho, T)$ creating difficulties are: $\tilde{c}_{V, \text{nonreg}}^r$ and $\tilde{c}_{V, \text{crit}}^r$. For $T < T_{\text{div}}$, $\tilde{c}_{V, \text{nonreg}}^r$ becomes negative which has no physical meaning; indeed, the thermodynamic thermal stability has always to be satisfied. And the term $\tilde{c}_{V, \text{crit}}^r$, for $T < T_{\text{div}}$, diverges when $T \rightarrow 0$, which has also no physical meaning. The easiest way to solve these problems is to take a symmetric function by changing the variable T_{div}/T into T/T_{div} , hence we obtain:

$$\tilde{c}_{V, \text{nonreg}}^r(\rho, T < T_{\text{div}}) = \frac{3}{2} n_{\text{nonreg}}(\rho) \times \exp \left[- \left(\frac{T}{T_{\text{div}}(\rho)} \right)^{-3/2} \right] \times \frac{1}{1 - \frac{T}{T_{\text{div}}(\rho)}} \quad (53)$$

$$\tilde{c}_{V, \text{crit}}^r(\rho, T < T_{\text{div}}) = \frac{3}{2} n_{\text{crit}}(\rho) \times \left(\frac{T}{T_{\text{div}}(\rho)} \right)^{\varepsilon_{\text{crit}}(\rho)} \quad (54)$$

However a problem remains as the two equations ($\tilde{c}_{V, \text{nonreg}}^r$ and $\tilde{c}_{V, \text{nonreg}}^r$) become infinite for $T = T_{\text{div}}$. In fact, this is the consequence of the extensive nature of C_V . Therefore, this divergence can be removed by introducing explicitly into the equations for C_V a finite number N_V of particles. N_V have to be the largest possible without to be infinity (which is the condition for an extensive property). Then, as these equations must converge for $T = T_{\text{div}}$, the terms $\frac{1}{1 - \frac{T}{T_{\text{div}}}}$ and $\frac{1}{1 - \frac{T_{\text{div}}}{T}}$ have to be corrected so that the two equations must tend to the same finite value for $T = T_{\text{div}}$. The following functions have the required properties:

- $\frac{1}{1 - \frac{T}{T_{\text{div}}}}$ is replaced by $\frac{1 - N_V \left(1 - \frac{T}{T_{\text{div}}}\right)}{1 - \frac{T}{T_{\text{div}}}}$, so $\tilde{c}_{V, \text{nonreg}}^r$ becomes now

$$\tilde{c}_{V,\text{outside}}^r = \frac{3}{2} n_{\text{nonreg}}(\rho) \times \exp\left[-\left(\frac{T_{\text{div}}(\rho)}{T}\right)^{-3/2}\right] \times \frac{1 - N_V^{-\left(1 - \frac{T}{T_{\text{div}}}\right)}}{1 - \frac{T}{T_{\text{div}}}} \quad (55)$$

- and $\frac{1}{1 - \frac{T}{T_{\text{div}}}}$ is replaced by $\frac{1 - N_V^{-\left(1 - \frac{T_{\text{div}}}{T}\right)}}{1 - \frac{T_{\text{div}}}{T}}$, so $\tilde{c}_{V,\text{inside}}^r$ becomes now

$$\tilde{c}_{V,\text{inside}}^r = \frac{3}{2} n_{\text{nonreg}}(\rho) \times \exp\left[-\left(\frac{T}{T_{\text{div}}(\rho)}\right)^{-3/2}\right] \times \frac{1 - N_V^{-\left(1 - \frac{T_{\text{div}}}{T}\right)}}{1 - \frac{T_{\text{div}}}{T}} \quad (56)$$

The two corrections tends to $\ln(N_V)$ when $T \rightarrow T_{\text{div}}$. N_V may be thought as a quantity representing the number of particles in the volume V for a given experiment, so we can write:

$$N_V = \text{fmol} \times \mathcal{N}_a \frac{\rho}{\rho_c} \quad (57)$$

where $\text{fmol} = 10^{20}$ is an arbitrary constant required to remove the divergence. This means that near the transition, C_V and its related quantities are no longer extensive quantities. This is not surprising since sample size effects are known to exist around the phase transition. Thus, the divergence occurs only for an infinite number of particles.

Outside the coexistence liquid-vapour region, the percentage deviation between $\tilde{c}_{V,\text{nonreg}}^r$ calculated by Eq. (18) and $\tilde{c}_{V,\text{nonreg}}^r$ calculated by Eq. (55) is shown on Fig. 7. We observe that the difference is only significant in the close vicinity of the critical point.

Figure 8 shows the behaviour of C_V on two isotherms that are crossing the coexistence phase: one can observe that, on both isotherms, the new model gives always positive values of C_V with maximum values as experimentally observed. It can be noticed that the model of Tegeler *et al.* leads to erroneous C_V variations in this coexistence region.

3.4.2. Choice of a reference state

The functions U , S and F are obtained by successive integrations of C_V along isochors; this means a reference temperature is necessary. From Eq. (55) and Eq. (56), it is evident that the only state which is identical for all isochors is for T infinite.

Due to the fact that, first, the development such as Eq. (18) for $\tilde{c}_{V,\text{nonreg}}^r$ becomes more complex with a much slower convergence of the series and, secondly, there are two expressions for this term inside the coexistence liquid-vapour region, it is preferable and easier to integrate numerically these terms. Thus the respective expressions for $\tilde{u}_{\text{nonreg}}^r$ and $\tilde{s}_{\text{nonreg}}^r$ are now:

$$\tilde{u}_{\text{nonreg}}^r(\rho, T) = T^{-1} \int_{\infty}^T \tilde{c}_{V,\text{nonreg}}^r(\rho, t) dt \quad (58)$$

$$\tilde{s}_{\text{nonreg}}^r(\rho, T) = \int_{\infty}^T \tilde{c}_{V, \text{nonreg}}^r(\rho, t) t^{-1} dt \quad (59)$$

$$\text{with } \tilde{c}_{V, \text{nonreg}}^r(\rho, T) = \begin{cases} \tilde{c}_{V, \text{nonreg}}^r \text{ outside}(\rho, T) & \text{if } T \geq T_{\text{div}} \\ \tilde{c}_{V, \text{nonreg}}^r \text{ inside}(\rho, T) & \text{otherwise} \end{cases}$$

To complete the description we also give the expression of the non-regular compressibility factor:

$$Z_{\text{nonreg}} = \rho \left(\frac{\partial \tilde{a}_{\text{nonreg}}^r}{\partial \rho} \right)_T = \frac{\rho}{T} \int_{\infty}^T \left(1 - \frac{T}{t} \right) \frac{\partial}{\partial \rho} \tilde{c}_{V, \text{nonreg}}^r(\rho, t) dt \quad (60)$$

To calculate the partial derivative of $\tilde{c}_{V, \text{nonreg}}^r$, N_V must be considered constant because the experiments that we imagine here to measure the pressure are performed on a closed system. Thus, the expressions of the partial derivative of $\tilde{c}_{V, \text{nonreg}}^r$ are:

$$\begin{aligned} \frac{\partial}{\partial \rho} \tilde{c}_{V, \text{nonreg}}^r \text{ outside}(\rho, T) &= \frac{3}{2} \frac{\exp\left(-\left(\frac{T_{\text{div}}(\rho)}{T}\right)^{-3/2}\right)}{1 - \frac{T_{\text{div}}(\rho)}{T}} \left\{ n'_{\text{nonreg}}(\rho) \left(1 - N_V^{-1 + \frac{T_{\text{div}}(\rho)}{T}} \right) \right. \\ &\quad \left. + n_{\text{nonreg}}(\rho) \frac{T_{\text{div}}(\rho)}{T} \left[\frac{1 - N_V^{-1 + \frac{T_{\text{div}}(\rho)}{T}}}{1 - \frac{T_{\text{div}}(\rho)}{T}} - N_V^{-1 + \frac{T_{\text{div}}(\rho)}{T}} \ln(N_V) + \frac{3}{2} \left(\frac{T_{\text{div}}(\rho)}{T} \right)^{-5/2} \left(1 - N_V^{-1 + \frac{T_{\text{div}}(\rho)}{T}} \right) \right] \right\} \end{aligned} \quad (61)$$

$$\begin{aligned} \frac{\partial}{\partial \rho} \tilde{c}_{V, \text{nonreg}}^r \text{ inside}(\rho, T) &= \frac{3}{2} \frac{\exp\left(-\left(\frac{T}{T_{\text{div}}(\rho)}\right)^{-3/2}\right)}{1 - \frac{T}{T_{\text{div}}(\rho)}} \left\{ n'_{\text{nonreg}}(\rho) \left(1 - N_V^{-1 + \frac{T}{T_{\text{div}}(\rho)}} \right) \right. \\ &\quad \left. - n_{\text{nonreg}}(\rho) \left(\frac{T}{T_{\text{div}}(\rho)} \right)^2 \frac{T'_{\text{div}}(\rho)}{T} \left[\frac{1 - N_V^{-1 + \frac{T}{T_{\text{div}}(\rho)}}}{1 - \frac{T}{T_{\text{div}}(\rho)}} - N_V^{-1 + \frac{T}{T_{\text{div}}(\rho)}} \ln(N_V) + \frac{3}{2} \left(\frac{T}{T_{\text{div}}(\rho)} \right)^{-5/2} \left(1 - N_V^{-1 + \frac{T}{T_{\text{div}}(\rho)}} \right) \right] \right\} \end{aligned} \quad (62)$$

In the same manner as previously, we can deduce primitives for U and S corresponding to the term $\tilde{c}_{V, \text{crit}}^r$ inside:

$$\tilde{u}_{\text{crit}}^r \text{ inside} = \frac{3}{2} n_{\text{crit}}(\rho) \left[\frac{(T/T_{\text{div}}(\rho))^{\varepsilon_{\text{crit}}(\rho)}}{1 + \varepsilon_{\text{crit}}(\rho)} + \frac{2\varepsilon_{\text{crit}}(\rho)}{1 - \varepsilon_{\text{crit}}(\rho)^2} \right] \quad (63)$$

$$\tilde{s}_{\text{crit}}^r \text{ inside} = \frac{3}{2} n_{\text{crit}}(\rho) \varepsilon_{\text{crit}}(\rho)^{-1} \left[\left(\frac{T}{T_{\text{div}}(\rho)} \right)^{\varepsilon_{\text{crit}}(\rho)} - 2 \right] \quad (64)$$

Then we deduce that:

$$\tilde{a}_{\text{inside}}^{\text{crit}}(\rho, T) = \frac{3}{2} n_{\text{crit}}(\rho) \left[\frac{(T/T_{\text{div}}(\rho))^{\varepsilon_{\text{crit}}(\rho)}}{\varepsilon_{\text{crit}}(\rho)(1 + \varepsilon_{\text{crit}}(\rho))} + \frac{2}{1 - \varepsilon_{\text{crit}}(\rho)^2} \right] \quad (65)$$

and

$$\begin{aligned} \frac{P_{\text{inside}}^{\text{crit}}(\rho, T)}{\rho R_A T} = & \frac{3}{2} \rho n'_{\text{crit}}(\rho) \left[\frac{(T/T_{\text{div}}(\rho))^{\varepsilon_{\text{crit}}(\rho)}}{\varepsilon_{\text{crit}}(\rho)(1 + \varepsilon_{\text{crit}}(\rho))} + \frac{2}{1 - \varepsilon_{\text{crit}}(\rho)^2} \right] \\ & + \frac{3}{2} \rho n_{\text{crit}}(\rho) \left\{ -\frac{1 + 2\varepsilon_{\text{crit}}(\rho)}{\varepsilon_{\text{crit}}(\rho)^2 (1 + \varepsilon_{\text{crit}}(\rho))^2} \varepsilon'_{\text{crit}}(\rho) \left(\frac{T}{T_{\text{div}}(\rho)} \right)^{\varepsilon_{\text{crit}}(\rho)} + \frac{4\varepsilon_{\text{crit}}(\rho)\varepsilon'_{\text{crit}}(\rho)}{(1 - \varepsilon_{\text{crit}}(\rho)^2)^2} \right. \\ & \left. + \frac{(T/T_{\text{div}}(\rho))^{\varepsilon_{\text{crit}}(\rho)}}{\varepsilon_{\text{crit}}(\rho)(1 + \varepsilon_{\text{crit}}(\rho))} \left[\varepsilon'_{\text{crit}}(\rho) \ln \left(\frac{T}{T_{\text{div}}(\rho)} \right) - \varepsilon_{\text{crit}}(\rho) \frac{T'_{\text{div}}(\rho)}{T_{\text{div}}(\rho)} \right] \right\} \quad (66) \end{aligned}$$

We emphasize here that the choice of these expressions to describe the coexistence region has no effect on the properties of the pure fluid up to the saturation curve.

The model with these new expressions of regular and non-critical terms is referred to as ‘**non-extensive model**’. The non-extensive residual part of the Helmholtz energy $\tilde{a}^{\text{r}}(\rho, T)$ and its partial derivatives with temperature are given in Table 7. The first partial derivative with density can be easily deduced from the expression of the compressibility factor Z . The second partial derivatives $\left. \frac{\partial^2 \tilde{a}^{\text{r}}}{\partial \rho \partial T} \right|_T$ and $\left. \frac{\partial^2 \tilde{a}^{\text{r}}}{\partial \rho^2} \right|_T$ can easily be deduced from the first derivatives of the compressibility factor which are given in Table 8 and Table 9.

Table 26 in Tegeler *et al.* paper summarizes how to calculate the thermodynamics properties from the empirical description of the Helmholtz free energy and its derivatives. In the present approach, the same thermodynamics properties are deduced from the isochoric heat capacity equation and the thermal equation of state, which are now two experimentally measured quantities.

The new equations of state corresponding to the non-extensive model can be *freely downloaded* as a Wolfram Mathematica application on the following web page:
<http://mathematica.g2elab.grenoble-inp.fr/neweosargon.html>

Table 7. Mathematical expressions of the dimensionless terms for the non-extensive residual Helmholtz function and its partial derivatives with temperature.

$$\begin{aligned} \tilde{a}_{\text{reg}}^r &= \frac{3}{2} n_{\text{reg}} \frac{T_c}{T} \left\{ \frac{1}{m} \left[\left(\frac{T}{T_c} \right)^m - 1 \right] + \frac{\lambda^{-m}}{2-m} \Gamma \left(\frac{m}{2-m}, \left(\frac{\lambda T}{T_c} \right)^{2-m} \right) \right\} \\ &\quad - \frac{3}{2} n_{\text{reg}} \left\{ \frac{1}{m-1} \left[\left(\frac{T}{T_c} \right)^{m-1} - 1 \right] + \frac{\lambda^{1-m}}{2-m} \Gamma \left(\frac{m-1}{2-m}, \left(\frac{\lambda T}{T_c} \right)^{2-m} \right) \right\} \\ T_c \left(\frac{\partial \tilde{a}_{\text{reg}}^r}{\partial T} \right)_\rho &= \frac{3}{2} n_{\text{reg}} \left(\frac{T_c}{T} \right)^2 m^{-1} \left\{ 1 - \left(\frac{T}{T_c} \right)^m + \frac{\lambda^{-m} m}{m-2} \Gamma \left(\frac{m}{2-m}, \left(\frac{\lambda T}{T_c} \right)^{2-m} \right) \right\} \\ T_c^2 \left(\frac{\partial^2 \tilde{a}_{\text{reg}}^r}{\partial T^2} \right)_\rho &= \frac{3}{2} n_{\text{reg}} \left(\frac{T_c}{T} \right)^3 \left\{ \left(\frac{T}{T_c} \right)^m \left(\frac{2-m}{m} + \exp \left(- \left(\frac{\lambda T}{T_c} \right)^{2-m} \right) \right) - \frac{2}{m} + \frac{2\lambda^{-m}}{m-2} \Gamma \left(\frac{m}{2-m}, \left(\frac{\lambda T}{T_c} \right)^{2-m} \right) \right\} \\ \tilde{a}_{\text{nonreg}}^r &= \int_\infty^T \tilde{c}_{V,\text{nonreg}}^r \left(1 - \frac{T}{t} \right) \frac{dt}{T} \\ T_c \left(\frac{\partial \tilde{a}_{\text{nonreg}}^r}{\partial T} \right)_\rho &= -\frac{T_c}{T^2} \int_\infty^T \tilde{c}_{V,\text{nonreg}}^r dt, \quad T_c^2 \left(\frac{\partial^2 \tilde{a}_{\text{nonreg}}^r}{\partial T^2} \right)_\rho = -\left(\frac{T_c}{T} \right)^2 \tilde{c}_{V,\text{nonreg}}^r + 2 \frac{T_c^2}{T^3} \int_\infty^T \tilde{c}_{V,\text{nonreg}}^r dt \\ \tilde{a}_{\text{crit}}^r &= \frac{3}{2} n_{\text{crit}} \begin{cases} \frac{(T_{\text{div}}/T)^{\varepsilon_{\text{crit}}}}{(1-\varepsilon_{\text{crit}})\varepsilon_{\text{crit}}} & \text{if } T \geq T_{\text{div}} \\ \frac{(T/T_{\text{div}})^{\varepsilon_{\text{crit}}}}{(1+\varepsilon_{\text{crit}})\varepsilon_{\text{crit}}} + \frac{2}{1-\varepsilon_{\text{crit}}^2} & \text{otherwise} \end{cases} \\ T_c \left(\frac{\partial \tilde{a}_{\text{crit}}^r}{\partial T} \right)_\rho &= \frac{3}{2} n_{\text{crit}} \frac{T_c}{T} \begin{cases} \frac{1}{\varepsilon_{\text{crit}} - 1} \left(\frac{T_{\text{div}}}{T} \right)^{\varepsilon_{\text{crit}}} & \text{if } T \geq T_{\text{div}} \\ \frac{1}{1 + \varepsilon_{\text{crit}}} \left(\frac{T}{T_{\text{div}}} \right)^{\varepsilon_{\text{crit}}} & \text{otherwise} \end{cases} \\ T_c^2 \left(\frac{\partial^2 \tilde{a}_{\text{crit}}^r}{\partial T^2} \right)_\rho &= \frac{3}{2} n_{\text{crit}} \left(\frac{T_c}{T} \right)^2 \begin{cases} \frac{1 + \varepsilon_{\text{crit}}}{\varepsilon_{\text{crit}} - 1} \left(\frac{T_{\text{div}}}{T} \right)^{\varepsilon_{\text{crit}}} & \text{if } T \geq T_{\text{div}} \\ \frac{\varepsilon_{\text{crit}} - 1}{1 + \varepsilon_{\text{crit}}} \left(\frac{T}{T_{\text{div}}} \right)^{\varepsilon_{\text{crit}}} & \text{otherwise} \end{cases} \\ \tilde{a}_0^r &= \frac{3}{2} \frac{T_c}{T} \hat{u}_0(\rho) - \{ \tilde{s}_0(\rho) + \ln(\rho) \} \\ T_c \left(\frac{\partial \tilde{a}_0^r}{\partial T} \right)_\rho &= -\frac{3}{2} \left(\frac{T_c}{T} \right)^2 \hat{u}_0(\rho) \\ T_c^2 \left(\frac{\partial^2 \tilde{a}_0^r}{\partial T^2} \right)_\rho &= 3 \left(\frac{T_c}{T} \right)^3 \hat{u}_0(\rho) \end{aligned}$$

Table 8. Mathematical expressions of the first partial derivatives with temperature of Z . All these derivatives are in K^{-1} .

$$\left(\frac{\partial Z_{\text{reg}}}{\partial T}\right)_{\rho} \text{ is given in Appendix 1}$$

$$\left(\frac{\partial Z_{\text{nonreg}}}{\partial T}\right)_{\rho} = -\frac{\rho}{T^2} \int_{\infty}^T \frac{\partial \tilde{c}_{V,\text{nonreg}}^r}{\partial \rho} \Big|_T dt$$

$$\left(\frac{\partial Z_{\text{crit}}}{\partial T}\right)_{\rho} = \frac{3}{2} \frac{\rho}{T} n'_{\text{crit}} \begin{cases} \frac{1}{\varepsilon_{\text{crit}} - 1} \left(\frac{T_{\text{div}}}{T}\right)^{\varepsilon_{\text{crit}}} & \text{if } T \geq T_{\text{div}} \\ \frac{1}{1 + \varepsilon_{\text{crit}}} \left(\frac{T}{T_{\text{div}}}\right)^{\varepsilon_{\text{crit}}} & \text{otherwise} \end{cases}$$

$$+ \frac{3}{2} \rho n_{\text{crit}} \begin{cases} \frac{(T_{\text{div}}/T)^{\varepsilon_{\text{crit}}-1}}{T^2 (\varepsilon_{\text{crit}} - 1)^2} \left\{ \varepsilon_{\text{crit}} (\varepsilon_{\text{crit}} - 1) T'_{\text{div}} + T_{\text{div}} \varepsilon'_{\text{crit}} \left((\varepsilon_{\text{crit}} - 1) \ln \left(\frac{T_{\text{div}}}{T} \right) \right) - 1 \right\} & \text{if } T \geq T_{\text{div}} \\ \frac{(T/T_{\text{div}})^{\varepsilon_{\text{crit}}-1}}{T_{\text{div}}^2 (1 + \varepsilon_{\text{crit}})^2} \left\{ \varepsilon_{\text{crit}} (1 + \varepsilon_{\text{crit}}) T'_{\text{div}} - T_{\text{div}} \varepsilon'_{\text{crit}} \left((1 + \varepsilon_{\text{crit}}) \ln \left(\frac{T}{T_{\text{div}}} \right) \right) - 1 \right\} & \text{otherwise} \end{cases}$$

$$\left(\frac{\partial Z_0}{\partial T}\right)_{\rho} = -\frac{3}{2} \frac{\rho}{T} \frac{T_c}{T} \hat{u}'_0(\rho)$$

Table 9. Mathematical expressions of the first partial derivatives with density of Z for $T \geq T_{\text{div}}$. All these derivatives are in cm^3/g .

$\left(\frac{\partial Z_{\text{reg}}}{\partial \rho}\right)_T$ is given in Appendix 1

$$\left(\frac{\partial Z_{\text{nonreg}}}{\partial \rho}\right)_T = \frac{1}{T} \int_{\infty}^T \left(1 - \frac{T}{t}\right) \frac{\partial \tilde{c}_{V,\text{nonreg}}^r}{\partial \rho} \Big|_T dt + \frac{\rho}{T} \int_{\infty}^T \left(1 - \frac{T}{t}\right) \frac{\partial^2 \tilde{c}_{V,\text{nonreg}}^r}{\partial \rho^2} \Big|_T dt$$

with

$$\frac{\partial^2 \tilde{c}_{V,\text{nonreg}}^r}{\partial \rho^2} \Big|_T = -\frac{3}{2} \frac{T'_{\text{div}}}{(T - T_{\text{div}})} \left[n'_{\text{nonreg}} + \frac{T'_{\text{div}}}{(T - T_{\text{div}})} n_{\text{nonreg}} + \frac{1}{2} \frac{T''_{\text{div}}}{T'_{\text{div}}} n_{\text{nonreg}} \right] \exp\left(-\left(\frac{T}{T_{\text{div}}}\right)^{3/2}\right) \times \left\{ 3 \left(\frac{T}{T_{\text{div}}}\right)^{5/2} \left(-1 + N_V^{-1 + \frac{T_{\text{div}}}{T}}\right) + 2 N_V^{-1 + \frac{T_{\text{div}}}{T}} \ln(N_V) \right\}$$

$$- \frac{3}{8} \frac{n_{\text{nonreg}} T_{\text{div}}'^2}{T_{\text{div}} (T - T_{\text{div}})} \exp\left(-\left(\frac{T}{T_{\text{div}}}\right)^{3/2}\right) \left(\frac{T}{T_{\text{div}}}\right)^{5/2} \left\{ 3 \left(\frac{T}{T_{\text{div}}}\right)^{3/2} - 5 \right\} \left(-1 + N_V^{-1 + \frac{T_{\text{div}}}{T}}\right) + 4 N_V^{-1 + \frac{T_{\text{div}}}{T}} \ln(N_V) \frac{T_{\text{div}}}{T} \left(3 + \ln(N_V) \left(\frac{T_{\text{div}}}{T}\right)^{5/2} \right) \right\}$$

$$- \frac{3}{2} \frac{T}{(T - T_{\text{div}})^3} \exp\left(-\left(\frac{T}{T_{\text{div}}}\right)^{3/2}\right) \left(-1 + N_V^{-1 + \frac{T_{\text{div}}}{T}}\right) \left\{ 2(T - T_{\text{div}}) T'_{\text{div}} n'_{\text{nonreg}} + (T - T_{\text{div}})^2 n''_{\text{nonreg}} + (2T_{\text{div}}'^2 + (T - T_{\text{div}}) T_{\text{div}}'') n_{\text{nonreg}} \right\}$$

$$\left(\frac{\partial Z_{\text{crit}}}{\partial \rho}\right)_T = \frac{3}{2} (n'_{\text{crit}} + \rho n''_{\text{crit}}) \frac{(T_{\text{div}}/T)^{\varepsilon_{\text{crit}}}}{(1 - \varepsilon_{\text{crit}}) \varepsilon_{\text{crit}}} + \frac{3}{2} (n_{\text{crit}} + 2\rho n'_{\text{crit}}) \frac{(T_{\text{div}}/T)^{\varepsilon_{\text{crit}}}}{(\varepsilon_{\text{crit}} - 1)} \left\{ \frac{2\varepsilon_{\text{crit}} - 1}{(\varepsilon_{\text{crit}} - 1) \varepsilon_{\text{crit}}} \frac{\varepsilon'_{\text{crit}}}{\varepsilon_{\text{crit}}} - \frac{T'_{\text{div}}}{T_{\text{div}}} - \ln\left(\frac{T_{\text{div}}}{T}\right) \frac{\varepsilon'_{\text{crit}}}{\varepsilon_{\text{crit}}} \right\} - \frac{3}{2} \rho n_{\text{crit}} \frac{(T_{\text{div}}/T)^{\varepsilon_{\text{crit}}}}{(\varepsilon_{\text{crit}} - 1)^2} \left\{ (\varepsilon_{\text{crit}} - 1)^2 \left(\frac{T'_{\text{div}}}{T_{\text{div}}}\right)^2 + \frac{2\varepsilon_{\text{crit}}'^2}{(\varepsilon_{\text{crit}} - 1) \varepsilon_{\text{crit}}^3} + \frac{T'_{\text{div}}}{T_{\text{div}}} \left[(\varepsilon_{\text{crit}} - 1) \frac{T_{\text{div}}''}{T_{\text{div}}'} + 2\varepsilon'_{\text{crit}} \left(-1 + \ln\left(\left(\frac{T_{\text{div}}}{T}\right)^{\varepsilon_{\text{crit}} - 1}\right)\right) \right] \right\} + \frac{1}{\varepsilon_{\text{crit}}^2} \left[\varepsilon_{\text{crit}}'' \left(1 - \varepsilon_{\text{crit}} \left(2 + \ln\left(\frac{T_{\text{div}}}{T}\right)\right)\right) + \varepsilon_{\text{crit}}^2 \ln\left(\frac{T_{\text{div}}}{T}\right) + 6\varepsilon_{\text{crit}}'^2 + \varepsilon_{\text{crit}}'^2 \ln\left(\frac{T_{\text{div}}}{T}\right) \left(2 - \varepsilon_{\text{crit}} \left(4 + \ln\left(\frac{T_{\text{div}}}{T}\right)\right)\right) + \varepsilon_{\text{crit}}^2 \ln\left(\frac{T_{\text{div}}}{T}\right) \right] \right\}$$

$$\left(\frac{\partial Z_0}{\partial \rho}\right)_T = \frac{3}{2} \frac{T_c}{T} [\hat{u}'_0(\rho) + \rho \hat{u}''_0(\rho)] - [\tilde{s}'_0(\rho) + \rho \tilde{s}''_0(\rho)]$$

4. Comparison of the New Equations of State with Experimental Data and the Equations of State of Tegeler *et al.*

In this section, the quality of the new equation of state in its **non-extensive formulation** (see Table 3 and Table 7) is analysed in comparison with selected experimental and theoretical data. Most figures also show a comparison with the values calculated using the most recent equation of state established by Tegeler *et al.* (1999). In the following, the model of Tegeler *et al.* will be simply noted **TSW model**.

4.1. Melting phase transition

In the work of Tegeler *et al.*, their equation (2.7) gives the melting-pressure variation. However, they discard arbitrarily some data sets for example the data of Zha *et al.* (1986). It is clear that these data are scattered but, as they are obtained at high temperature and pressure, it should be interesting to use them. New and more accurate data from Datchi *et al.* (2000) are almost in the same range of temperature of those of Zha *et al.* and are consistent with these data. It is possible to have a complete view of the melting line for the range of temperature corresponding to the Ronchi's data set by adding the data of Jephcoat *et al.* (1996).

Thus, using a two parameters Simon-Glatzel type function, it is possible to represent in a coherent manner and with continuity the data of Hardy *et al.* (1971), Zha *et al.*, Datchi *et al.* and Jephcoat *et al.*:

$$P_m - P_t = a_1 \left[\left(\frac{T}{T_t} \right)^{a_2} - 1 \right] \quad (67)$$

with $a_1 = 225.2858$ MPa and $a_2 = 1.5284$. We have used this equation for the representation of the melting line in this paper.

It must be noticed that for determining the parameters in Eq. (67) we have also used the data from Bridgman (1935), Lahr *et al.* (1962), Crawford *et al.* (1968) and L'Air Liquide (1976).

Figure 9 compares some different data sets with values calculated from Eq. (67) (solid line), from Eq. (2) written by Datchi *et al.* (dashed curve) and from Eq. (1) written by Abramson (2011) (dot dashed curve). Equation (67) is very close to the function written by Datchi *et al.* and both equations are consistent with the data of Jephcoat *et al.* The main difference between Eq. (67) and Eq. (2) from Datchi *et al.* is at low temperature where this last one is very inaccurate and cannot be used when approaching the triple point. Equation (1) from Abramson is determined for the representation of its own data and it can be seen that the extrapolation of this function is not consistent with the data of Jephcoat *et al.* Also the Eq. (1) of Abramson is not very accurate at low temperature.

Some of the previous authors have also measured the liquid density on the melting line. But as it can be seen on Fig. 10 all the data sets have a large dispersion which makes difficult their representation. In particular the data of Lahr *et al.* at low temperature seem incompatible with the other data sets and at high temperature these data are incompatible with the data of Crawford *et al.* For these reasons, we can propose two equations which give a greater importance at high temperature either the data from Lahr *et al.* either the data from Crawford *et al.*:

$$T_{m,Low}(\rho) = T_t + 1015.4 \times \left(\frac{\rho}{\rho_{t,Liq}} - 1 \right)^{1.843} + 250.46 \times \left(\frac{\rho}{\rho_{t,Liq}} - 1 \right) \quad (67-Low)$$

$$T_{m,High}(\rho) = T_t + 677.25 \times \left(\frac{\rho}{\rho_{t,Liq}} - 1 \right)^{1.236} + 94.955 \times \left[1 - \exp \left(- \left(\frac{\rho - \rho_{t,Liq}}{0.25} \right)^{10.442} \right) \right] \quad (67-High)$$

These two empirical functions are represented on Fig. 10. As can be seen, for a liquid density smaller than 1.6 g/cm³ the two functions are almost identical.

4.2. Single Phase Region

4.2.1. Isochoric Heat Capacities

Our model is mainly based on C_V 's data provided by NIST but since the NIST data are identical, with some exceptions, to the numerical values deduced from the Eq. (4.1) of Tegeler *et al.*, a comparison between the results obtained with the two models is necessary. In the pressure-temperature region covered by NIST data, the relative differences ΔC_V observed between Tegeler's data and our data are less than the uncertainties given on Fig. 44 of Tegeler *et al.* The most important relative difference is obtained in the vicinity of the critical point as shown in Fig. 11. We can also notice in Fig. 11, that outside the critical region, the error oscillates almost regularly with density (for all temperatures). These oscillations come from the different mathematical forms used in the two models. For our model, a perfectly smooth monotonic function has been used for C_V while Tegeler *et al.* used a polynomial equation. This polynomial equation induced small oscillations on C_V and these oscillations can be seen on ΔC_V (Fig. 11). Such oscillations, more or less amplified, should also appear on other relative differences between thermodynamic quantities calculated from the two models.

In the paper of Ronchi (1981) there are no C_V 's data, then, no direct comparison is possible with our calculated data. However, in the region covered by the paper of Ronchi, Vrabec *et al.* (1996) have calculated C_V 's data using a molecular dynamics calculation based on a (12,6) Lennard-Jones potential. Figure 12 shows plots of the isochoric heat capacity on three high density isochors. The isochors with $\rho = 1.196$ g/cm³ and $\rho = 1.393$ g/cm³ are smaller than the density $\rho_{t,Liq}$ of the liquid at the triple point and hence are limited by the saturated liquid line at low temperatures. The isochor $\rho = 1.6$ g/cm³ is limited by the solidification line. As can be seen, in the pressure-temperature region covered by NIST data, the difference between our model and the TSW model is insignificant. The difference becomes only significant for temperatures larger than 1000 K and for densities higher than $\rho_{t,Liq}$. For these conditions, the data of Vrabec *et al.* are better fitted with our model than with the TSW model. This result was expected since our model has been built to reproduce the data of Ronchi; data which are also based on a statistical model using a potential of type (12,7).

In the region covered by the data of Ronchi and not covered by the data from NIST, we found the data from L'Air Liquide that have clearly not been analysed by Tegeler *et al.* Figure 13 shows plots of L'Air Liquide data on their highest isotherm at 1100 K and the corresponding calculated curves from our model and the TSW model. The maximum relative error is around 3% and, once again, these data are better fitted with our model than with the TSW model.

Even if the calculated values of Ronchi (1981) are not enough accurate, the isochors of C_V show the right variation with a maximum when temperature tends to zero as expected for

all liquids (Fig. 14). These maxima of C_V are observed in water, and they must also exist in argon. The maximum is also well understood as an extension in the single phase of the same very sharp maximum which is observed in the region of vapour-liquid coexistence. On the contrary, with the TSW model, C_V tends to infinity when temperature tends to zero (see Fig. 14), which is an improper variation.

4.2.2. Thermal Properties

As explained in section 3.1, the $P\rho T$ data from NIST and from Ronchi were used to determine the arbitrary functions $U_0(\rho)$ and $S_0(\rho)$ of the internal energy and entropy respectively. Therefore, our equation of state $P(\rho, T)$ is dependent on the accuracy obtained on the modelling of $U_0(\rho)$ and $S_0(\rho)$. Although the slopes of the straight lines $P - P_{C_V}$ are more accurately determined than the ordinates at the origin of these curves, Figs. 15 and 16 show that the average absolute errors obtained for $U(\rho, T)$ and $S(\rho, T)$ respectively, on all the isochors located in the region of pressure and temperature covered by NIST, are very small and of the same order of magnitude for a given temperature. Figs 15 and 16 show in both cases an oscillation of the average error value that is nearly centred on zero. Errors bars represent the standard deviation of the absolute error and given the value of these standard deviations from the average one, it can be understood that the error on each isochor is nearly identical for all values of temperature. This indicates that the shape of the isochors as function of temperature is very well reproduced and the errors are due to small oscillations in the data arising from the mathematical form used in the TSW model. However from the mathematical expressions we used, it is not possible to compensate for such oscillations.

Thus, for $T > T_c$ and for all densities in the range from $\rho_{t, \text{Gas}}$ to $\rho_{t, \text{Liq}}$, we find that the relative error on pressure between the NIST data (or TSW model) and our calculated data shows a “beautiful” oscillation in density (i.e. along isotherms) between -0.2% to +0.4%. In the gas phase, the relative error remains well below 0.2%, value which is only reached on the coexistence curve and in the vicinity of $\rho = 0.3 \text{ g/cm}^3$. In the liquid phase, the relative error remains well below 0.5% except close to the coexistence line. These largest errors are due to the fact that in dense phase, small variations of density can lead to large variations of pressure. We will come back on this question in section 4.3.2 but it can be noticed that, to analyse clearly this problem, we must look at the inverse equation $\rho(P, T)$ obtained by inversion of equation (45).

Due to the strong nonlinearity of the equation $P(\rho, T)$, whatever the model (TSW, Ronchi or ours), it is not possible to obtain an analytical form of the inverse equation $\rho(P, T)$, so we used a numerical method. The calculated data $\rho(P, T)$ from the different models are now compared. Fig. 17 shows the relative error on density between our calculated data and NIST data. We used the same tolerance range (from $\pm 0.03\%$ to $\pm 0.5\%$ in density) that the one proposed by Tegeler *et al.* on their Fig. 42. It is evident that Fig. 17 and Fig. 42 of Tegeler *et al.* are comparable though the distribution of tolerance regions is different.

For $P > P_c$ and for all temperatures corresponding to NIST data, we find from our model that the relative error on density and their oscillations (Fig. 17) are lower or close to the error obtained from the TSW model (see Fig. 42 in the paper of Tegeler *et al.*) except in the vicinity of the critical point. It can however be noticed that in this region, Tegeler *et al.* used an uncertainty on pressure, such uncertainty is obviously smaller than uncertainty on density.

For $P < P_c$ and for all the gaseous phase, the relative error on density (in the range ± 0.03 to $\pm 0.1\%$) is close to the one given by Tegeler *et al.*; globally our error is in the range $\pm 0.03\%$, i.e. category C of the paper of Tegeler *et al.*.

Before discussing these different tolerance diagrams, we will first look at the comparison of the calculated density data (from TSW model and ours) with data from L'Air Liquide. The accuracy claimed by L'Air Liquide on density measurements spread between $\pm 0.1\%$ and $\pm 1.5\%$ depending on the experimental method used.

Figures 18 and 19 display the relative error on density as a function of temperature between calculated data and L'Air Liquide data along two isobars. The data along the 0.1 MPa isobar are all in the gaseous phase while the data along the 100 MPa isobar spread from the liquid phase to the supercritical one. The both relative errors show comparable variations with temperature. Fig. 18 shows that, using the TSW model, the relative errors are in agreement with the uncertainty obtained with our model. Our relative errors are slightly larger at low temperature but the error variation, in all the temperature range, is better centred on zero. This means that the shape of the isobars is better reproduced by our model. On Fig. 19 we can notice that the relative errors using the TSW model agree again with the uncertainty obtained with our model. The relative errors from our model are almost everywhere slightly larger but remains in the tolerance range given by Tegeler *et al.*

Some data from L'Air Liquide are outside the range of NIST data but are connected to data calculated from the model of Ronchi. Then, such data from L'Air Liquide can be compared to the calculated data from the two models (TSW and ours). Figure 20 shows plots of the relative errors on density between calculated and L'Air Liquide data, as a function of pressure on the highest isotherm at 1100 K. The maximum relative error is around 0.3% and the two models lead to a similar variation with temperature. The error variation is slightly better centred on zero using our model than the TSW one.

It finally appears that our model can ultimately better reproduce the thermal properties in the gas phase than in the liquid phase. This is consistent with the fact that the state equations for U and S are better reproduced at low densities than at high densities. So if we want to better reproduce the data in the liquid phase, it is necessary to increase the accuracy on these two functions going towards high densities. It can however be noticed that the relative errors on pressure and density as defined by NIST remain very comparable for the two models, with a few exceptions.

In the region covered by the calculated data of Ronchi, it is only possible to use the thermal equations of state $P(\rho, T)$ to compare data. Figure 21 shows the relative error on pressure vs. temperature for different isochors. In the region of density covered by NIST data, the relative error from our model below 700 K is similar to the relative error deduced from the TSW model (see Fig. 1). Above 700 K, the maximum of the error is -2.5% on the isochor $\rho = 1.1784 \text{ g/cm}^3$ and, above 1000 K, the relative error on all the isochors decreases towards zero. Therefore, up to 2300 K, the overall error using our model does not exceed the error obtained in the region covered by NIST data. Outside the region of density covered by NIST, Fig. 22 shows that the relative error corresponding to our model is in the range $\pm 5\%$, except at low temperature on the two isochors $\rho = 1.84944 \text{ g/cm}^3$ and $\rho = 2.01758 \text{ g/cm}^3$. For these isochors, the relative error can be reduced to zero by decreasing the density value corresponding to these isochors by about 0.6%. The uncertainty of $\pm 5\%$ corresponds to the uncertainty claimed by Ronchi between his model and the many experimental data he used. If we compare the data of Ronchi with the extrapolation of the TSW model, Fig. 23 shows that the relative error increase with increasing the isochor's density and reach the value of 60% on the highest density isochor. This result was already mentioned by Tegeler *et al.*

New experimental $P\rho T$ data in the supercritical phase at 300 K have been determined by Hanna *et al.* (2010). There results have been compared with the model of Tegeler *et al.* and are consistent with it. But due to the large error bars, our model is also consistent with these new data.

New precise experimental $P\rho T$ data in the gaseous phase, in the range of temperature from 234 K to 505 K, have been made by McLinden (2006). These results have been compared with the values calculated from the model of Tegeler *et al.* and are consistent with them. In the pressure and temperature ranges covered by these data, our model has the same precision as that of Tegeler *et al.* hence these data are also consistent with our model.

4.2.3. Isobaric Heat Capacities, Sound Velocities and Isothermal Throttling Coefficient

As we can observe from Table 26 in the paper of Tegeler *et al.* the isobaric heat capacity $C_P(\rho, T)$, the speed of sound $c(\rho, T)$ and the isothermal throttling coefficient $\delta_T(\rho, T) = (\partial H / \partial P)_T$ are functions expressed with first and second derivatives of the Helmholtz free energy, therefore these quantities are more complex with respect to the quantities shown in the previous sections. Given that our model is not built on free energy but on the equation of state of $C_V(\rho, T)$ and thermal state equation $P(\rho, T)$, it is preferable to express the three above quantities as:

$$C_P = C_V + TVK_T \left(\frac{\partial P}{\partial T} \right)_V^2 = C_V + TV \frac{\beta^2}{K_T} \quad (68)$$

$$c^2 = \frac{V}{K_T} \frac{C_P}{C_V} \quad (69)$$

$$\delta_T = V(1 - T\beta) \quad (70)$$

where $K_T = -\frac{1}{V} \left(\frac{\partial V}{\partial P} \right)_T$ represents the isothermal compressibility coefficient and

$\beta = \frac{1}{V} \left(\frac{\partial V}{\partial T} \right)_P$ represents the isobaric coefficient of thermal expansion. These quantities

include the derivatives of pressure along the two directions ρ and T . The two quantities c and δ_T are functions of K_T and of the ratio C_P/C_V . So the errors on these two last quantities will reflect in a different way the errors on the state equations for pressure and for the isochoric heat capacity.

Since C_P diverges at the critical point it is only possible to compare the two models (TSW model and our model) outside the region of coexistence. Fig. 24 shows the relative error on C_P between the TSW model and our model. The relative error is everywhere inside the uncertainty given on Fig. 44 in the paper of Tegeler *et al.* In particular, Fig. 24 shows that, for most of the states, our relative error oscillates globally, without going into the details, between $\pm 0.5\%$, except for high density states and states in the vicinity of the critical point.

It is again interesting to compare the results of the two models with the data from L'Air Liquide. Figure 25 displays the data values of L'air Liquide on two isotherms at 700 K and 1100 K (i.e. the highest isotherm) and, the corresponding calculated curves from our model and the TSW model. As for the C_V data, our model shows a closer fitting of the data from L'Air Liquide than the TSW model. The highest relative error (about 1%) is obtained for the isotherm at 1100K using the TSW model.

The sound velocity c does not diverge at the critical point, but exhibits a very pronounced minimum. However in our model, c is expressed on the basis of C_P which diverges itself (Eq. (69)). Then for numerical reasons, we will compare the data calculated from the two models with the exception of the data on the respective curves of coexistence. The relative error on c (see Fig. 26) between the TSW model and our model presents a very similar variation with ρ and T that the one displayed by C_P on Fig. 24. In the largest part of the (ρ, T) diagram, the relative error oscillates globally between $\pm 0.5\%$, except for high density states and near the critical point where the error reaches 2%. On Fig. 43 of the paper of Tegeler *et al.*, the tolerance diagram for c shows similar uncertainties that we obtained on Fig. 26, however some regions of their diagram present lower uncertainties ($\pm 0.02\%$ and $\pm 0.1\%$).

If we compare the calculated data using the two models with the data of L'Air Liquide we can observe on Fig. 27 and 28 that, although the corresponding errors in our model are sometimes higher than those of the TSW model, they are generally better centred on zero. This means that the isobars and isotherms variations are better predicted using our model. Unfortunately, there are no data of sound speed from L'Air Liquide in the range 700 to 1100 K.

Equation (70) can be easily derived from the Gibbs-Helmholtz relations and its non-dimensional formulation $V^{-1}\delta_T$ reflects almost the behaviour of thermal expansion coefficient. When this quantity is equal to zero, the fluid behaves as an ideal perfect gas. Due to the fact that zero is a possible value for this function; it is not possible to make a relative error analysis. Figure 29 shows the absolute $\rho\delta_T$ vs P diagram for the same isotherms plotted on Fig. 33 of the paper of Tegeler *et al.* We can observe that the difference between the two models is very small and only more pronounced in the vicinity of the minimum of $\rho\delta_T$. On the isotherm at 162 K, the shape of our isotherm with a deeper well seems slightly better in the light of data from Kim (1974).

Finally, it is important to note that, since our model gives overall numerical results very close to those of the TSW model, both models have the same weakness for the representation of most of the experimental data very close to the critical point.

4.2.4. The “Ideal Curves”

Ideal curves are curves along which one property of a real fluid is equal to the corresponding property of the hypothetical ideal gas in the same state. The most important ideal curves can be derived from the compressibility factor Z and its first derivatives, i.e., the classical ideal curve ($Z = 1$), the Boyle curve [$(\partial Z/\partial P)_T = 0$ or $(\partial Z/\partial V)_T = 0$], the Joule-Thomson inversion curve (or Charles curve) [$(\partial Z/\partial T)_p = 0$ or $(\partial Z/\partial V)_p = 0$], and the Amagat curve (or Joule curve) [$(\partial Z/\partial P)_\rho = 0$ or $(\partial Z/\partial T)_\rho = 0$]. For Argon, all ideal curves lie within the range covered by data from NIST and Ronchi (1981). The only relevant exception is the high-temperature part of the Amagat curve.

Figure 30 shows the plot of the ideal curves calculated from Eq. (46) and its derivatives and from TSW equation of state. Inside the single phase domain where reliable data exists, both equations show the expected variations of ideal curves. Visible differences occur only for the very low density part of each curve. Thus Z and its first derivatives are well represented by our model.

4.2.5. Extrapolation to High Temperatures

Tegeler *et al.* compared their model to data resulting from the shock wave experiments of van Thiel *et al.* (1966), Nellis *et al.* (1980) and Grigor'ev *et al.* (1985). The pressure and density are calculated from the Hugoniot relations by using experimental velocity measurements. All of these data are in the pressure range and density range of the Ronchi's data but not in its temperature range. For example, all the data of Grigor'ev *et al.* correspond to a temperature range from 3700 K to 17000 K. In addition, for most of these experiments argon is ionized and the corresponding physics is clearly not included in our approach but also it is not explicitly included in the TSW model.

For all the data that lie in the Ronchi's domain, our Hugoniot curve is consistent with the data as the Hugoniot curve calculated by Tegeler *et al.* This can be easily understood because the Hugoniot states depend mainly of the behaviour of the Poisson adiabatic curves which have close variations till to the melting line as can be seen on Fig. 31 for the two different initial states which corresponds to those of van Thiel *et al.*

From these results we suggest not to use our model outside the highest limit of the Ronchi's domain.

4.3. Liquid-Vapour Phase Boundary

4.3.1. Isochoric Heat Capacities

Along the coexistence curve, the relative errors between the data from NIST and from our model oscillate about $\pm 0.45\%$ (see Fig. 11). This result can be compared to the uncertainties given on Fig. 44 of the paper of Tegeler *et al.*. Our relative error on the saturated liquid side is smaller than the one given in Fig. 44 ($\pm 0.45\%$ instead of $\pm 2\%$) and slightly larger on the saturated vapour side ($\pm 0.45\%$ instead of $\pm 0.3\%$).

Along this coexistence line, no NIST data are available in the density range 0.5 - 0.6 g/cm³. However, this region that extends on both sides of the critical point is covered along some isochors that crossed the coexistence curve by the data of Voronel *et al.* (1967 and 1973). Figure 32 shows that the two models (TSW and ours) lead to similar variations with T and the discrepancies with the data of Voronel *et al.* increase more and more as we approach the coexistence curve. Inside the coexistence phase, the data of Voronel *et al.* show a peak in C_V which is not symmetrical. Such C_V variation is in any case impossible to reproduce using the TSW model (see Fig. 8). On the other hand, our model could be modified to correctly describe such C_V variation. Indeed, the parameter T_{div} was inserted into the model (Eq. 10) to qualitatively describe the C_V divergence inside the coexistence phase (see Fig. 8). It is however evident, from the data of Voronel *et al.*, that the T_{div} values we defined are not quantitatively suitable. The peak position of C_V along the entire coexistence curve could be used to establish a new equation for T_{div} leading to a reliable fitting of C_V divergence inside the coexistence phase. The other side of T_{div} (i.e. for $T < T_{\text{div}}$) could also be easily modelled without changing any properties for the single phase region. Unfortunately, the data of Voronel *et al.* which are limited to a very small density range are insufficient to be taken into account in view to improve our model into the coexistence phase. We can also notice that the data of Voronel *et al.* have been correctly modelled by Rizi *et al.* (2012) using the crossover model. However, this model, which contains coefficients among which a number are unknown, cannot be put in practice.

Table 10. Characteristic values of the coexistence line calculated from the thermal equation of state and using the NIST values.

	Unit	NIST	Model of Tegeler <i>et al.</i>	Our non-extensive model Eq. (45)
$P_c(\rho_c, T_c)$	MPa	4.863	4.86299	4.86298
$\rho_c(P_c, T_c)$	g/cm ³	0.535599	0.549928	0.535526
$P_t(\rho_{t,Liq}, T_t)$	MPa	0.068891	0.082671	0.0688907
$\rho_{t,Liq}(P_t, T_t)$	g/cm ³	1.4168	1.41676	1.41680
$P_t(\rho_{t,Gas}, T_t)$	MPa	0.068891	0.0688913	0.068891
$\rho_{t,Gas}(P_t, T_t)$	g/cm ³	0.0040546	0.00405458	0.00405460

Table 11. Characteristic values of the coexistence line calculated from the Maxwell relations: Eq. (50) to (52).

	NIST	Model of Tegeler <i>et al.</i>	Our non-extensive model
T_c (K)	150.687	150.687	151.396
P_c (MPa)	4.863	4.86295	4.99684
ρ_c (g/cm ³)	0.535599	0.533136	0.543786
T_t (K)	83.8058	83.8058	83.8058
P_t (MPa)	0.068891	0.0688908	0.0689657
$\rho_{t,Liq}$ (g/cm ³)	1.4168	1.41676	1.416802
$\rho_{t,Gas}$ (g/cm ³)	0.0040546	0.00405457	0.00405912

4.3.2. Thermal Properties

The coexistence phase is characterized by three specific points which are the saturated liquid triple point, the saturated vapour triple point and the critical point. These points correspond to different well-known thermodynamic states.

From the thermal equation of state $P(\rho, T)$ of Tegeler *et al.* and the one we develop (Eq. (45)), the specific points have been calculated using for ρ and T the NIST data. Table 10 shows that the calculated values of the three characteristic states using our model are globally more accurate than the one calculated using the model of Tegeler *et al.* and, particularly for the triple point on the saturated liquid curve. As shown in Table 10, near the liquid saturated curve, even a tiny variation on density produces a large variation on the calculated pressure, i.e. the density values for these states must be extremely accurate. Thus, the TSW model gives an error of 0.003% on $\rho_{t, \text{Liq}}(P_t, T_t)$ and this leads to an error of 20% on $P_t(\rho_{t, \text{Liq}}, T_t)$.

At a given temperature, the vapour pressure and the densities of the coexisting phases (ρ_{ol} and ρ_{ov}) can also be calculated from the Maxwell criterion of phase equilibrium conditions and therefore the characteristics values of the coexistence line (triple and critical points) as well. Table 11 shows these characteristics values calculated from the TSW model and our model (Eq. (50) to (52)). The NIST data and those calculated with the TSW model are in good agreement, but this is not the case for our model particularly for the critical point. However, it can be noticed that T_c and T_t are imposed values for the TSW model whereas only T_t is fixed in ours. Then, the critical values (P_c , T_c , ρ_c) are calculated ones in our approach. Our thermal equation of state leads to better results for characteristics values than those calculated with the TSW model while, using the Maxwell equations, it is the opposite.

How to explain this result? The Maxwell equations represent the equality of pressure, temperature and specific Gibbs energy in the coexisting phases. Our model built all the required thermodynamics quantities (U , S , F , etc.) from the empirical description of the experimental data of $C_V(\rho, T)$ and $P(\rho, T)$. The accuracy of these empirical equations to describe the experimental data has been shown to be very good. Therefore, the discrepancy between our calculated critical values (P_c , T_c , ρ_c) and the NIST ones can be attributed to the inconsistency of the data in this critical state. The agreement between the calculated liquid triple point and the experimental one is better using our model: this means that, on the liquid side, our isochors network is slightly twisted compared to the TSW network used by Tegeler *et al.* This slight distortion of the isochors network on the liquid side has then a strong impact on the construction of the coexistence curve as already shown in Table 11. Indeed, considering that there is good agreement with the TSW model on the gas side but not as good on the liquid side, it is clear that the equilibrium conditions deduced from the Maxwell relations must be different.

Figure 33 shows that the relative error between the TSW model and ours for the saturated liquid density is less than $\pm 0.2\%$ in the range T_t to 139 K, which is in the uncertainty of the data selected by Tegeler *et al.* (see Fig. 5 in Tegeler *et al.*). Hence, on the liquid side our isochors network below 139 K is clearly more realistic.

Also, Figure 33 shows that the relative error between the TSW model and ours for the saturated vapour density is in the uncertainty of the data selected by Tegeler *et al.* (see Fig. 6 in Tegeler *et al.*) in the range 100 K to 149.5 K. Below 100 K, our error is 3 to 4 times larger than the claimed experimental uncertainties of Gilgen *et al.* (1994). But, as mentioned by Tegeler *et al.*, the densities on the saturated vapour curve were extrapolated from measurement in the homogeneous region close to the phase boundary. Such density values are obviously depending on the method used for doing the extrapolation. Although our error in

this region is relatively high, the calculated density values are compatible with the experimental data.

Finally, Fig. 33 also shows that the relative error between the TSW model and ours for the saturated vapour pressure is in the uncertainty of the data selected by Tegeler *et al.* in the range 97 K to 144 K. Below 97 K, our error oscillates slightly around -0.1% which is in the uncertainty of the data assigned to Group 2 by Tegeler *et al.* so we can say that these results are also in agreement with the experimental data.

However, in the vicinity of the critical state, the two models lead to very different values. This is due to the different approaches used for the two models. For the TSW model, the parameters of the critical point are imposed, whereas they are calculated in our model. Apart from the numerical values, Fig. 34 shows that the shape of the saturated vapour pressure curve around the critical point depends on the model. The TSW model generates an extremely "flat" variation on a wide range of density around the critical point when our model produces a more rounded variation in the same range of density. This last variation is closer of the experimental saturated vapour pressure curve from L'Air Liquide than the one given by the TSW model. The fact that the critical state is imposed in the TSW model seems to lead to a forced flattening-out of the saturated vapour pressure curve at the critical point.

If we use $T_{\text{sat}}(\rho)$ on the phase boundary derived from NIST data and calculate the saturated pressure curve using our thermal state equation Eq. (45), then Fig. 35 shows that the relative error on the saturated vapour pressure curve $P_{\text{sat}}(\rho)$ is less than $\pm 0.2\%$ below ρ_c . This uncertainty is compatible with the uncertainty of the data assigned to Group 2 by Tegeler *et al.* On the other hand, the relative error on the saturated liquid pressure curve $P_{\text{sat}}(\rho)$ in the range ρ_c to 0.85 g/cm^3 is compatible with the uncertainty of the data assigned to Group 3 by Tegeler *et al.* From this, we can conclude that our thermal equation of state is probably not enough accurate in the range 145 K to T_c .

From the analysis of the latent heat of vaporization $L_v = H_{\sigma v} - H_{\sigma l}$, we can determine the effect of the cumulative errors between the properties on the saturated vapour side and on the liquid saturated one. Figure 36 shows that until 149.5 K, the relative error between the TSW model and ours is far insight of the experimental data uncertainties shown on Fig. 15 in the paper of Tegeler *et al.* and, more particularly from T_t to 134 K, the relative error is less than $\pm 0.1\%$.

Owing to the fact that the "ideal curves" are correctly described - in particular near the critical point- but the saturated pressure is not correctly reproduced in the vicinity of the critical point, we can conclude that the problem comes from the fact that the experimental data in this region are not correctly described and, more are not enough coherent between themselves. These arguments can be easily observed with the spinodal properties.

4.3.3. The spinodal properties

The spinodal properties correspond to the metastable states of the fluid system. The knowledge of these metastable states is important for industrial processes that are involving ever increasing heat fluxes and rapid transients but also for testing the validity of a new equation of state formulation.

Most of the available experimental data pertain to states much closer to the saturated liquid state than the spinodal limit except very close to the critical point. The experimental data of Voronel *et al.* (1967, 1973) crossed the spinodal limit in a very narrow range of density around the critical point and the divergence states are shown on Fig. 37. Figure 37 shows also the liquid spinodal data points from Bařidakov *et al.* (1975). These data were determined from experimental $P\rho T$ data combined with a simple theoretical equation of $C_V(\rho, T)$. So these data points are dependent of the theoretical variations of C_V chosen by

Bařidakov *et al.* Figure 37 shows that these data decrease rapidly as the density increase but they are compatible with the spinodal states determined from our approach or from the TSW model, excepted for the TSW model around the density of 0.8 g/cm^3 where a strong unphysical hole appears due to uncontrollable strong oscillations of the polynomial terms.

Figure 37 shows that globally the two spinodal curves determined from our approach and from the TSW model are very close except close the liquid triple point where our spinodal curve shows a strong decrease vs. density. This is due to the fact that in this region the $P\rho T$ data are not represented with enough accuracy by the TSW model. We have already seen in previous sections that our approach have a better accuracy in this region, accuracy that was obtained by “twisting“ the isochors network. The strong decrease of the spinodal curve near the liquid triple point is simply the results of this locally network deformation.

From Fig. 37 we can also compare our divergence curve of C_V with the spinodal curve. If the data set of C_V and of $P\rho T$ used for the theoretical developments were sufficiently coherent the both curves would be identical. This is approximately true only on the liquid side for densities higher than 0.9 g/cm^3 and on the gaseous side in the range of density from 0.025 g/cm^3 to 0.15 g/cm^3 . Elsewhere this is not the case showing that the variations of C_V close to the saturation line are not correctly represented. Given that we have high accuracy with the TSW model it means that the variations of C_V calculated from the TSW model have not the good shape. This shows that it is not enough to have great precision with *a priori* selected set of data to ensure a coherent representation. Local variations of some measured quantities have physical non-negligible importance.

Table 12 : Thermodynamic parameters of saturated argon.

Temperature (K)	Pressure (MPa)	Density (g cm ⁻³)	Enthalpy (kJ kg ⁻¹)	Entropy (kJ kg ⁻¹ K ⁻¹)	C_V (kJ kg ⁻¹ K ⁻¹)	C_P (kJ kg ⁻¹ K ⁻¹)	c (m s ⁻¹)
83.8058 ^a	0.068 891	1.41680	-121.39	1.3297	0.548 64	1.11895	856.17
		0.0040546	42.23	3.2824	0.326 40	0.55734	168.02
84	0.070 522	1.41561	-121.17	1.3323	0.547 95	1.11968	854.73
		0.0041430	42.31	3.2786	0.326 60	0.55794	168.17
86	0.088 193	1.40321	-118.92	1.3586	0.540 97	1.12304	840.88
		0.0050845	43.08	3.2425	0.328 55	0.56400	169.74
88	0.109 096	1.39072	-116.67	1.3844	0.534 26	1.12305	828.22
		0.0061790	43.82	3.2082	0.330 63	0.57071	171.24
90	0.133 597	1.37815	-114.41	1.4095	0.527 82	1.12402	815.37
		0.0074416	44.52	3.1755	0.332 84	0.57812	172.67
92	0.162 078	1.36549	-112.15	1.4342	0.521 64	1.12613	802.28
		0.0088882	45.18	3.1443	0.335 19	0.58629	174.02
94	0.194 930	1.35271	-109.88	1.4583	0.515 69	1.12944	788.92
		0.0105356	45.80	3.1145	0.337 68	0.59531	175.30
96	0.232 558	1.33979	-107.60	1.4820	0.509 96	1.13400	775.28
		0.0124010	46.37	3.0859	0.340 32	0.60523	176.51
98	0.275 373	1.32672	-105.31	1.5053	0.504 45	1.13988	761.35
		0.0145031	46.89	3.0584	0.343 11	0.61617	177.64
100	0.323 796	1.31346	-103.00	1.5282	0.499 15	1.14718	747.12
		0.0168613	47.36	3.0319	0.346 07	0.62824	178.69
102	0.378 255	1.29999	-100.68	1.5508	0.494 05	1.15597	732.59
		0.0194966	47.78	3.0063	0.349 19	0.64156	179.68
104	0.439 185	1.28630	-98.34	1.5730	0.489 16	1.16640	717.75
		0.0224312	48.14	2.9816	0.352 51	0.65630	180.58
106	0.507 023	1.27233	-95.97	1.5951	0.484 46	1.17859	702.59
		0.0256892	48.43	2.9575	0.356 03	0.67264	181.41
108	0.582 216	1.25808	-93.58	1.6169	0.479 97	1.19271	687.10
		0.0292969	48.67	2.9341	0.359 77	0.69081	182.17
110	0.665 211	1.24349	-91.15	1.6385	0.475 68	1.20896	671.25
		0.0332828	48.83	2.9112	0.363 75	0.71110	182.84
112	0.756 461	1.22855	-88.70	1.6600	0.471 60	1.22758	655.04
		0.0376785	48.92	2.8888	0.368 01	0.73383	183.44
114	0.856 424	1.21319	-86.20	1.6814	0.467 75	1.24886	638.45
		0.0425194	48.94	2.8669	0.372 57	0.75942	183.97
116	0.965 560	1.19739	-83.66	1.7027	0.464 15	1.27315	621.45
		0.0478449	48.86	2.8452	0.377 47	0.78839	184.41
118	1.0843	1.18108	-81.07	1.7240	0.460 80	1.30090	604.01
		0.0537001	48.70	2.8238	0.382 76	0.82138	184.77
120	1.2132	1.16422	-78.43	1.7452	0.457 74	1.33265	586.10
		0.0601365	48.44	2.8026	0.388 49	0.85921	185.05
122	1.3526	1.14673	-75.72	1.7666	0.455 01	1.36910	567.70
		0.0672141	48.08	2.7814	0.394 73	0.90296	185.24
124	1.5032	1.12853	-72.95	1.7880	0.452 64	1.41114	548.75
		0.0750035	47.60	2.7603	0.401 54	0.95400	185.33

126	1.6653	1.10955	-70.11	1.8097	0.450 70	1.45995	529.20
		0.0835889	46.99	2.7390	0.409 04	1.01421	185.34
128	1.8394	1.08966	-67.17	1.8315	0.449 26	1.51708	509.01
		0.0930725	46.24	2.7176	0.417 33	1.08612	185.24
130	2.0261	1.06875	-64.14	1.8536	0.448 41	1.58468	488.11
		0.103580	45.33	2.6958	0.426 58	1.17327	185.03
132	2.2260	1.04666	-61.00	1.8762	0.448 30	1.66578	466.42
		0.115272	44.23	2.6735	0.436 97	1.28078	184.69
134	2.4395	1.02319	-57.73	1.8992	0.449 09	1.76485	443.85
		0.128351	42.94	2.6505	0.448 77	1.41628	184.21
136	2.6672	0.998082	-54.31	1.9229	0.451 02	1.88882	420.29
		0.143090	41.39	2.6266	0.462 33	1.59167	183.57
138	2.9099	0.970997	-50.71	1.9474	0.454 42	2.04902	395.56
		0.159864	39.55	2.6015	0.478 18	1.82657	182.73
140	3.1682	0.941443	-46.88	1.9730	0.459 84	2.26491	369.39
		0.179210	37.35	2.5747	0.497 06	2.15574	181.63
142	3.4430	0.908698	-42.77	2.0000	0.468 24	2.57120	341.35
		0.201946	34.68	2.5455	0.520 30	2.64684	180.19
144	3.7351	0.871668	-38.28	2.0292	0.481 83	3.03858	310.73
		0.229420	31.38	2.5129	0.550 34	3.45008	178.23
146	4.0460	0.828488	-33.24	2.0614	0.505 66	3.85590	276.57
		0.264135	27.13	2.4749	0.592 79	4.97016	175.27
148	4.3773	0.775089	-27.30	2.0989	0.550 48	5.71750	237.51
		0.311718	21.29	2.4273	0.662 71	8.72009	169.94
150	4.7323	0.698343	-19.28	2.1495	0.647 63	13.9176	190.54
		0.390945	11.82	2.3569	0.809 39	26.4188	157.52
150.687 ^b	4.8607	0.656707	-15.14	2.1758	0.715 68	29.7562	171.24
		0.439127	6.406	2.3188	0.891 67	56.4503	149.66
151.396 ^c	4.99684	0.543786	-4.184	2.2468	0.879 26	3580	146.56

^a Triple-point temperature

^b Critical temperature from NIST

^c Critical temperature from Maxwell relations Eq. (50) to (52)

5. The Uncertainty of the New Equation of State

Mainly guided by comparison with the model of Tegeler *et al.*, estimates for the uncertainty of calculated densities ρ , speeds of sound c , and isobaric heat capacities C_P calculated from Eq. (39) have been made. These uncertainties are illustrated in the following tolerance diagrams, Figs. 17, 38, 39. For all these tolerance diagrams, the variables are the pressure P and the temperature T . Since the quantities c and C_P depend on ρ and T , the pressure was converted to density by inversion of Eq. (45). In order to make an easier comparison with tolerance diagrams given in the paper of Tegeler *et al.* (1999), we have used the same tolerance ranges (± 0.03 to $\pm 5\%$) and identical notations (A, B, C, D, E, F).

We do not plot a tolerance diagram for C_V as it will not bring different information from Fig. 11. Moreover, the relative error on C_V between the TSW model and ours is everywhere far inside the errors shown in Fig. 44 in the paper of Tegeler *et al.* (1999).

Comparisons with the data of L'Air Liquide allow completing the tolerance diagrams in temperature range from 700 K to 1100 K. These uncertainties for calculated densities ρ , isobaric heat capacities C_P and isochoric heat capacities C_V are illustrated in the tolerance diagrams, Figs. 40–42.

6. Conclusions

A new equation of state for argon has been developed, which can be written in the form of a fundamental equation explicit in the reduced Helmholtz free energy. This equation has been derived from the measured quantities $C_V(\rho, T)$ and $P(\rho, T)$. It is valid for the whole fluid region (single-phase and coexistence states) from the melting line to 2300 K and for pressures up to 50 000 MPa. The formulation is based on data from NIST (or equivalently on the calculated values from the TSW model) and calculated values from the model of Ronchi (1981).

Our new approach using mainly power laws with density dependent exponents involves much less coefficients than the TSW model and, more, eliminates the very small oscillations introduced by a polynomial description. This leads to a more physical description of the thermodynamic properties. On the other hand, the cut in the number of terms and parameters does not modify in an appreciable way the uncertainties of the calculated data (see the different diagrams of tolerance). However, in an unexpected way, our approach which generates more regular and monotonous expressions raises greater difficulty for the reversal of certain equations of state due to a highly nonlinear behaviour of these expressions.

The new equation of state also shows a more physical behaviour along isochors when T tends to zero for the basic properties such as the isochoric heat capacity and the compressibility factor. It also shows a more reasonable behaviour for the crossing of the coexistence phase. However it does not describe correctly the properties in the vicinity of the critical point, in the same way as the model of Tegeler *et al.* (1999) does not properly describe the properties in the vicinity of the critical point with the exception of the saturation curve. Comparison of the model with data of L'Air Liquide (1976), which had not previously been taken into account, shows that our model is consistent with these data up to 1100 K and 100 MPa, which allows, regardless of the data of Ronchi (1981), to extend the range of NIST data.

7. References

- 1 Abramson E.H., High Pres. Res. **31** (4), 549 (2011).
2 Baïdakov V.G., V.P. Skripov and A.M. Kaverin, Sov. Phys.-JETP **40** (2), 335 (1975).
3 Bridgman P.W., Proc. Am. Acad. Arts Sci. **70**, 1 (1935).
4 Crawford R.K. and W.B. Daniels, Phys. Rev. Lett. **21** (6), 367 (1968).
5 Datchi D., P. Loubeyre and R. LeToullec, Phys. Rev. B **61** (10), 6535 (2000).
6 Gilgen R., R. Kleinrahm and W. Wagner, J. Chem. Thermodyn. **26**, 399 (1994b).
7 Grigor'ev F.V., S.B. Kormer, O.L. Mikhailova, M.A. Mochalov and V.D. Urlin, Sov.
Phy.-JETP **61**, 751 (1985).
8 Hanna G.J. and M.D. McCluskey, Phys. Rev. B **81**, 132104 (2010).
9 Hardy W.H., R.K. Crawford and W.B. Daniels, J. Chem. Phys. **54**, 1005 (1971).
10 Jephcoat A.P. and S.P. Besedin, Phil. Trans. R. Soc. Lond. A **354**, 1333 (1996).
11 Kim K.Y., Calorimetric studies on argon and hexafluoroethane and a generalized
correlation of maxima in isobaric heat capacity, PhD thesis, University of Michigan,
1974.
12 McLinden M.O., Meas. Sci. Technol. **17**, 2597 (2006).
13 Lahr P.H. and W.G. Eversole, J. Chem. Eng. Data **7** (1), 42 (1962).
14 L'Air Liquide, *Gaz Encyclopaedia* (Elsevier, 1976).
15 Nellis W.J. and A.C. Mitchell, J. Chem. Phys. **73**, 6137 (1980).
16 *NIST Chemistry Webbook*, <http://webbook.nist.gov/chemistry/>. NIST Standard
Reference Database Number 69.
17 Rizi A. and A. Abbaci, J. Molecular Liquids **171**, 64 (2012).
18 Ronchi C., J. Nucl. Mater. **96**, 314 (1981).
19 Tegeler Ch., R. Span and W. Wagner, J. Phys. Chem. Ref. Data **28**, 779 (1999).
20 M. Van Thiel and B.J. Alder, J. Chem. Phys. **44**, 1056 (1966).
21 Voronel' A.V. and Yu.R. Chashkin, Sov. Phys. JETP **24**, 263 (1967).
22 Voronel' A.V., V.G. Gorbunova, V.A. Smirnov, N.G. Shmakov and V.V.
Shchekochikhina, Sov. Phys. JETP **36**, 505 (1973).
23 Vrabc J. and J. Fisher, private communication cited in ref. 8.
24 W. van Witzenburg and J.C. Stryland, Can. J. Phys. **46**, 811 (1968).
25 Zha C.-S., R. Boehler, D. A. Young and M. Ross, J. Chem. Phys. **85**, 1034 (1986).

Appendix 1 : Expression of the Regular Term of Pressure P_{reg}

The regular term of pressure is formed by the difference of two terms which come respectively from the derivative of the energy and entropy we have:

$$P_{\text{reg}}(\rho, T) = P_{\text{Ureg}}(\rho, T) - P_{\text{Sreg}}(\rho, T) \quad (71)$$

and

$$Z_{\text{reg}}(\rho, T) = \frac{P_{\text{reg}}(\rho, T)}{\rho R_A T} = Z_{\text{Ureg}}(\rho, T) - Z_{\text{Sreg}}(\rho, T) \quad (72)$$

with

$$\begin{aligned} Z_{\text{Ureg}} &= \frac{P_{\text{Ureg}}(\rho, T)}{\rho R_A T} = \rho \left(\frac{\partial \tilde{u}_{\text{reg}}}{\partial \rho} \right)_T = \frac{3}{2} \rho n'_{\text{reg}}(\rho) \frac{T_c}{T} \left[\frac{(T/T_c)^{m(\rho)} - 1}{m(\rho)} + \frac{\lambda^{-m(\rho)}}{2-m(\rho)} \Gamma \left(\frac{m(\rho)}{2-m(\rho)}, \left(\frac{\lambda T}{T_c} \right)^{2-m(\rho)} \right) \right] \\ &+ \frac{3}{2} n_{\text{reg}}(\rho) \frac{T_c}{T} \rho m'(\rho) \left\{ \frac{1 - (T/T_c)^{m(\rho)}}{m(\rho)^2} + \frac{(T/T_c)^{m(\rho)} \ln(T/T_c)}{m(\rho)} + \frac{\lambda^{-m(\rho)}}{2-m(\rho)} \left(\frac{\lambda T}{T_c} \right)^{m(\rho)} \ln \left(\frac{\lambda T}{T_c} \right) \exp \left(- \left(\frac{\lambda T}{T_c} \right)^{\frac{5}{2}-m(\rho)} \right) \right\} \\ &+ \frac{3}{2} n_{\text{reg}}(\rho) \frac{T_c}{T} \rho m'(\rho) \frac{\lambda^{-m(\rho)}}{[2-m(\rho)]^2} \Gamma \left(\frac{m(\rho)}{2-m(\rho)}, \left(\frac{\lambda T}{T_c} \right)^{2-m(\rho)} \right) \left\{ 1 - \ln(\lambda^{2-m(\rho)}) + \frac{2}{2-m(\rho)} \ln \left(\left(\frac{\lambda T}{T_c} \right)^{2-m(\rho)} \right) \right\} \\ &+ 3 n_{\text{reg}}(\rho) \frac{T_c}{T} \rho m'(\rho) \frac{\lambda^{-m(\rho)}}{[2-m(\rho)]^3} G_{23}^{30} \left(\left(\frac{\lambda T}{T_c} \right)^{2-m(\rho)} \middle| \begin{array}{c} 1, 1 \\ 0, 0, \frac{m(\rho)}{2-m(\rho)} \end{array} \right) \end{aligned} \quad (73)$$

and

$$\begin{aligned} Z_{\text{Sreg}} &= \frac{P_{\text{Sreg}}(\rho, T)}{\rho R_A T} = \rho \left(\frac{\partial \tilde{s}_{\text{reg}}}{\partial \rho} \right)_T = \frac{3}{2} \rho n'_{\text{reg}}(\rho) \left[\frac{(T/T_c)^{m(\rho)-1} - 1}{m(\rho)-1} + \frac{\lambda^{1-m(\rho)}}{2-m(\rho)} \Gamma \left(\frac{m(\rho)-1}{2-m(\rho)}, \left(\frac{\lambda T}{T_c} \right)^{2-m(\rho)} \right) \right] \\ &+ \frac{3}{2} n_{\text{reg}}(\rho) \rho m'(\rho) \left\{ \frac{1 - (T/T_c)^{m(\rho)-1}}{[m(\rho)-1]^2} + \frac{(T/T_c)^{m(\rho)-1} \ln(T/T_c)}{m(\rho)-1} + \frac{\lambda^{1-m(\rho)}}{2-m(\rho)} \left(\frac{\lambda T}{T_c} \right)^{m(\rho)-1} \ln \left(\frac{\lambda T}{T_c} \right) \exp \left(- \left(\frac{\lambda T}{T_c} \right)^{2-m(\rho)} \right) \right\} \\ &+ \frac{3}{2} n_{\text{reg}}(\rho) \rho m'(\rho) \frac{\lambda^{1-m(\rho)}}{[2-m(\rho)]^2} \Gamma \left(\frac{m(\rho)-1}{2-m(\rho)}, \left(\frac{\lambda T}{T_c} \right)^{2-m(\rho)} \right) \left\{ 1 - \ln(\lambda^{2-m(\rho)}) + \frac{1}{2-m(\rho)} \ln \left(\left(\frac{\lambda T}{T_c} \right)^{2-m(\rho)} \right) \right\} \\ &+ \frac{3}{2} n_{\text{reg}}(\rho) \rho m'(\rho) \frac{\lambda^{1-m(\rho)}}{[2-m(\rho)]^3} G_{23}^{30} \left(\left(\frac{\lambda T}{T_c} \right)^{2-m(\rho)} \middle| \begin{array}{c} 1, 1 \\ 0, 0, \frac{m(\rho)-1}{2-m(\rho)} \end{array} \right) \end{aligned} \quad (74)$$

where $G_{p,q}^{m,n} \left(z \left| \begin{matrix} a_1, \dots, a_p \\ b_1, \dots, b_q \end{matrix} \right. \right)$ represents the Meijer G function. It is worth noting that the Meijer

functions in Z_{Ureg} and Z_{Sreg} are equal to zero when $T \geq T_t$ whatever the value of density.

For calculating some thermodynamics parameters, we need the first partial derivatives of this pressure term.

We give below the first partial derivatives of Z_{Ureg} and Z_{Sreg} with temperature:

$$\begin{aligned}
\left(\frac{\partial Z_{\text{Ureg}}}{\partial T} \right)_{\rho} &= \frac{3}{2} \frac{T_c}{T} \frac{\rho}{T} n'_{\text{reg}} \lambda^{-m} \left[\left(\frac{\lambda T}{T_c} \right)^m \left(\frac{m-1}{m} - \exp \left(- \left(\frac{\lambda T}{T_c} \right)^{2-m} \right) \right) + \frac{\lambda^m}{m} + \frac{1}{m-2} \Gamma \left(\frac{m}{2-m}, \left(\frac{\lambda T}{T_c} \right)^{2-m} \right) \right] \\
&+ \frac{3}{2} \frac{T_c}{T} \frac{\rho}{T} n'_{\text{reg}} \frac{m'}{m^2} \left\{ -1 + \left(\frac{T}{T_c} \right)^m \left[1 + m(m-1) \ln \left(\frac{T}{T_c} \right) \right] \right\} \\
&- 3 \frac{T_c}{T} \frac{\rho}{T} n'_{\text{reg}} m' \frac{\lambda^{-m}}{(2-m)^3} \Gamma \left(\frac{m}{2-m}, \left(\frac{\lambda T}{T_c} \right)^{2-m} \right) \left\{ \ln \left(\left(\frac{\lambda T}{T_c} \right)^{2-m(\rho)} \right) + \frac{1}{2} (1 + \ln(\lambda^{2-m})) (m-2) \right\} \\
&+ \frac{3}{2} \frac{T_c}{T} \frac{\rho}{T} n'_{\text{reg}} m' \frac{\lambda^{-m}}{(2-m)} \left(\frac{\lambda T}{T_c} \right)^2 \exp \left(- \left(\frac{\lambda T}{T_c} \right)^{2-m} \right) \left\{ \left(\frac{\lambda T}{T_c} \right)^{m-2} \left[\ln(\lambda^{2-m}) - \ln \left(\frac{\lambda T}{T_c} \right)^2 \right] - \ln \left(\frac{\lambda T}{T_c} \right)^{2-m} \left(1 + \left(\frac{\lambda T}{T_c} \right)^{m-2} \frac{m-1}{m-2} \right) \right\} \\
&+ 3 \frac{T_c}{T} \frac{\rho}{T} n'_{\text{reg}} m' \frac{\lambda^{-m}}{(2-m)^3} \left\{ (m-2) G_{12}^{20} \left(\frac{\lambda T}{T_c} \right)^{2-m} \left| \begin{matrix} 1 \\ 0, \frac{m}{2-m} \end{matrix} \right. - G_{23}^{30} \left(\frac{\lambda T}{T_c} \right)^{2-m} \left| \begin{matrix} 1, 1 \\ 0, 0, \frac{m}{2-m} \end{matrix} \right. \right\}
\end{aligned} \tag{75}$$

and

$$\begin{aligned}
\left(\frac{\partial Z_{\text{Sreg}}}{\partial T} \right)_{\rho} &= \frac{3}{2} \frac{\rho}{T} n'_{\text{reg}} \left(\frac{T}{T_c} \right)^{m-1} \left[1 - \exp \left(- \left(\frac{\lambda T}{T_c} \right)^{2-m} \right) \right] + \frac{3}{2} \frac{\rho}{T} n'_{\text{reg}} m' \left(\frac{T}{T_c} \right)^{m-1} \ln \left(\frac{T}{T_c} \right) \\
&+ \frac{3}{2} \frac{\rho}{T} n'_{\text{reg}} m' \frac{\lambda^{1-m}}{(m-2)^2} \left\{ \Gamma \left(\frac{1-m}{m-2}, \left(\frac{\lambda T}{T_c} \right)^{2-m} \right) - G_{12}^{20} \left(\frac{\lambda T}{T_c} \right)^{2-m} \left| \begin{matrix} 1 \\ 0, \frac{1-m}{m-2} \end{matrix} \right. \right\} \\
&+ \frac{3}{2} \frac{\rho}{T} n'_{\text{reg}} m' \frac{\lambda^{1-m}}{(m-2)} \left(\frac{\lambda T}{T_c} \right)^{2-m} \exp \left(- \left(\frac{\lambda T}{T_c} \right)^{2-m} \right) \left\{ \left(1 + \left(\frac{\lambda T}{T_c} \right)^{2-m} \right) \ln \left(\left(\frac{\lambda T}{T_c} \right)^{2-m} \right) - \ln(\lambda^{2-m}) \right\}
\end{aligned} \tag{76}$$

We give below the first partial derivatives of Z_{Ureg} and Z_{Sreg} with density:

$$\begin{aligned}
\left(\frac{\partial Z_{\text{Ureg}}}{\partial \rho}\right)_T &= \frac{3}{2} \frac{T_c}{T} (n'_{\text{reg}} + \rho n''_{\text{reg}}) \left[\frac{\lambda^{-m}}{2-m} \Gamma\left(\frac{m}{2-m}, \left(\frac{\lambda T}{T_c}\right)^{2-m}\right) - m^{-1} \left(1 - \left(\frac{T}{T_c}\right)^m\right) \right] \\
&+ \frac{3}{2} \frac{T_c}{T} \rho n_{\text{reg}} \frac{m'^2}{m^3} \left\{ -2 + 2 \left(\frac{T}{T_c}\right)^m \left[1 - \ln\left(\left(\frac{T}{T_c}\right)^m\right) + \frac{1}{2} \ln\left(\left(\frac{T}{T_c}\right)^2\right) \right] \right\} \\
&+ \frac{3}{2} \frac{T_c}{T} \rho n'_{\text{reg}} m' \frac{\lambda^{-m}}{(m-2)^2} \Gamma\left(\frac{m}{2-m}, \left(\frac{\lambda T}{T_c}\right)^{2-m}\right) (1 + \ln(\lambda^{m-2})) \\
&+ \frac{3}{2} \frac{T_c}{T} (n_{\text{reg}} m' + \rho n_{\text{reg}} m'' + 2 \rho n'_{\text{reg}} m') \left[m^{-2} \left(1 - \left(\frac{T}{T_c}\right)^m\right) + m^{-1} \left(\frac{T}{T_c}\right)^m \ln\left(\frac{T}{T_c}\right) \right] \\
&- \frac{3}{2} \frac{T_c}{T} (n_{\text{reg}} m' + \rho n_{\text{reg}} m'' + \rho n'_{\text{reg}} m') \frac{\lambda^{-m}}{(m-2)^3} \left\{ \Gamma\left(\frac{m}{2-m}, \left(\frac{\lambda T}{T_c}\right)^{2-m}\right) \left[2 \ln\left(\left(\frac{\lambda T}{T_c}\right)^{2-m}\right) - (m-2)(1 + \ln(\lambda^{m-2})) \right] \right. \\
&\quad \left. + (m-2)^2 \left(\frac{\lambda T}{T_c}\right)^m \ln\left(\frac{\lambda T}{T_c}\right) \exp\left(-\left(\frac{\lambda T}{T_c}\right)^{2-m}\right) + 2G_{2,3}^{3,0}\left(\frac{\lambda T}{T_c}\right)^{2-m} \left| \begin{matrix} 1, & 1 \\ 0, & 0, & \frac{m}{2-m} \end{matrix} \right. \right\} \\
&+ \frac{3}{2} \frac{T_c}{T} \rho m' \left[(2-m)n'_{\text{reg}} + n_{\text{reg}} m' \left(1 + 2 \ln\left(\frac{T}{T_c}\right) + \ln(\lambda^m)\right) \right] \frac{\lambda^{-m}}{(m-2)^4} \left\{ (2-m) \left(\frac{\lambda T}{T_c}\right)^m \exp\left(-\left(\frac{\lambda T}{T_c}\right)^{2-m}\right) \ln\left(\left(\frac{\lambda T}{T_c}\right)^{2-m}\right) \right. \\
&\quad \left. + 2 \Gamma\left(\frac{m}{2-m}, \left(\frac{\lambda T}{T_c}\right)^{2-m}\right) \ln\left(\left(\frac{\lambda T}{T_c}\right)^{2-m}\right) + 2G_{2,3}^{3,0}\left(\frac{\lambda T}{T_c}\right)^{2-m} \left| \begin{matrix} 1, & 1 \\ 0, & 0, & \frac{m}{2-m} \end{matrix} \right. \right\} \\
&- \frac{3}{2} \frac{T_c}{T} \rho n_{\text{reg}} m'^2 \frac{\lambda^{-m}}{(m-2)^3} \left\{ \Gamma\left(\frac{m}{2-m}, \left(\frac{\lambda T}{T_c}\right)^{2-m}\right) \left[2 + (2 + \ln(\lambda^{m-2})) \left(2 \ln\left(\frac{T}{T_c}\right) + \ln(\lambda^m)\right) \right] \right. \\
&\quad \left. + \left(\frac{\lambda T}{T_c}\right)^m \exp\left(-\left(\frac{\lambda T}{T_c}\right)^{2-m}\right) \ln\left(\left(\frac{\lambda T}{T_c}\right)^{2-m}\right) \left[1 + \ln\left(\left(\frac{T}{T_c}\right)^{2-m}\right) + \left(\frac{\lambda T}{T_c}\right)^{2-m} \ln\left(\left(\frac{\lambda T}{T_c}\right)^{2-m}\right) \right] \right\} \\
&- 3 \frac{T_c}{T} \rho n_{\text{reg}} m'^2 \frac{\lambda^{-m}}{(m-2)^5} \left\{ (2-m) \left(\frac{\lambda T}{T_c}\right)^{m-2} \ln\left(\left(\frac{\lambda T}{T_c}\right)^{2-m}\right) G_{1,2}^{2,0}\left(\frac{\lambda T}{T_c}\right)^{2-m} \left| \begin{matrix} 2 \\ 1, & \frac{m}{2-m} \end{matrix} \right. \right. \\
&\quad \left. \left. + (2-m) \left(3 + 2 \ln\left(\frac{T}{T_c}\right) + \ln(\lambda^m)\right) G_{2,3}^{3,0}\left(\frac{\lambda T}{T_c}\right)^{2-m} \left| \begin{matrix} 1, & 1 \\ 0, & 0, & \frac{m}{2-m} \end{matrix} \right. + 4G_{3,4}^{4,0}\left(\frac{\lambda T}{T_c}\right)^{2-m} \left| \begin{matrix} 1, & 1, & 1 \\ 0, & 0, & 0, & \frac{m}{2-m} \end{matrix} \right. \right\} \quad (77)
\end{aligned}$$

and

$$\begin{aligned}
\left(\frac{\partial Z_{\text{Sreg}}}{\partial \rho}\right)_T &= \frac{3}{2} (n'_{\text{reg}} + \rho n''_{\text{reg}}) \left[\frac{\lambda^{1-m}}{2-m} \Gamma\left(\frac{1-m}{m-2}, \left(\frac{\lambda T}{T_c}\right)^{2-m}\right) - (m-1)^{-1} \left(1 - \left(\frac{T}{T_c}\right)^{m-1}\right) \right] \\
&+ \frac{3}{2} (n_{\text{reg}} m' + \rho n_{\text{reg}} m'' + 2\rho n'_{\text{reg}} m') \frac{1}{(m-1)^2} \left[\left(1 - \left(\frac{T}{T_c}\right)^{m-1}\right) + (m-1) \left(\frac{T}{T_c}\right)^{m-1} \ln\left(\frac{T}{T_c}\right) \right] \\
&+ \frac{3}{2} (n_{\text{reg}} m' + \rho n_{\text{reg}} m'' + \rho n'_{\text{reg}} m') \frac{\lambda^{1-m}}{(2-m)^2} \left\{ \Gamma\left(\frac{1-m}{m-2}, \left(\frac{\lambda T}{T_c}\right)^{2-m}\right) \left[1 + \ln\left(\frac{\lambda T}{T_c}\right) - \ln(\lambda^{2-m}) \right] \right. \\
&\quad \left. + \left(\frac{\lambda T}{T_c}\right)^{m-1} \ln\left(\left(\frac{\lambda T}{T_c}\right)^{2-m}\right) \exp\left(-\left(\frac{\lambda T}{T_c}\right)^{2-m}\right) \right\} \\
&+ \frac{3}{2} \rho n'_{\text{reg}} m' \frac{\lambda^{1-m}}{(m-2)^2} \Gamma\left(\frac{1-m}{m-2}, \left(\frac{\lambda T}{T_c}\right)^{2-m}\right) (1 + \ln(\lambda^{m-2})) \\
&- \frac{3}{2} \rho n_{\text{reg}} m'^2 \frac{1}{(m-1)^3} \left[2 \left(1 - \left(\frac{T}{T_c}\right)^{m-1}\right) + 2 \left(\frac{T}{T_c}\right)^{m-1} \ln\left(\left(\frac{T}{T_c}\right)^{m-1}\right) - \left(\frac{T}{T_c}\right)^{m-1} \ln\left(\left(\frac{T}{T_c}\right)^{m-1}\right)^2 \right] \\
&- \frac{3}{2} \rho n_{\text{reg}} m'^2 \frac{\lambda^{1-m}}{(m-2)^3} (3 + \ln(\lambda^{m-2})) \left\{ \Gamma\left(\frac{1-m}{m-2}, \left(\frac{\lambda T}{T_c}\right)^{2-m}\right) \left[1 + \ln\left(\frac{\lambda T}{T_c}\right) - \ln(\lambda^{2-m}) \right] \right. \\
&\quad \left. + \left(\frac{\lambda T}{T_c}\right)^{m-1} \ln\left(\left(\frac{\lambda T}{T_c}\right)^{2-m}\right) \exp\left(-\left(\frac{\lambda T}{T_c}\right)^{2-m}\right) \right\} \\
&- \frac{3}{2} \rho n_{\text{reg}} m'^2 \frac{\lambda^{1-m}}{(2-m)^3} \left\{ \Gamma\left(\frac{1-m}{m-2}, \left(\frac{\lambda T}{T_c}\right)^{2-m}\right) \left[1 + \ln\left(\frac{\lambda T}{T_c}\right) - 2 \ln(\lambda^{2-m}) \right] - \left(\frac{\lambda T}{T_c}\right) \ln\left(\left(\frac{\lambda T}{T_c}\right)^{2-m}\right)^2 \exp\left(-\left(\frac{\lambda T}{T_c}\right)^{2-m}\right) \right. \\
&\quad \left. + \left(\frac{\lambda T}{T_c}\right)^{m-1} \ln\left(\left(\frac{\lambda T}{T_c}\right)^{2-m}\right) \left(2 - \ln\left(\left(\frac{\lambda T}{T_c}\right)^{2-m}\right) \right) \exp\left(-\left(\frac{\lambda T}{T_c}\right)^{2-m}\right) - \left(\frac{\lambda T}{T_c}\right)^{m-2} \ln\left(\frac{\lambda T}{T_c}\right) G_{12}^{20}\left(\left(\frac{\lambda T}{T_c}\right)^{2-m} \middle| 1, \frac{2}{2-m}\right) \right\} \\
&+ \frac{3}{2} \rho m' \left[(2-m)n'_{\text{reg}} + n_{\text{reg}} m' \left(1 + \ln\left(\frac{\lambda T}{T_c}\right) - \ln(\lambda^{2-m}) \right) \right] \frac{\lambda^{1-m}}{(m-2)^4} \ln\left(\left(\frac{\lambda T}{T_c}\right)^{2-m}\right) \left\{ (2-m) \left(\frac{\lambda T}{T_c}\right)^{m-1} \exp\left(-\left(\frac{\lambda T}{T_c}\right)^{2-m}\right) \right. \\
&\quad \left. + \Gamma\left(\frac{1-m}{m-2}, \left(\frac{\lambda T}{T_c}\right)^{2-m}\right) \right\} \\
&- 3 \rho n_{\text{reg}} m'^2 \frac{\lambda^{1-m}}{(m-2)^5} \left\{ \ln\left(\left(\frac{\lambda T}{T_c}\right)^{2-m}\right) + (2-m)(2 - \ln(\lambda^{2-m})) \right\} G_{23}^{30}\left(\left(\frac{\lambda T}{T_c}\right)^{2-m} \middle| \begin{matrix} 1, & 1 \\ 0, & 0, & \frac{1-m}{m-2} \end{matrix} \right) \\
&\quad + G_{34}^{40}\left(\left(\frac{\lambda T}{T_c}\right)^{2-m} \middle| \begin{matrix} 1, & 1, & 1 \\ 0, & 0, & 0, & \frac{1-m}{m-2} \end{matrix} \right) \right\} \\
&+ \frac{3}{2} \frac{\lambda^{1-m}}{(2-m)^3} (n_{\text{reg}} m' + \rho n_{\text{reg}} m'' + 2\rho n'_{\text{reg}} m') G_{23}^{30}\left(\left(\frac{\lambda T}{T_c}\right)^{2-m} \middle| \begin{matrix} 1, & 1 \\ 0, & 0, & \frac{1-m}{m-2} \end{matrix} \right)
\end{aligned} \tag{78}$$

Appendix 2 : Expression of the First and Second Derivatives of the Coefficients in C_V

We give here the expressions of the first derivatives of coefficients that appear in C_V which are useful for calculating the pressure.

$$\begin{aligned} \rho n'_{\text{reg}}(\rho) = & \alpha_{\text{reg},1} \left(\frac{\rho}{\rho + \rho_{\text{t,Liq}}} \right)^{\varepsilon_{\text{reg},1a}} \exp \left(- \left(\frac{\rho}{\rho_{\text{t,Gas}}} \right)^{\varepsilon_{\text{reg},1b}} \right) \left\{ \varepsilon_{\text{reg},1a} \frac{\rho_{\text{t,Liq}}}{\rho + \rho_{\text{t,Liq}}} - \varepsilon_{\text{reg},1b} \left(\frac{\rho}{\rho_{\text{t,Gas}}} \right)^{\varepsilon_{\text{reg},1b}} \right\} \\ & - \alpha_{\text{reg},2} \left(\frac{\rho}{\rho_{\text{t,Liq}}} \right)^{\varepsilon_{\text{reg},2a}} \left\{ - \varepsilon_{\text{reg},2a} \left(1 - \exp \left(- \left(\frac{\rho}{\rho_{\text{reg,Ronc}}} \right)^{-\varepsilon_{\text{reg},2b}} \right) \right) + \varepsilon_{\text{reg},2b} \left(\frac{\rho}{\rho_{\text{reg,Ronc}}} \right)^{-\varepsilon_{\text{reg},2b}} \exp \left(- \left(\frac{\rho}{\rho_{\text{reg,Ronc}}} \right)^{-\varepsilon_{\text{reg},2b}} \right) \right\} \end{aligned} \quad (79)$$

$$\begin{aligned} \rho m'(\rho) = & - \left\{ \alpha_{m,4} + \alpha_{m,3} \left(-\frac{3}{2} + \frac{\rho}{\rho_c} \right) \left(\frac{\rho}{\rho_c} \right)^{\frac{3}{2}} \exp \left(-\frac{\rho}{\rho_c} \right) + \frac{3}{2} \alpha_{m,2} \left(\frac{\rho}{\rho_{\text{t,Liq}}} \right)^{\frac{3}{2}} \exp \left(- \left(\frac{\rho}{\rho_{\text{t,Liq}}} \right)^{\frac{3}{2}} \right) \right\} \\ & + \rho m'_{\text{Ronc}}(\rho) \end{aligned} \quad (80)$$

$$\begin{aligned} \rho m'_{\text{Ronc}} \left(\rho \geq \frac{M}{12.9} \text{ g/cm}^3 \right) = & \frac{\rho}{\rho_{\text{m,Ronc}}} \left(\frac{\rho + \rho_{\text{m,Ronc}}}{\rho_{\text{m,Ronc}}} \right)^{\varepsilon_{m,5a}-1} \exp \left(- \exp \left(\left(\frac{\rho_{\text{m,Ronc}}}{\rho} \right)^{\varepsilon_{m,5b}} \right) \right) \\ & \times \left\{ \alpha_{m,1} \varepsilon_{m,5a} + \alpha_{m,4} \left(1 + \frac{\rho_{\text{m,Ronc}}}{\rho} + \varepsilon_{m,5a} \ln \left(\frac{\rho}{\rho_c} \right) \right) + \varepsilon_{m,5b} \left(\frac{\rho + \rho_{\text{m,Ronc}}}{\rho_{\text{m,Ronc}}} \right) \left(\frac{\rho_{\text{m,Ronc}}}{\rho} \right)^{\varepsilon_{m,5b}} \right. \\ & \left. \times \exp \left(\left(\frac{\rho_{\text{m,Ronc}}}{\rho} \right)^{\varepsilon_{m,5b}} \right) \left(\alpha_{m,1} + \alpha_{m,4} \ln \left(\frac{\rho}{\rho_c} \right) \right) \right\} \end{aligned} \quad (81)$$

$$\begin{aligned} \rho n'_{\text{nonreg}}(\rho \leq \rho_{\text{t,Liq}}) = & \alpha_{\text{nonreg},1} \left(\frac{\rho}{\rho_{\text{t,Gas}}} \right)^{\varepsilon_{\text{nonreg},1a}} \left(\frac{\rho_{\text{t,Liq}}}{\rho} \right) \exp \left(- \left(\frac{\rho_{\text{t,Liq}}}{\rho_{\text{t,Gas}}} \right)^{\varepsilon_{\text{nonreg},1b}} \left(\frac{\rho}{\rho_{\text{t,Liq}} - \rho} \right)^{\varepsilon_{\text{nonreg},1b}} \right) \\ & \times \left\{ \varepsilon_{\text{nonreg},1a} \frac{\rho}{\rho_{\text{t,Liq}}} - \varepsilon_{\text{nonreg},1b} \left(\frac{\rho_{\text{t,Liq}}}{\rho_{\text{t,Gas}}} \right)^{\varepsilon_{\text{nonreg},1b}} \left(\frac{\rho}{\rho_{\text{t,Liq}} - \rho} \right)^{1+\varepsilon_{\text{nonreg},1b}} \right\} \\ & + \alpha_{\text{nonreg},2} \left(\frac{\rho}{\rho_{\text{t,Gas}}} \right)^{\varepsilon_{\text{nonreg},2a}} \left(\frac{\rho_{\text{t,Liq}}}{\rho} \right) \exp \left(- \left(\frac{\rho_{\text{t,Liq}}}{\rho_{\text{t,Gas}}} \right)^{\varepsilon_{\text{nonreg},2b}} \left(\frac{\rho}{\rho_{\text{t,Liq}} - \rho} \right)^{\varepsilon_{\text{nonreg},2b}} \right) \\ & \times \left\{ \varepsilon_{\text{nonreg},2a} \frac{\rho}{\rho_{\text{t,Liq}}} - \varepsilon_{\text{nonreg},2b} \left(\frac{\rho_{\text{t,Liq}}}{\rho_{\text{t,Gas}}} \right)^{\varepsilon_{\text{nonreg},2b}} \left(\frac{\rho}{\rho_{\text{t,Liq}} - \rho} \right)^{1+\varepsilon_{\text{nonreg},2b}} \right\} \end{aligned} \quad (82)$$

$$\begin{aligned} \rho T'_{\text{div}}(\rho) &= \alpha_{\text{div},1} \left(\frac{\rho}{\rho_c} \right)^{\varepsilon_{\text{div},1a}} \exp \left(- \left(\frac{\rho}{\rho_c} \right)^{\varepsilon_{\text{div},1b}} \right) \left\{ \varepsilon_{\text{div},1a} - \varepsilon_{\text{div},1b} \left(\frac{\rho}{\rho_c} \right)^{\varepsilon_{\text{div},1b}} \right\} \\ &+ \alpha_{\text{div},2} \left(\frac{\rho}{\rho_{\text{t,Liq}}} \right)^{\varepsilon_{\text{div},2a}} \exp \left(- \left(\frac{\rho}{\rho_{\text{t,Liq}}} \right)^{\varepsilon_{\text{div},2b}} \right) \left\{ \varepsilon_{\text{div},2a} - \varepsilon_{\text{div},2b} \left(\frac{\rho}{\rho_{\text{t,Liq}}} \right)^{\varepsilon_{\text{div},2b}} \right\} \end{aligned} \quad (83)$$

$$\begin{aligned} \rho n'_{\text{crit}}(\rho) &= \alpha_{\text{crit},a} \left(\frac{\rho}{\rho_c} \right)^{\varepsilon_{\text{crit},a}} \times \exp \left[- \left(\left(\alpha_{\text{crit},b} \frac{\rho - \rho_c}{\rho_c} \right)^2 \right)^{\varepsilon_{\text{crit},b}} \right] \\ &\times \left\{ \varepsilon_{\text{crit},a} - 2\varepsilon_{\text{crit},b} \rho \left(\frac{\alpha_{\text{crit},b}}{\rho_c} \right)^{2\varepsilon_{\text{crit},b}} \left((\rho - \rho_c)^2 \right)^{\varepsilon_{\text{crit},b} - \frac{1}{2}} \text{sgn}(\rho - \rho_c) \right\} \end{aligned} \quad (84)$$

$$\begin{aligned} \rho_c \varepsilon'_{\text{crit}}(\rho) &= 2\varepsilon_{\text{crit},d} \varepsilon_{\text{crit},e}^2 \frac{\rho_{\text{crit},a} - \rho}{\rho_{\text{crit},a}} \frac{\rho_c}{\rho_{\text{crit},a}} \exp \left(- \left(\varepsilon_{\text{crit},e} \frac{\rho - \rho_{\text{crit},a}}{\rho_{\text{crit},a}} \right)^2 \right) \\ &+ 2\varepsilon_{\text{crit},f} \varepsilon_{\text{crit},g}^2 \frac{\rho_{\text{crit},b} - \rho}{\rho_{\text{crit},b}} \frac{\rho_c}{\rho_{\text{crit},b}} \exp \left(- \left(\varepsilon_{\text{crit},g} \frac{\rho - \rho_{\text{crit},b}}{\rho_{\text{crit},b}} \right)^2 \right) \end{aligned} \quad (85)$$

It is interesting to note that the limits of $\rho n'_{\text{crit}}(\rho)$, $\rho T'_{\text{div}}(\rho)$, $\rho n'_{\text{nonreg}}(\rho)$ and $\rho n'_{\text{reg}}(\rho)$ are equal to zero when $\rho \rightarrow 0$. Moreover the limit of $\rho m'(\rho)$ is equal to 0.240087 when $\rho \rightarrow 0$. We give now the expressions of the second derivatives of coefficients that appear in C_V and are useful for calculating the compressibility factor.

$$\begin{aligned} \rho^2 n''_{\text{reg}}(\rho) &= \alpha_{\text{reg},1} \left(\frac{\rho}{\rho + \rho_{\text{t,Liq}}} \right)^{\varepsilon_{\text{reg},1a}} \exp \left(- \left(\frac{\rho}{\rho_{\text{t,Gas}}} \right)^{\varepsilon_{\text{reg},1b}} \right) \left\{ \varepsilon_{\text{reg},1b}^2 \left(\frac{\rho}{\rho_{\text{t,Gas}}} \right)^{\varepsilon_{\text{reg},1b}} \left(-1 + \left(\frac{\rho}{\rho_{\text{t,Gas}}} \right)^{\varepsilon_{\text{reg},1b}} \right) \right. \\ &+ \varepsilon_{\text{reg},1a} \left(\frac{\rho_{\text{t,Liq}}}{\rho + \rho_{\text{t,Liq}}} \right)^2 \left(-2 \frac{\rho}{\rho_{\text{t,Liq}}} - 1 + \varepsilon_{\text{reg},1a} \right) + \varepsilon_{\text{reg},1b} \left(\frac{\rho}{\rho_{\text{t,Gas}}} \right)^{\varepsilon_{\text{reg},1b}} \left(1 - 2\varepsilon_{\text{reg},1a} \frac{\rho_{\text{t,Liq}}}{\rho + \rho_{\text{t,Liq}}} \right) \left. \right\} \\ &+ \alpha_{\text{reg},2} \varepsilon_{\text{reg},2b} \left(\frac{\rho}{\rho_{\text{t,Liq}}} \right)^{\varepsilon_{\text{reg},2a}} \left(\frac{\rho}{\rho_{\text{reg,Ronc}}} \right)^{-2\varepsilon_{\text{reg},2b}} \exp \left(- \left(\frac{\rho}{\rho_{\text{reg,Ronc}}} \right)^{-\varepsilon_{\text{reg},2b}} \right) \\ &\times \left\{ -\varepsilon_{\text{reg},2b} + (1 - 2\varepsilon_{\text{reg},2a} + \varepsilon_{\text{reg},2b}) \left(\frac{\rho}{\rho_{\text{reg,Ronc}}} \right)^{\varepsilon_{\text{reg},2b}} \right\} \\ &+ \alpha_{\text{reg},2} \varepsilon_{\text{reg},2a} (\varepsilon_{\text{reg},2a} - 1) \left(\frac{\rho}{\rho_{\text{t,Liq}}} \right)^{\varepsilon_{\text{reg},2a}} \left(1 - \exp \left(- \left(\frac{\rho}{\rho_{\text{reg,Ronc}}} \right)^{\varepsilon_{\text{reg},2b}} \right) \right) \end{aligned} \quad (86)$$

$$\begin{aligned}
\rho^2 m''(\rho) = & \alpha_{m,4} + \alpha_{m,3} \left(\frac{\rho}{\rho_c} \right)^{\frac{3}{2}} \exp\left(-\frac{\rho}{\rho_c}\right) \left(\frac{3}{4} - 3\frac{\rho}{\rho_c} + \left(\frac{\rho}{\rho_c} \right)^2 \right) \\
& + \frac{3}{2} \alpha_{m,2} \left(\frac{\rho}{\rho_{t,Liq}} \right)^{\frac{3}{2}} \exp\left(-\left(\frac{\rho}{\rho_{t,Liq}} \right)^{\frac{3}{2}}\right) \left(1 + \frac{3}{2} \left(-1 + \left(\frac{\rho}{\rho_{t,Liq}} \right)^{\frac{3}{2}} \right) \right) + \rho^2 m''_{\text{Ronc}}(\rho)
\end{aligned} \tag{87}$$

$$\begin{aligned}
\rho^2 m''_{\text{Ronc}} \left(\rho \geq \frac{M}{12.9} \text{ g/cm}^3 \right) = & \left(\frac{\rho + \rho_{m,\text{Ronc}}}{\rho_{m,\text{Ronc}}} \right)^{\varepsilon_{m,5a}} \exp\left(-\exp\left(\left(\frac{\rho_{m,\text{Ronc}}}{\rho} \right)^{\varepsilon_{m,5b}}\right)\right) \\
& \times \left\{ \alpha_{m,4} \left[-1 + 2\varepsilon_{m,5a} \frac{\rho}{\rho + \rho_{m,\text{Ronc}}} + 2\varepsilon_{m,5b} \left(\frac{\rho_{m,\text{Ronc}}}{\rho} \right)^{\varepsilon_{m,5b}} \exp\left(\left(\frac{\rho_{m,\text{Ronc}}}{\rho} \right)^{\varepsilon_{m,5b}}\right) \right] \right. \\
& + \left(\alpha_{m,1} + \alpha_{m,4} \ln\left(\frac{\rho}{\rho_c}\right) \right) \left[\varepsilon_{m,5a} (\varepsilon_{m,5a} - 1) \left(\frac{\rho}{\rho + \rho_{m,\text{Ronc}}} \right)^2 \right. \\
& - \varepsilon_{m,5b}^2 \left(\frac{\rho_{m,\text{Ronc}}}{\rho} \right)^{2\varepsilon_{m,5b}} \exp\left(\left(\frac{\rho_{m,\text{Ronc}}}{\rho} \right)^{\varepsilon_{m,5b}}\right) \left(1 - \exp\left(\left(\frac{\rho_{m,\text{Ronc}}}{\rho} \right)^{\varepsilon_{m,5b}}\right) \right) \\
& \left. \left. - \varepsilon_{m,5b} \left(\frac{\rho_{m,\text{Ronc}}}{\rho} \right)^{\varepsilon_{m,5b}} \exp\left(\left(\frac{\rho_{m,\text{Ronc}}}{\rho} \right)^{\varepsilon_{m,5b}}\right) \left(1 + \varepsilon_{m,5b} - 2\varepsilon_{m,5a} \frac{\rho}{\rho + \rho_{m,\text{Ronc}}} \right) \right] \right\}
\end{aligned} \tag{88}$$

$$\begin{aligned}
\rho^2 n''_{\text{nonreg}} (\rho \leq \rho_{t,Liq}) = & \left(\frac{\rho_{t,Liq}}{\rho - \rho_{t,Liq}} \right)^2 \left\{ \alpha_{\text{nonreg},1} \left(\frac{\rho}{\rho_{t,\text{Gas}}} \right)^{\varepsilon_{\text{nonreg},1a}} \exp\left(-\left(\frac{\rho_{t,Liq}}{\rho_{t,\text{Gas}}} \right)^{\varepsilon_{\text{nonreg},1b}} \left(\frac{\rho}{\rho_{t,Liq} - \rho} \right)^{\varepsilon_{\text{nonreg},1b}} \right) \right. \\
& \times \left[\varepsilon_{\text{nonreg},1a} (\varepsilon_{\text{nonreg},1a} - 1) \left(\frac{\rho}{\rho_{t,Liq}} - 1 \right)^2 + \varepsilon_{\text{nonreg},1b}^2 \left(\frac{\rho_{t,Liq}}{\rho_{t,\text{Gas}}} \right)^{2\varepsilon_{\text{nonreg},1b}} \left(\frac{\rho}{\rho_{t,Liq} - \rho} \right)^{2\varepsilon_{\text{nonreg},1b}} \right. \\
& + \varepsilon_{\text{nonreg},1b} \left(\frac{\rho_{t,Liq}}{\rho_{t,\text{Gas}}} \right)^{\varepsilon_{\text{nonreg},1b}} \left(\frac{\rho}{\rho_{t,Liq} - \rho} \right)^{\varepsilon_{\text{nonreg},1b}} \left(2(\varepsilon_{\text{nonreg},1a} - 1) \frac{\rho}{\rho_{t,Liq}} + 1 - 2\varepsilon_{\text{nonreg},1a} - \varepsilon_{\text{nonreg},1b} \right) \\
& \left. + \alpha_{\text{nonreg},2} \left(\frac{\rho}{\rho_{t,\text{Gas}}} \right)^{\varepsilon_{\text{nonreg},2a}} \exp\left(-\left(\frac{\rho_{t,Liq}}{\rho_{t,\text{Gas}}} \right)^{\varepsilon_{\text{nonreg},2b}} \left(\frac{\rho}{\rho_{t,Liq} - \rho} \right)^{\varepsilon_{\text{nonreg},2b}} \right) \right. \\
& \times \left[\varepsilon_{\text{nonreg},2a} (\varepsilon_{\text{nonreg},2a} - 1) \left(\frac{\rho}{\rho_{t,Liq}} - 1 \right)^2 + \varepsilon_{\text{nonreg},2b}^2 \left(\frac{\rho_{t,Liq}}{\rho_{t,\text{Gas}}} \right)^{2\varepsilon_{\text{nonreg},2b}} \left(\frac{\rho}{\rho_{t,Liq} - \rho} \right)^{2\varepsilon_{\text{nonreg},2b}} \right. \\
& \left. \left. + \varepsilon_{\text{nonreg},2b} \left(\frac{\rho_{t,Liq}}{\rho_{t,\text{Gas}}} \right)^{\varepsilon_{\text{nonreg},2b}} \left(\frac{\rho}{\rho_{t,Liq} - \rho} \right)^{\varepsilon_{\text{nonreg},2b}} \left(2(\varepsilon_{\text{nonreg},2a} - 1) \frac{\rho}{\rho_{t,Liq}} + 1 - 2\varepsilon_{\text{nonreg},2a} - \varepsilon_{\text{nonreg},2b} \right) \right] \right\}
\end{aligned} \tag{89}$$

$$\begin{aligned}
\rho^2 T_{\text{div}}''(\rho) &= \alpha_{\text{div},1} \left(\frac{\rho}{\rho_c} \right)^{\varepsilon_{\text{div},1a}} \exp \left(- \left(\frac{\rho}{\rho_c} \right)^{\varepsilon_{\text{div},1b}} \right) \\
&\times \left\{ \varepsilon_{\text{div},1a} (\varepsilon_{\text{div},1a} - 1) - \varepsilon_{\text{div},1b} (\varepsilon_{\text{div},1b} + 2\varepsilon_{\text{div},1a} - 1) \left(\frac{\rho}{\rho_c} \right)^{\varepsilon_{\text{div},1b}} + \varepsilon_{\text{div},1b}^2 \left(\frac{\rho}{\rho_c} \right)^{2\varepsilon_{\text{div},1b}} \right\} \\
&+ \alpha_{\text{div},2} \left(\frac{\rho}{\rho_{\text{t,Liq}}} \right)^{\varepsilon_{\text{div},2a}} \exp \left(- \left(\frac{\rho}{\rho_{\text{t,Liq}}} \right)^{\varepsilon_{\text{div},2b}} \right) \\
&\times \left\{ \varepsilon_{\text{div},2a} (\varepsilon_{\text{div},2a} - 1) - \varepsilon_{\text{div},2b} (\varepsilon_{\text{div},2b} + 2\varepsilon_{\text{div},2a} - 1) \left(\frac{\rho}{\rho_{\text{t,Liq}}} \right)^{\varepsilon_{\text{div},2b}} + \varepsilon_{\text{div},2b}^2 \left(\frac{\rho}{\rho_{\text{t,Liq}}} \right)^{2\varepsilon_{\text{div},2b}} \right\}
\end{aligned} \tag{90}$$

$$\begin{aligned}
\rho^2 n_{\text{crit}}''(\rho) &= \alpha_{\text{crit},a} \left(\frac{\rho}{\rho - \rho_c} \right)^2 \left(\frac{\rho}{\rho_c} \right)^{\varepsilon_{\text{crit},a}} \exp \left[- \left(\left(\alpha_{\text{crit},b} \frac{\rho - \rho_c}{\rho_c} \right)^2 \right)^{\varepsilon_{\text{crit},b}} \right] \\
&\times \left\{ \varepsilon_{\text{crit},a} (\varepsilon_{\text{crit},a} - 1) \left(\frac{\rho - \rho_c}{\rho} \right)^2 + 4\varepsilon_{\text{crit},b}^2 \left(\left(\alpha_{\text{crit},b} \frac{\rho - \rho_c}{\rho_c} \right)^2 \right)^{2\varepsilon_{\text{crit},b}} \right. \\
&\quad \left. - 2\varepsilon_{\text{crit},b} \left(\left(\alpha_{\text{crit},b} \frac{\rho - \rho_c}{\rho_c} \right)^2 \right)^{\varepsilon_{\text{crit},b}} \left(-1 + 2\varepsilon_{\text{crit},b} + 2\varepsilon_{\text{crit},a} \left(1 - \frac{\rho_c}{\rho} \right) \right) \right\}
\end{aligned} \tag{91}$$

$$\begin{aligned}
\rho_c^2 \varepsilon_{\text{crit}}''(\rho) &= 2\varepsilon_{\text{crit},d} \varepsilon_{\text{crit},e}^2 \left(\frac{\rho_c}{\rho_{\text{crit},a}} \right)^2 \left(2\varepsilon_{\text{crit},e}^2 \left(\frac{\rho - \rho_{\text{crit},a}}{\rho_{\text{crit},a}} \right)^2 - 1 \right) \exp \left(- \left(\varepsilon_{\text{crit},e} \frac{\rho - \rho_{\text{crit},a}}{\rho_{\text{crit},a}} \right)^2 \right) \\
&+ 2\varepsilon_{\text{crit},f} \varepsilon_{\text{crit},g}^2 \left(\frac{\rho_c}{\rho_{\text{crit},b}} \right)^2 \left(2\varepsilon_{\text{crit},g}^2 \left(\frac{\rho - \rho_{\text{crit},b}}{\rho_{\text{crit},b}} \right)^2 - 1 \right) \exp \left(- \left(\varepsilon_{\text{crit},g} \frac{\rho - \rho_{\text{crit},b}}{\rho_{\text{crit},b}} \right)^2 \right)
\end{aligned} \tag{92}$$

It is interesting to note that the limits of $\rho^2 n_{\text{crit}}''(\rho)$, $\rho^2 T_{\text{div}}''(\rho)$, $\rho^2 n_{\text{nonreg}}''(\rho)$ and $\rho^2 n_{\text{reg}}''(\rho)$ are also equal to zero when $\rho \rightarrow 0$ and the limit of $\rho^2 m''(\rho)$ is same absolute value as that of the limit of $\rho m'(\rho)$ but with opposite sign.

List of Figure captions

Figure 1: Percentage pressure deviations on different isochors in the common region of data from NIST and from Ronchi. The lines are eyeguides.

Figure 2: Plot of $n_{\text{reg}}(\rho)$, $n_{\text{nonreg}}(\rho)$ and $n_{\text{crit}}(\rho)$ between $\rho = 0$ and $\rho = \rho_{\text{t,Liq}}$.

Figure 3: Plot of $m(\rho)$ from $\rho_{\text{t,Gas}}$ to $\rho_{\text{max,Ronc}}$.

Figure 4: Plot of $T_{\text{div}}(\rho)$ and $T_{\text{sat}}(\rho)$ from $\rho_{\text{t,Gas}}$ to $\rho_{\text{t,Liq}}$. The curve $T_{\text{sat}}(\rho)$ is deduced from the NIST data.

Figure 5: Representation of $P - P_{C_r}$ versus temperature T for different isochors with $\rho < \rho_{\text{t,Liq}}$.

Figure 6: Plot of $\tilde{u}_0(\rho)$ and $\tilde{s}_0(\rho)$ between $\rho = 0$ to $\rho = \rho_{\text{max,Ronc}}$.

Figure 7: Percentage deviations $\Delta C_{V,\text{nonreg}}^r = \left(C_{V,\text{nonreg}}^r \text{ from Eq. (18)} - C_{V,\text{nonreg}}^r \text{ from Eq. (55)} \right) / C_{V,\text{nonreg}}^r \text{ from Eq. (18)}$ for the

single phase region in the temperature range from T_t to 160 K and the density range from $\rho_{\text{t,Gas}}$ to $\rho_{\text{t,Liq}}$.

Figure 8: Plot of C_V/R_A as a function of density from $\rho_{\text{t,Gas}}$ to $\rho_{\text{t,Liq}}$ for two isotherms (110 K and 140 K). The plotted curves correspond to values calculated from Eq. (1) with Eq. (53) to (57) and from TSW equations of state.

Figure 9: Plot of the melting pressure data determined by Zha *et al.*, Hardy *et al.*, Datchi *et al.*, Abramson and Jephcoat *et al.* The plotted curves correspond to values calculated from Eq. (67) (solid line), from Eq. (2) written by Datchi *et al.* (dashed curve) and from Eq. (1) written by Abramson (2011) (dot dashed curve).

Figure 10: Plot of the liquid density data on the melting line determined by Bridgman, Lahr *et al.*, Crawford *et al.*, Witzenburg *et al.* and L'Air Liquide. The plotted curves correspond to values calculated from the functions $T_{\text{m,Low}}(\rho)$ (dashed line) and $T_{\text{m,High}}(\rho)$ (solid line).

Figure 11: Percentage deviations $\Delta C_V = \left(C_V \begin{matrix} \text{from Tegeler } et \text{ al.} \\ \text{from Eq.(1)} \end{matrix} - C_V \begin{matrix} \text{calculated} \\ \text{from Tegeler } et \text{ al.} \end{matrix} \right) / C_V \begin{matrix} \text{calculated} \\ \text{from Tegeler } et \text{ al.} \end{matrix}$

from the TSW equations of state and from Eq. (1) in the range of density from $\rho_{t, Gas}$ to $\rho_{t, Liq}$.

The black lines correspond to values of ΔC_V equal to zero.

Figure 12: Isochoric heat capacity as a function of temperature (200 K to 2000 K) for 3 different liquid densities. The plotted curves correspond to values calculated from Eq. (1) and from TSW equations of state.

Figure 13: Plot of the isochoric heat capacity data determined by L'Air Liquide on the isotherm at 1100 K. The plotted curves correspond to values calculated from Eq. (1) and from TSW equations of state.

Figure 14: Isochoric heat capacity versus temperature at very high densities.

Figure 15: Percentage deviations of NIST internal energy data from values calculated from Eq. (39) along isochors up to 700 K. The error bars correspond to standard deviations. The lines are eyeguides.

Figure 16: percentage deviations of NIST entropy data from values calculated from Eq. (39) along isochors up to 700 K. The error bars correspond to standard deviations. The lines are eyeguides.

Figure 17: Tolerance diagram for densities calculated from inversion of Eq. (45). The red curve corresponds to the vapour pressure curve and the black one to the melting pressure curve.

Figure 18: Percentage deviations $\Delta \rho = (\rho_{L'Air Liquide} - \rho_{calc}) / \rho_{L'Air Liquide}$ of L'Air Liquide data on isobar 0.1 Mpa from inversion of Eq. (45) up to 1100 K. Values calculated from TSW equations are plotted for comparison. The lines are eyeguides.

Figure 19: Percentage deviations $\Delta \rho = (\rho_{L'Air Liquide} - \rho_{calc}) / \rho_{L'Air Liquide}$ of L'Air Liquide data on isobar 100 Mpa from inversion of Eq. (45) up to 1100 K. Values calculated from TSW equations of state are plotted for comparison. The lines are eyeguides.

Figure 20: Percentage deviations $\Delta\rho = (\rho_{L'Air\ Liquide} - \rho_{calc}) / \rho_{L'Air\ Liquide}$ of L'Air Liquide data on isotherm 1100 K from inversion of Eq. (45) up to 100 Mpa. Values calculated from TSW equations of state are plotted for comparison. The lines are eyeguides.

Figure 21: Percentage deviations of Ronchi data from Eq. (45) along isochors for densities less than $\rho_{t,Liq}$.

Figure 22: Percentage deviations of Ronchi data from Eq. (45) along isochors for densities greater than $\rho_{t,Liq}$.

Figure 23: Percentage deviations of Ronchi data from TSW equations of state along isochors for densities greater than $\rho_{t,Liq}$.

Figure 24: Percentage deviations $\Delta C_p = \left(C_p_{\text{from Tegeler et al.}} - C_p_{\text{from Eq. (68)}} \right) / C_p_{\text{from Tegeler et al.}}$ of

Tegeler *et al.* isobaric heat capacity from values calculated from Eq. (68) in the range of density from $\rho_{t,Gas}$ to $\rho_{t,Liq}$. The black lines correspond to values of ΔC_p equal to zero.

Figure 25: Representation of isobaric heat capacity from data of L'Air Liquide on the two isotherms 700 K and 1100 K. The plotted curves correspond to values calculated from Eq. (39) and from TSW equations of state.

Figure 26: Percentage deviations $\Delta c = (c_{\text{from Tegeler et al.}} - c_{\text{from Eq. (69)}}) / c_{\text{from Tegeler et al.}}$ of Tegeler *et al.* sound speed from values calculated from Eq. (69) in the range of density from $\rho_{t,Gas}$ to $\rho_{t,Liq}$. The black lines correspond to values of Δc equal to zero.

Figure 27: Percentage deviations $\Delta c = (c_{L'Air\ Liquide} - c_{calc}) / c_{L'Air\ Liquide}$ of L'Air Liquide data on isotherm 153.15 K from Eq. (69) up to 30.4 Mpa. Values calculated from TSW equations of state are plotted for comparison. The lines are eyeguides.

Figure 28: Percentage deviations $\Delta c = (c_{L'Air Liquide} - c_{calc})/c_{L'Air Liquide}$ of L'Air Liquide data on isobar 1000 atmospheres from Eq. (69) up to 473.15 K. Values calculated from TSW equations of state are plotted for comparison. The lines are eyeguides.

Figure 29: Representation of the dimensionless isothermal throttling coefficient. The plotted curves correspond to values calculated from Eq. (70) and from TSW equations of state.

Figure 30: The so-called “ideal curves” calculated from Eq. (39) and from TSW equations of state in the range of temperature covered by the data from NIST and from Ronchi. The curves are plotted in a double logarithmic P/P_c vs T/T_c diagram.

Figure 31: Representation of the Poisson adiabatic curves calculated from Eq. (39) and from TSW equations of state for the two different initial states corresponding to those of van Thiel *et al.*

Figure 32: Representation of the isochoric heat capacity in the vicinity of the critical point. The data points are from Voronel' *et al.* (1967 and 1973) and the plotted curves correspond to values calculated from Eq. (1) and from TSW equations of state.

Figure 33: Percentage deviations $\Delta y = (y_{NIST} - y_{calc})/y_{NIST}$ of the selected thermal data at saturation from values calculated from Eq. (39) in the range of temperature from T_t to 149.5K.

Figure 34: Representation of the saturated pressure vs density in the vicinity of the critical point (i.e. from 0.35 g/cm³ to 0.75 g/cm³). The plotted curves correspond to values calculated from Maxwell relations Eq. (50) to Eq. (52), from TSW equations of state and from the data of L'Air Liquide (1976).

Figure 35: Percentage deviations $\Delta P_{sat} = (P_{Tegeler et al.}(T_{sat}(\rho), \rho) - P(T_{sat}(\rho), \rho))/P_{Tegeler et al.}(T_{sat}(\rho), \rho)$ of Tegeler *et al.* saturated pressure from Eq. (45) in the range of density from $\rho_{t, Gas}$ to 0.85 g/cm³. The curve $T_{sat}(\rho)$ used is a fit with the data from NIST. The dashed lines correspond to the values $\Delta P_{sat} = \pm 0.2\%$.

Figure 36: Percentage deviations $\Delta L_v = (L_{v, \text{Tegeler et al.}} - L_{v, \text{from Eq. (39)}}) / L_{v, \text{Tegeler et al.}}$ of Tegeler *et al.* latent heat of vaporization from values calculated from Eq. (39) in the range of temperature from T_t to 149.5 K.

Figure 37: Representation of temperature vs. density for the spinodal states. The plotted curves correspond to the divergence curve of C_V and from calculated values using derivation of Eq. (45) or TSW equations of state. The data points are from Voronel *et al.* (1967 and 1973) and Baidakov *et al.* (1975)

Figure 38: Tolerance diagram for isobaric heat capacities calculated from Eq. (68) with the use of Eq. (45) for determining densities as function of pressure. The red curve corresponds to the vapour pressure curve and the black one to the melting pressure curve.

Figure 39: Tolerance diagram for sound speed calculated from Eq. (69) with the use of Eq. (45) for determining densities as function of pressure. The red curve corresponds to the vapour pressure curve and the black one to the melting pressure curve.

Figure 40: Tolerance diagram for densities calculated from inversion of Eq. (45) in the range of temperature from 700 K to 1100 K.

Figure 41: Tolerance diagram for isobaric heat capacities calculated from Eq. (68) with the use of Eq. (45) for determining densities as function of pressure in the range of temperature from 700 K to 1100 K.

Figure 42: Tolerance diagram for isochoric heat capacities calculated from Eq. (1) with the use of Eq. (45) for determining densities as function of pressure in the range of temperature from 700 K to 1100 K.

Figure 1

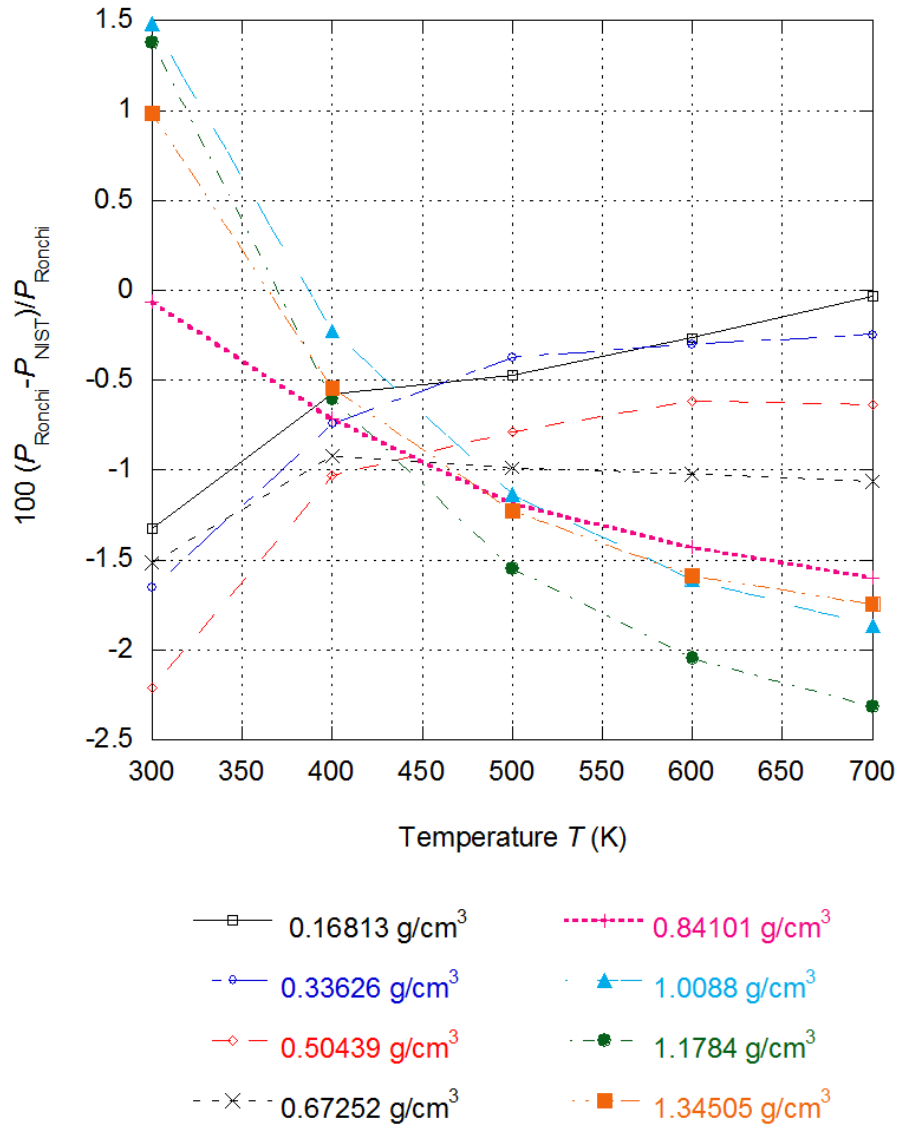


Figure 2

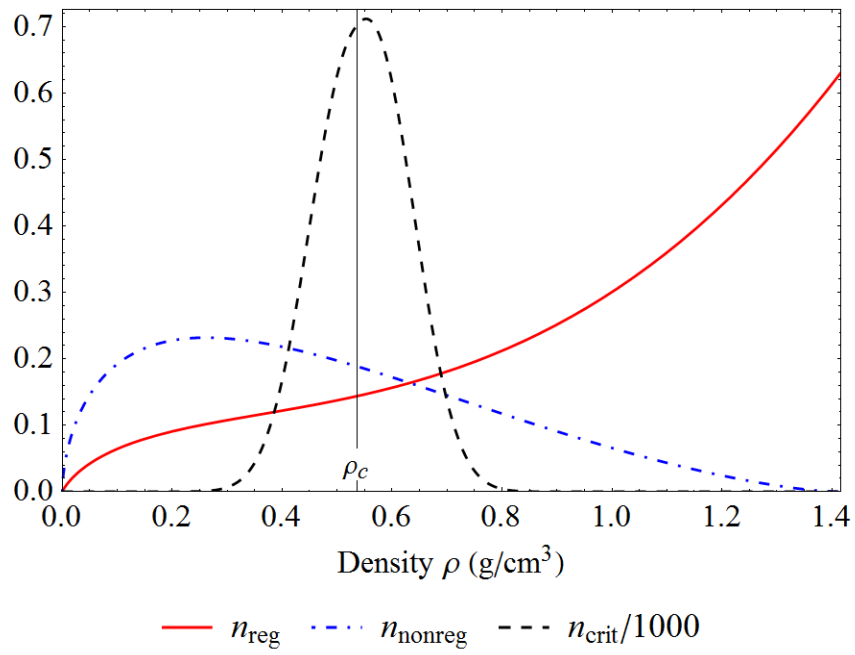


Figure 3

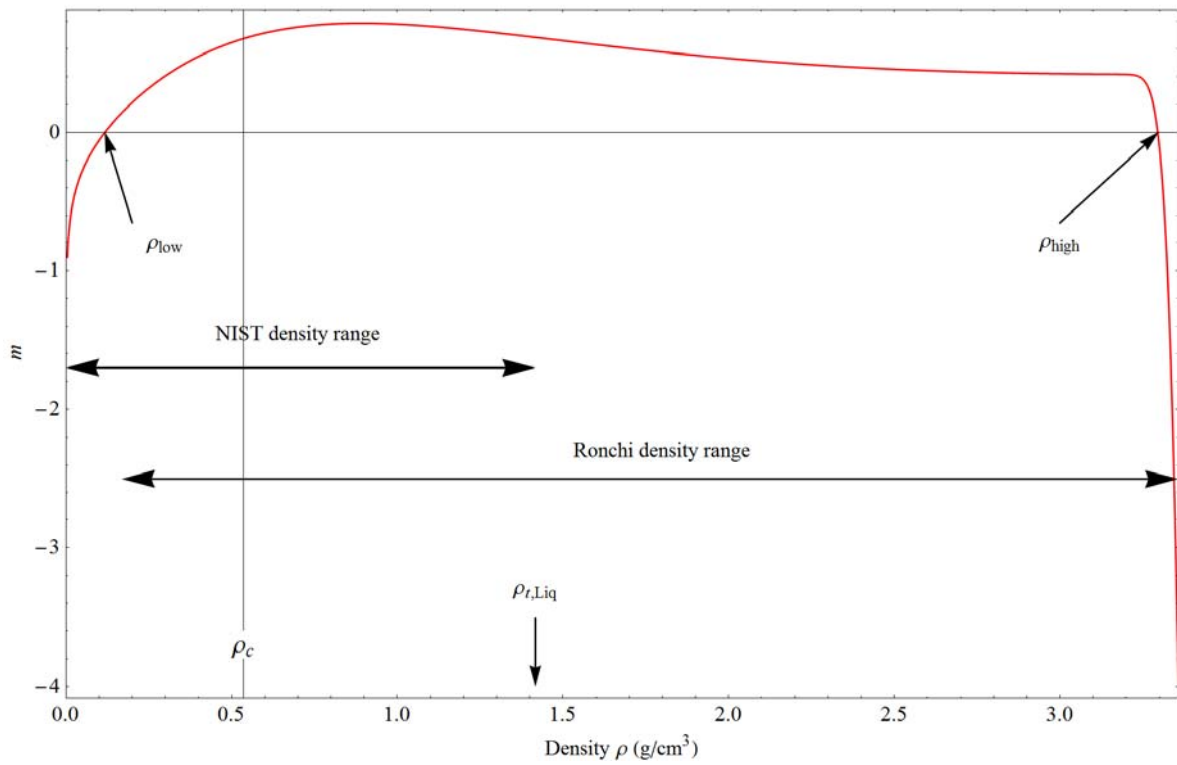


Figure 4

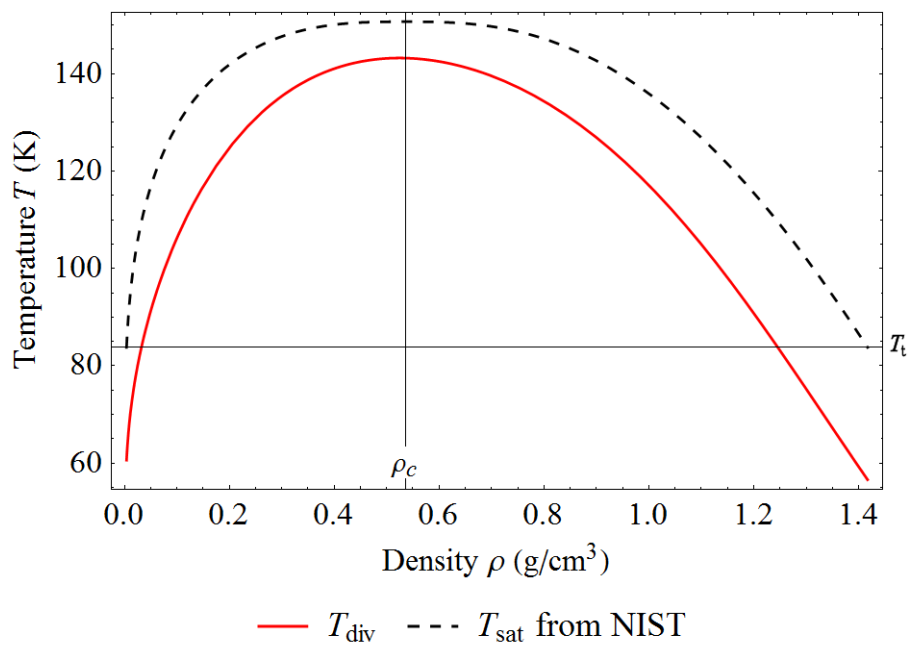


Figure 5

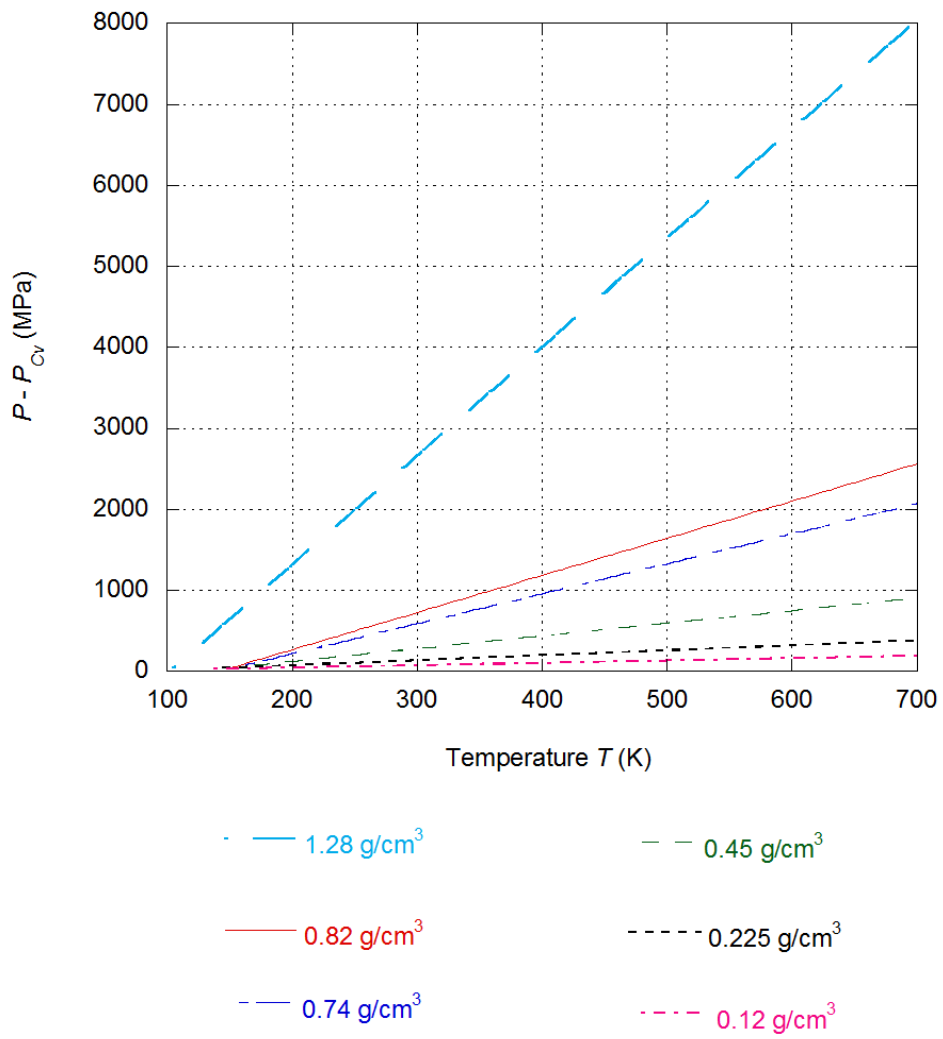


Figure 6

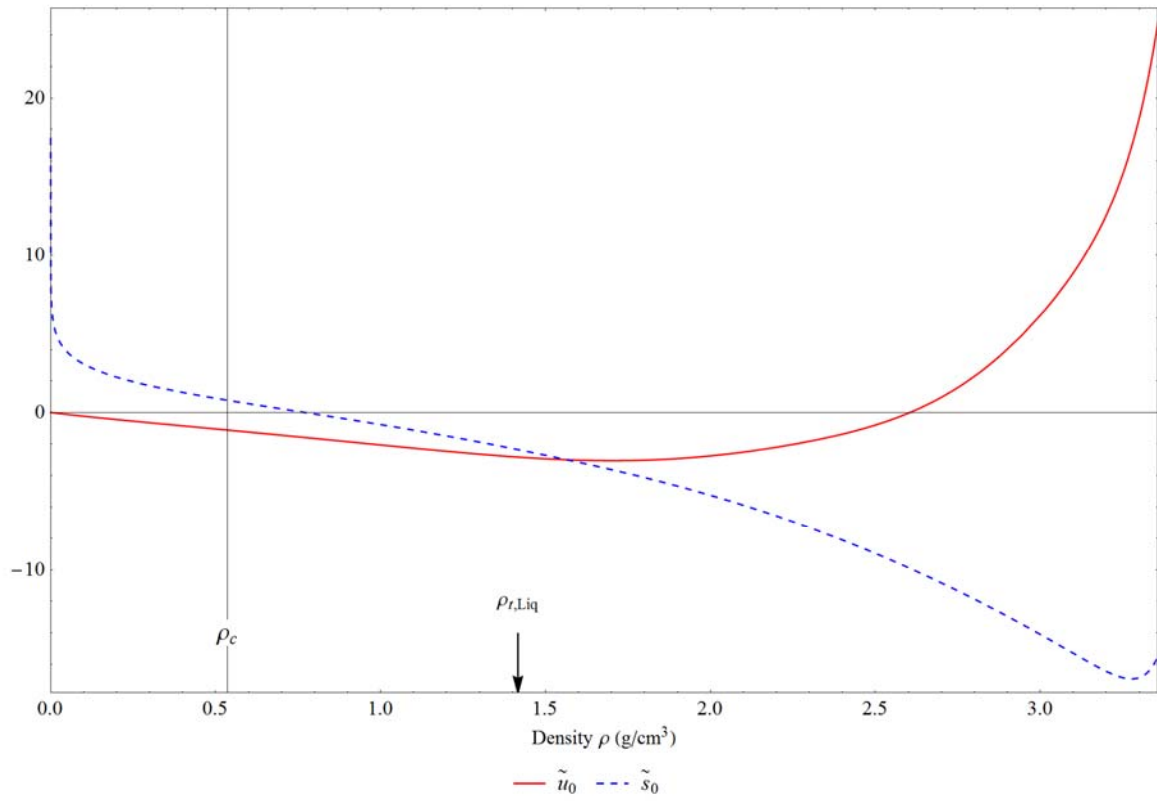


Figure 7

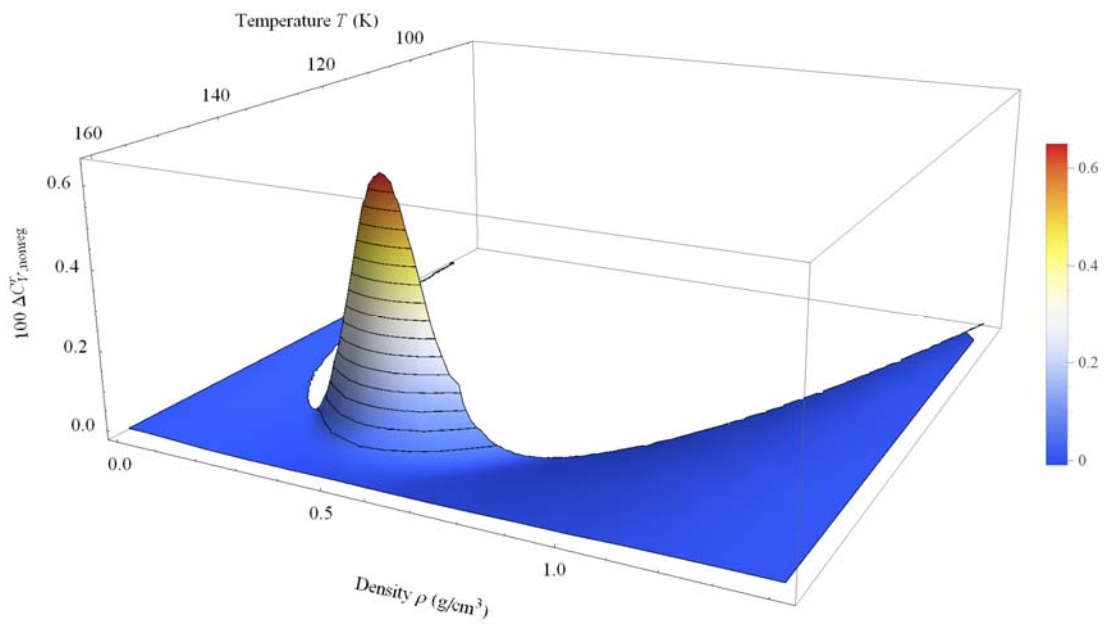
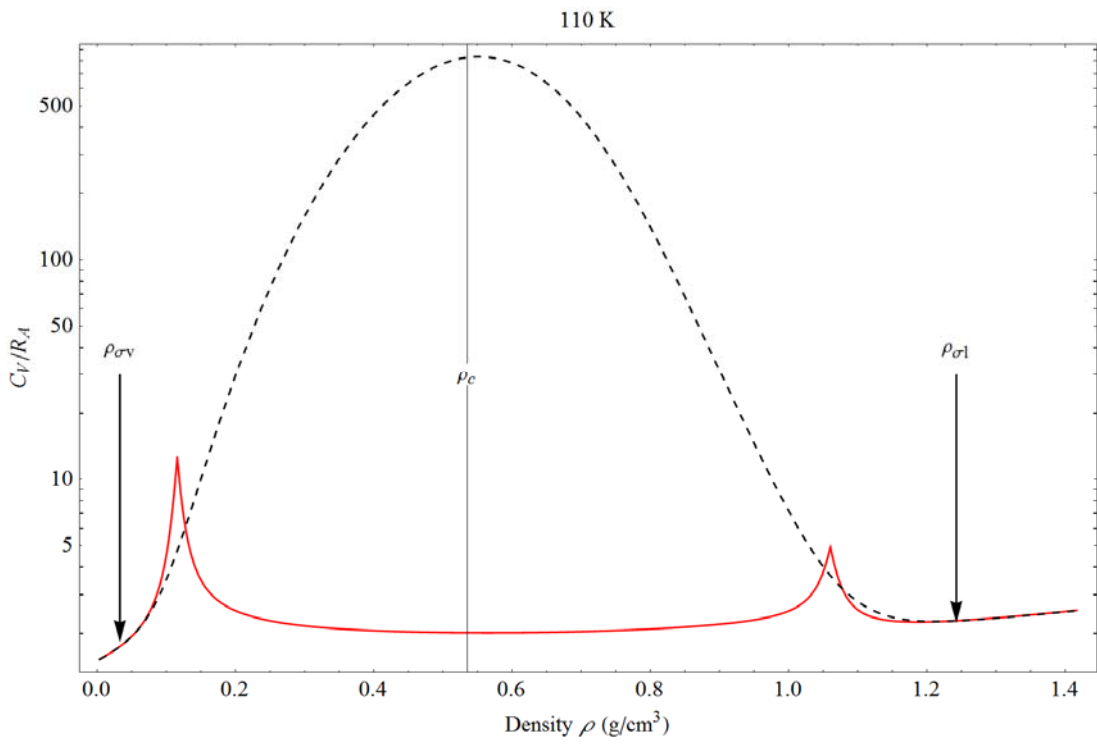


Figure 8

(a)



(b)

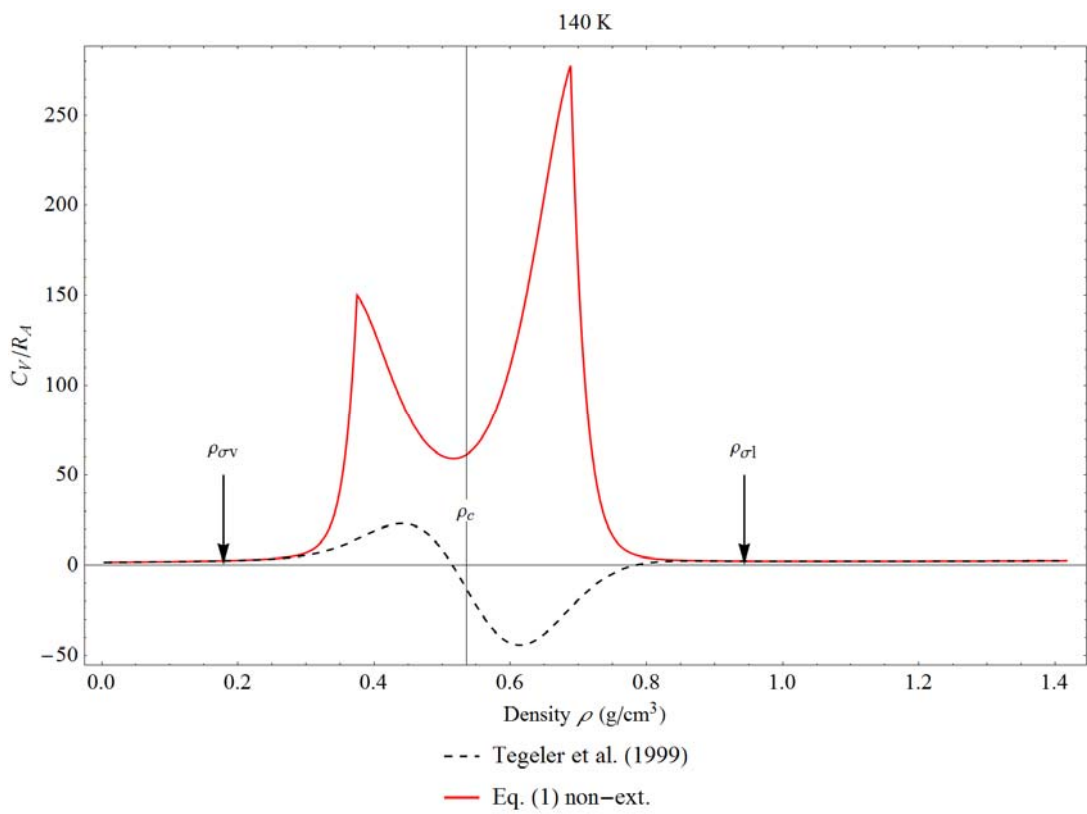
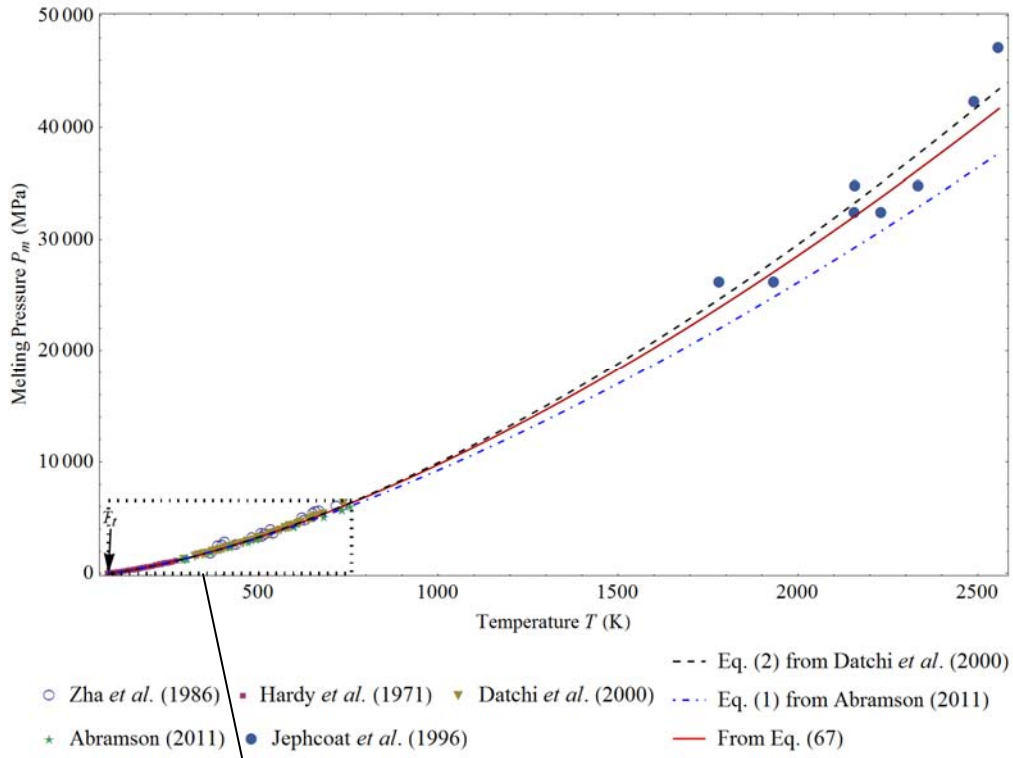


Figure 9

(a)



(b)

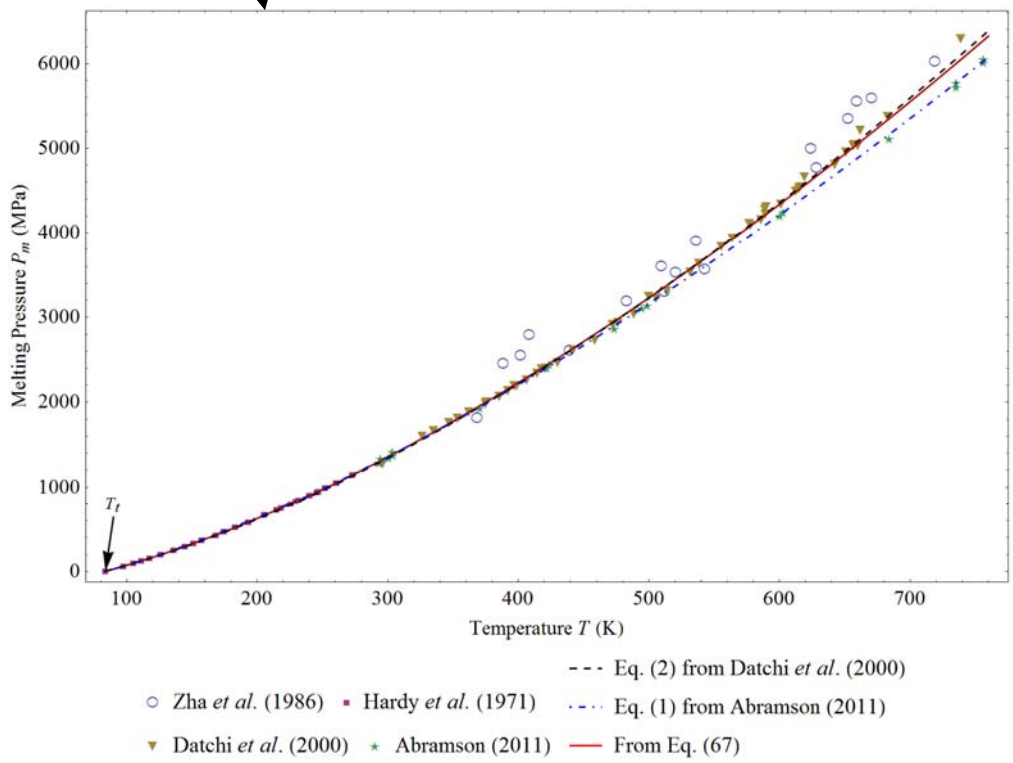


Figure 10

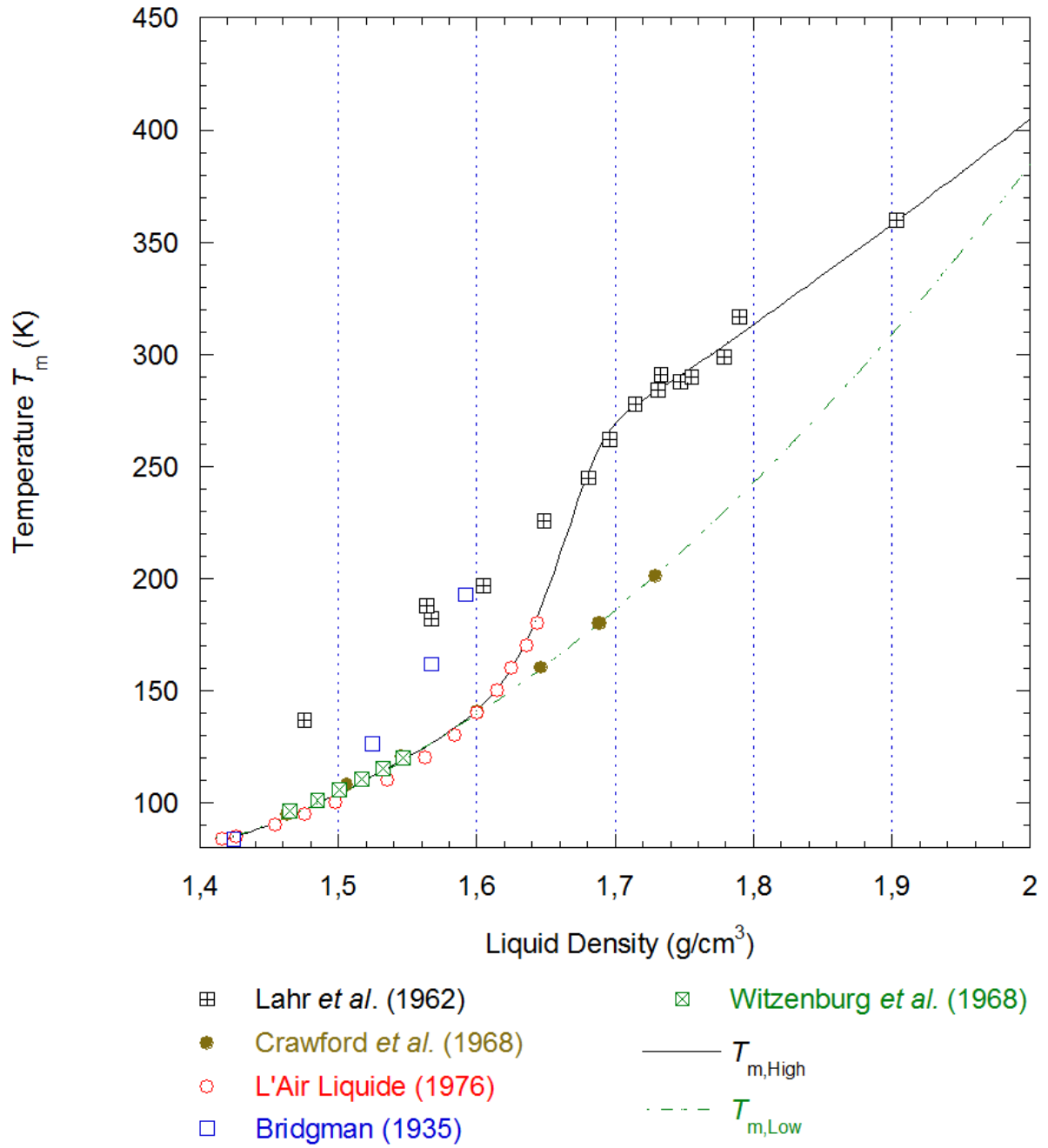
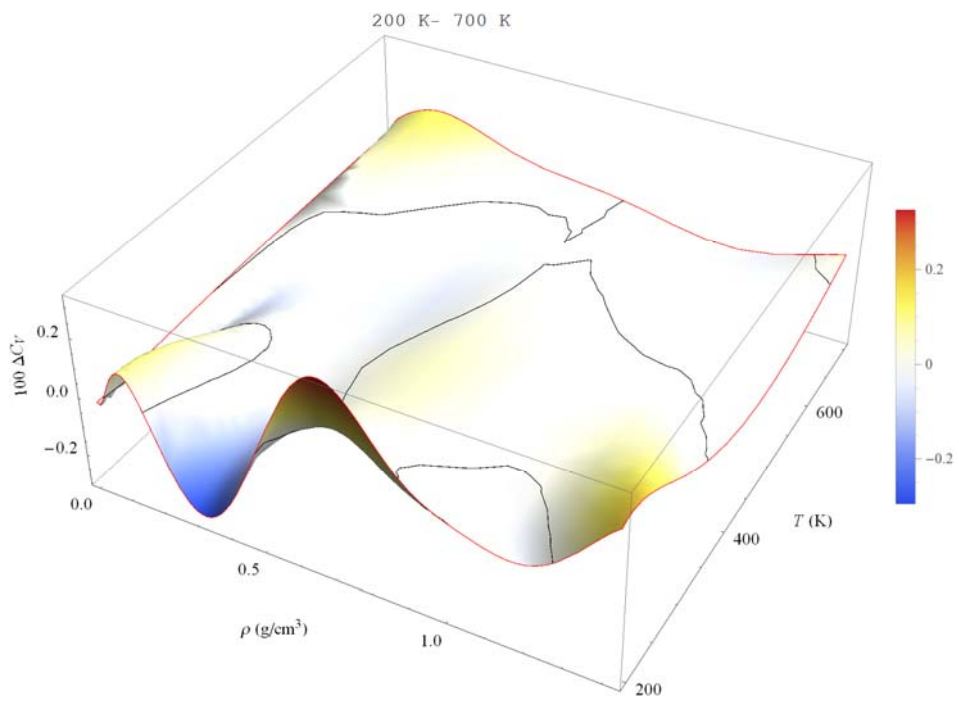


Figure 11

(a)



(b)

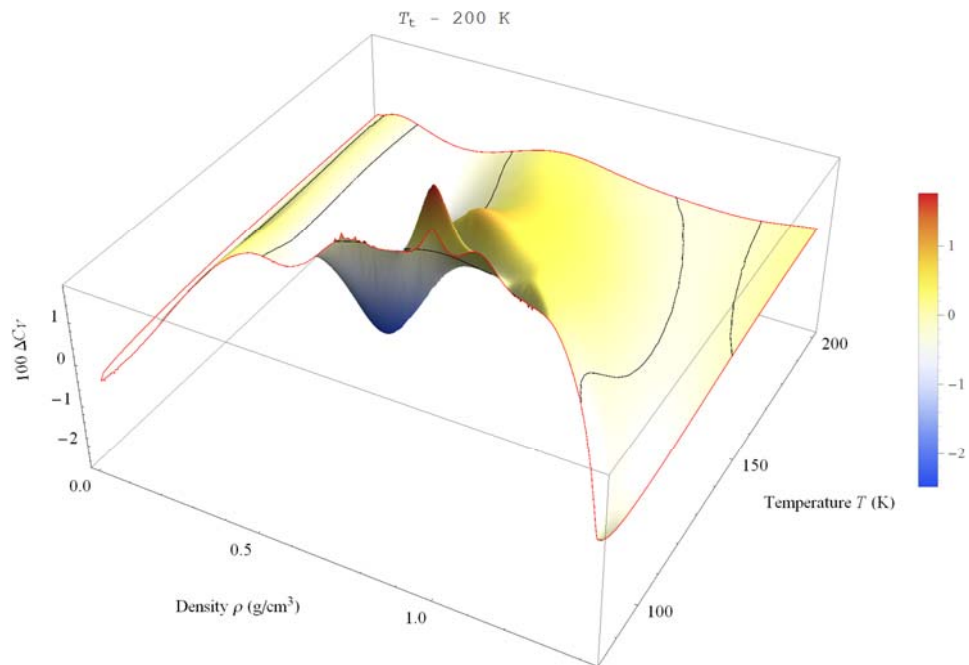


Figure 12

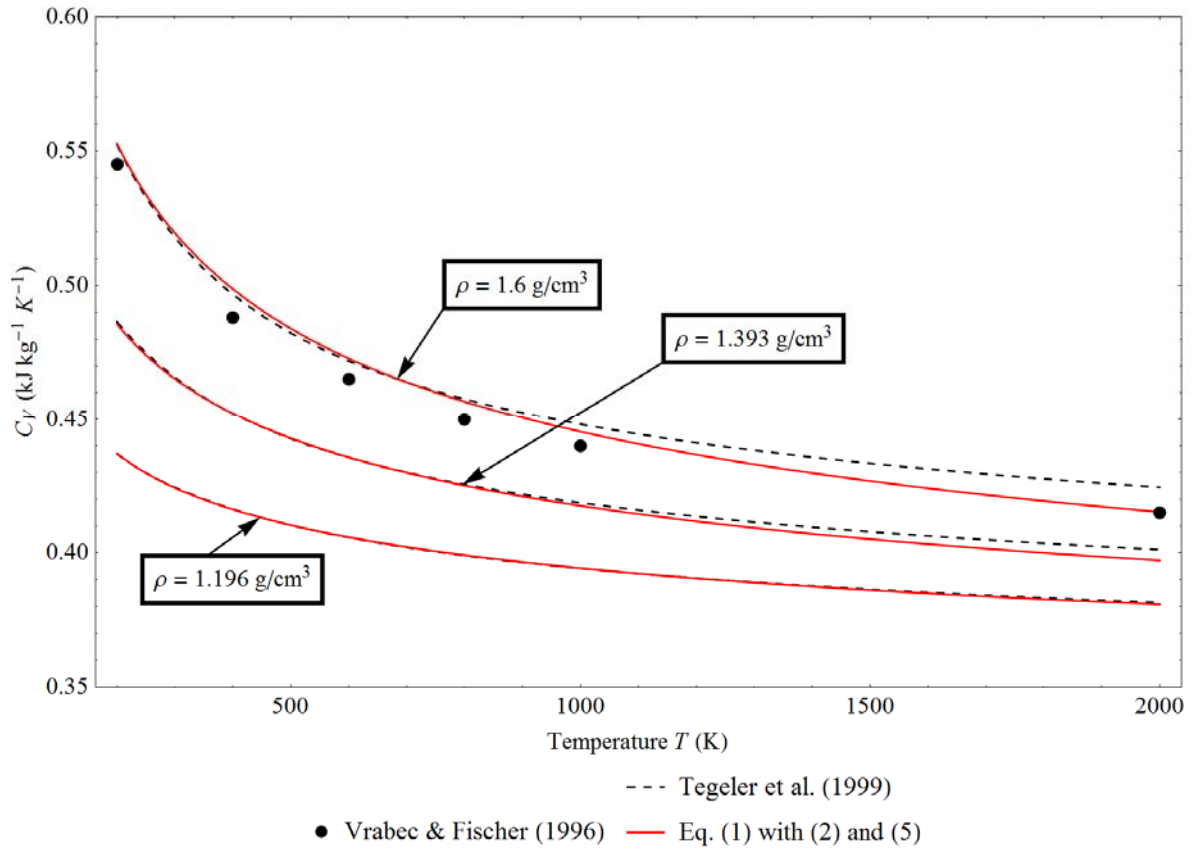


Figure 13

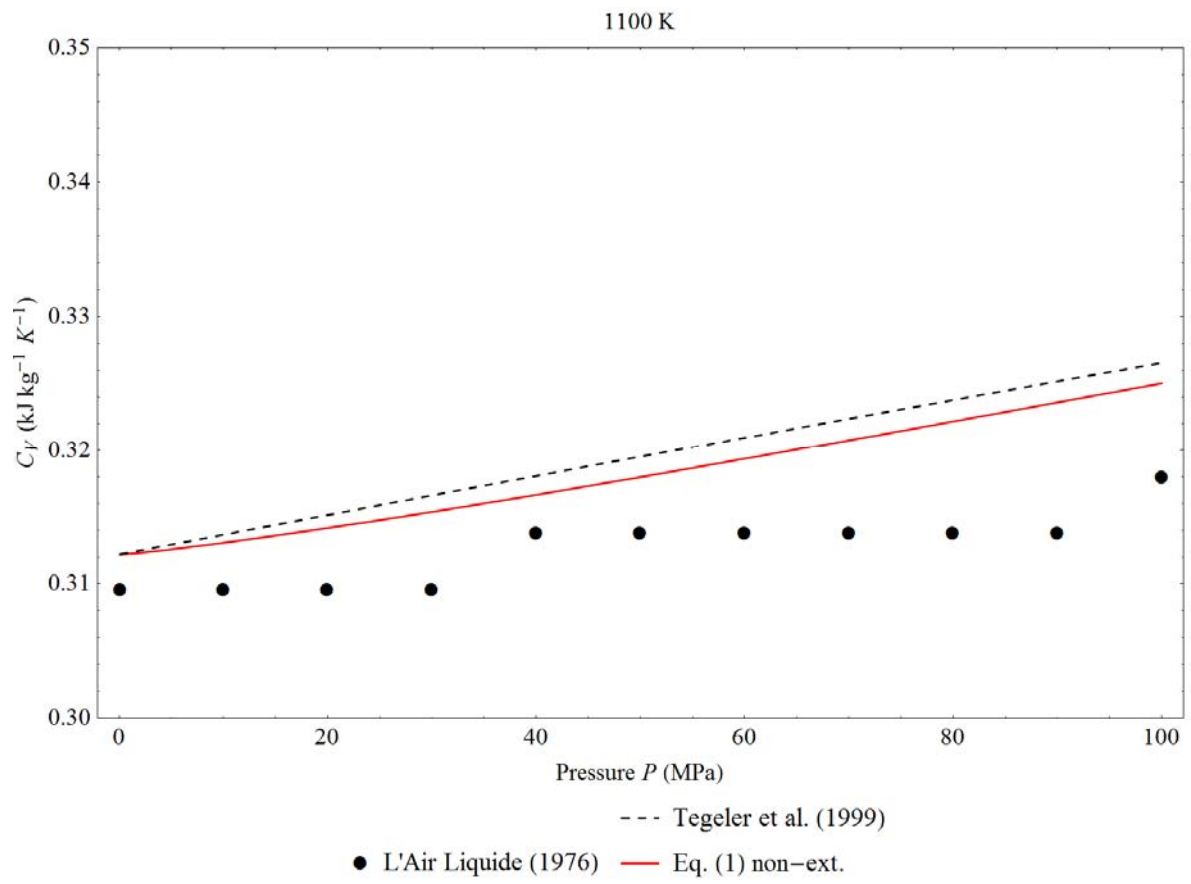


Figure 14

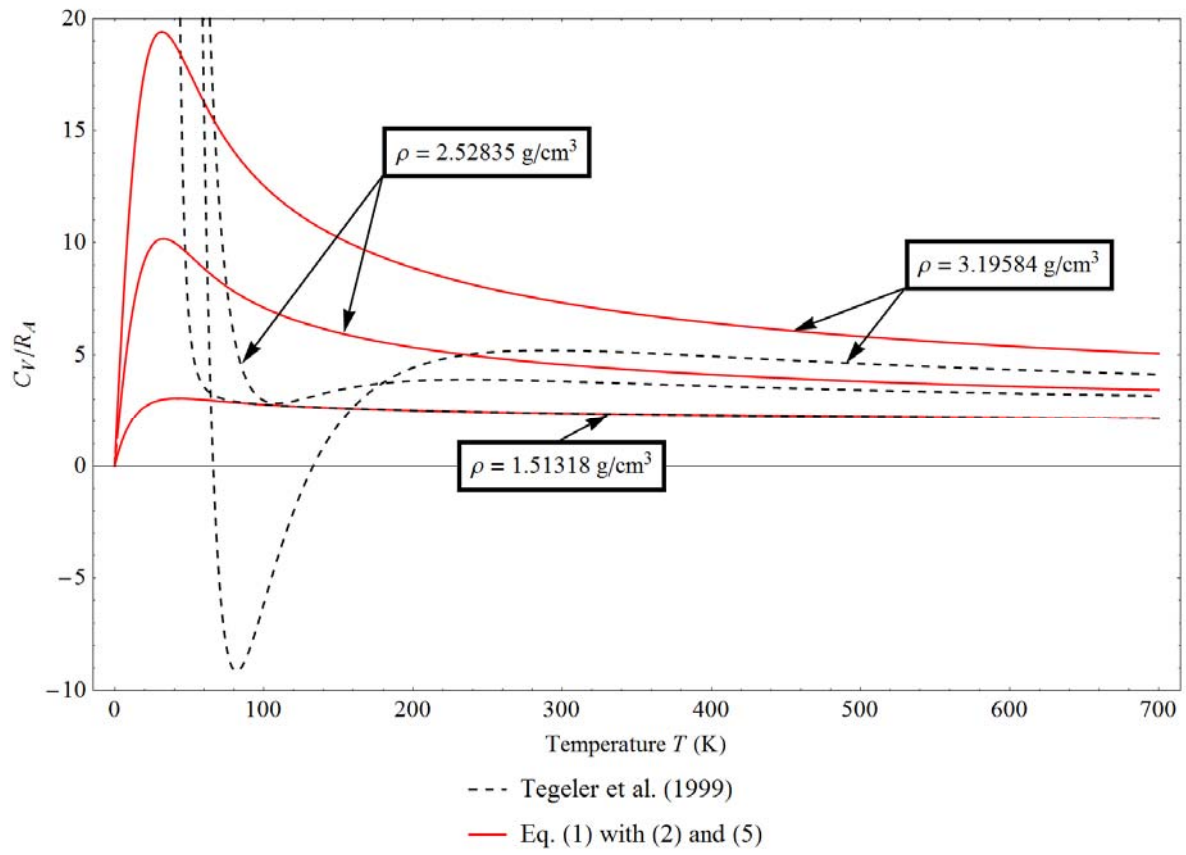


Figure 15

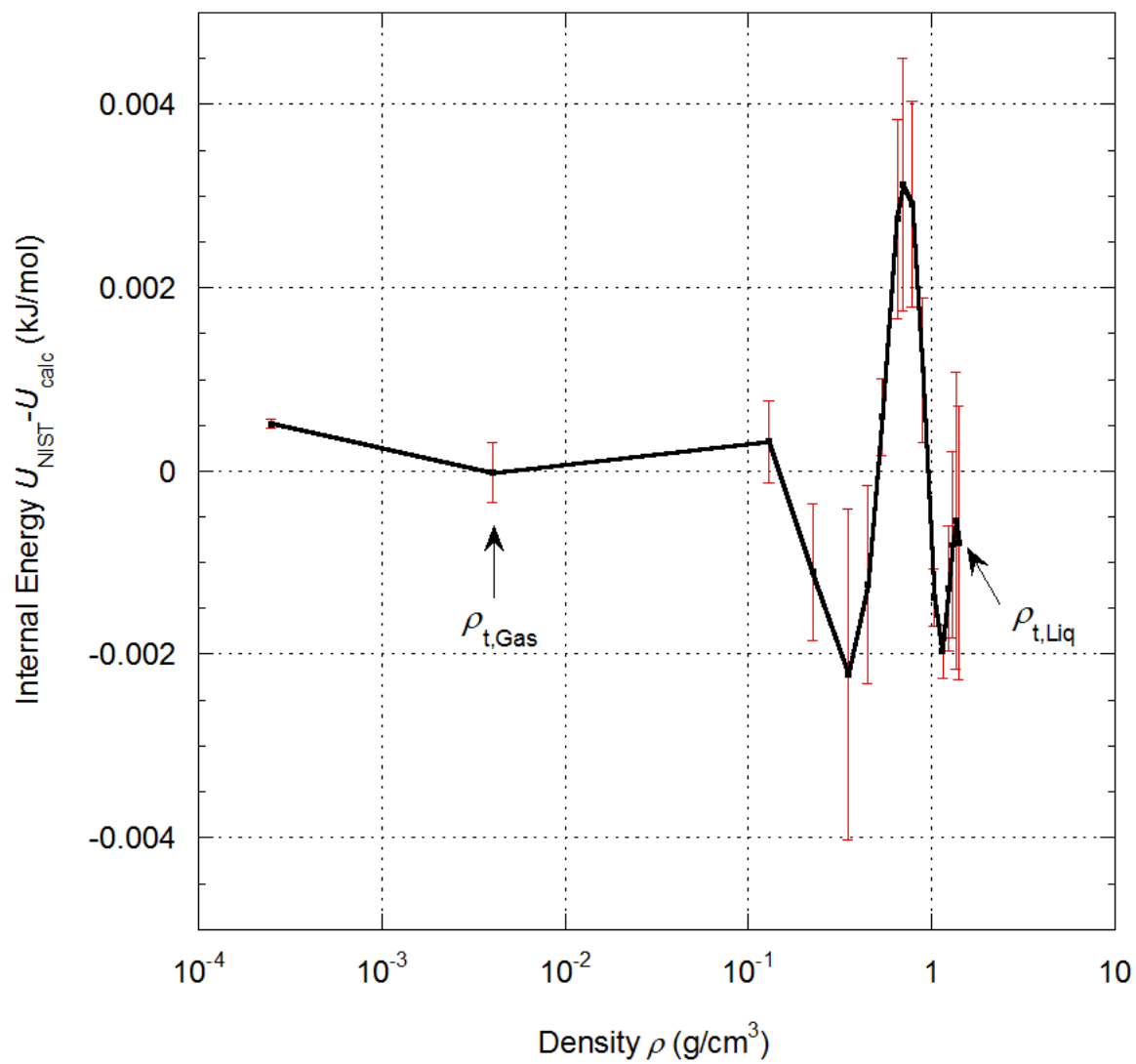


Figure 16

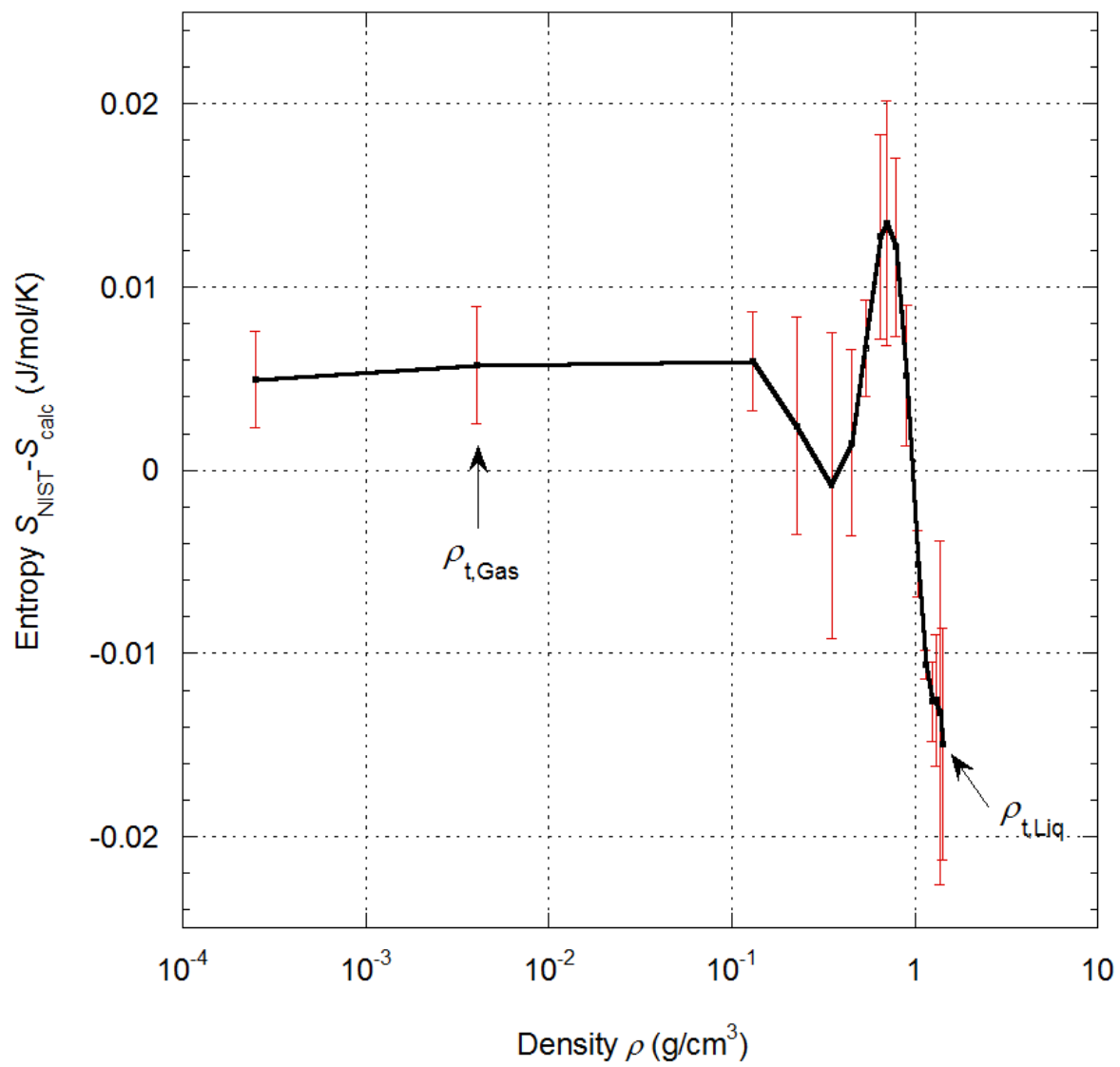


Figure 17

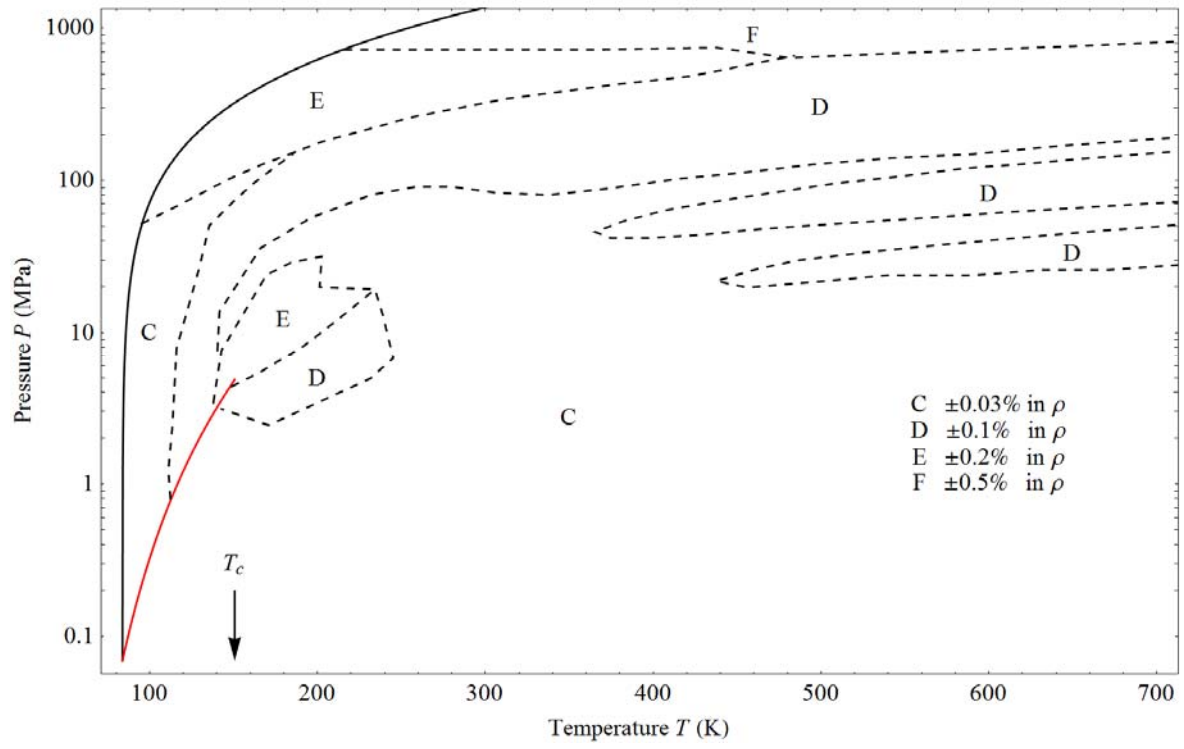
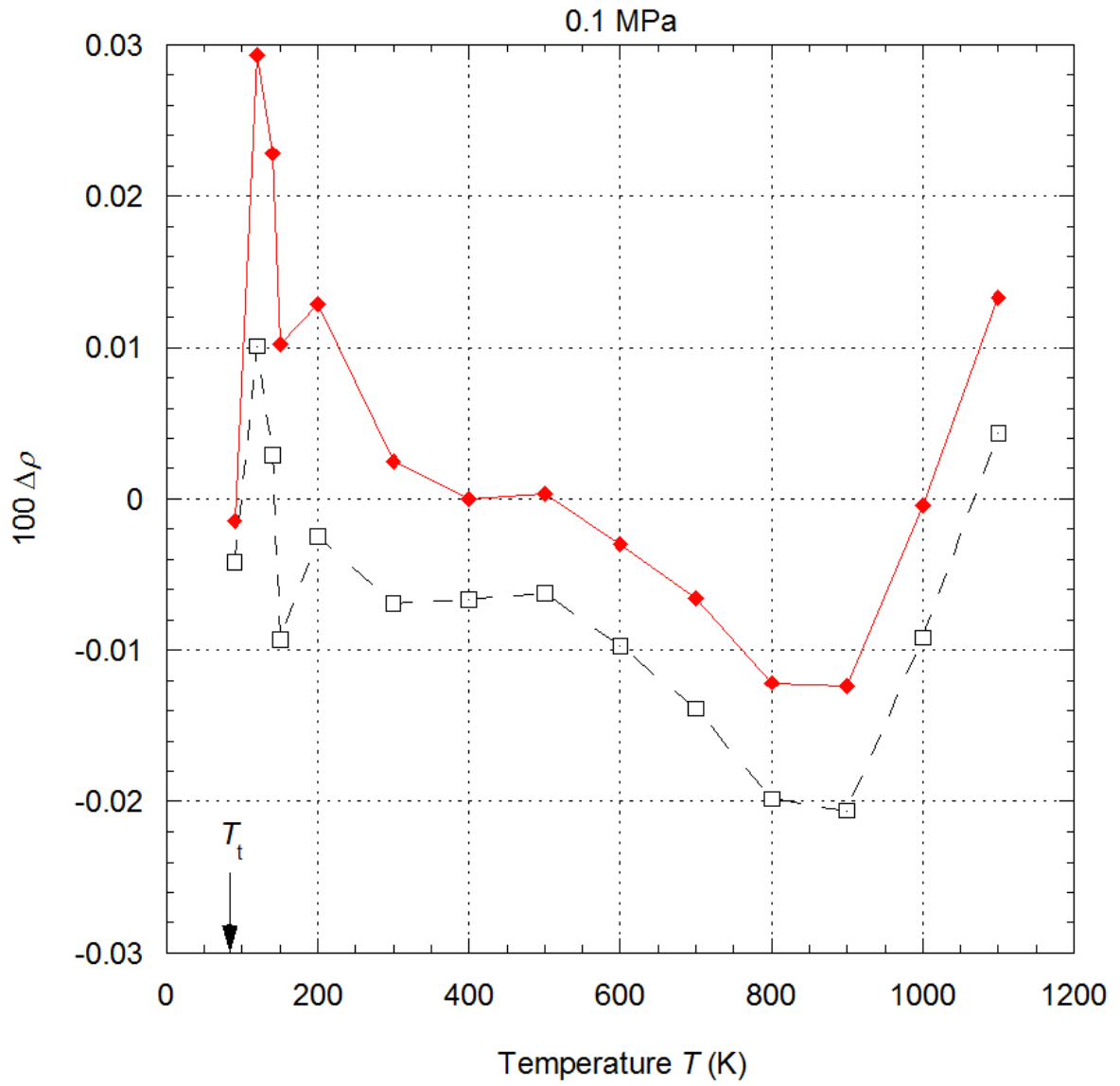
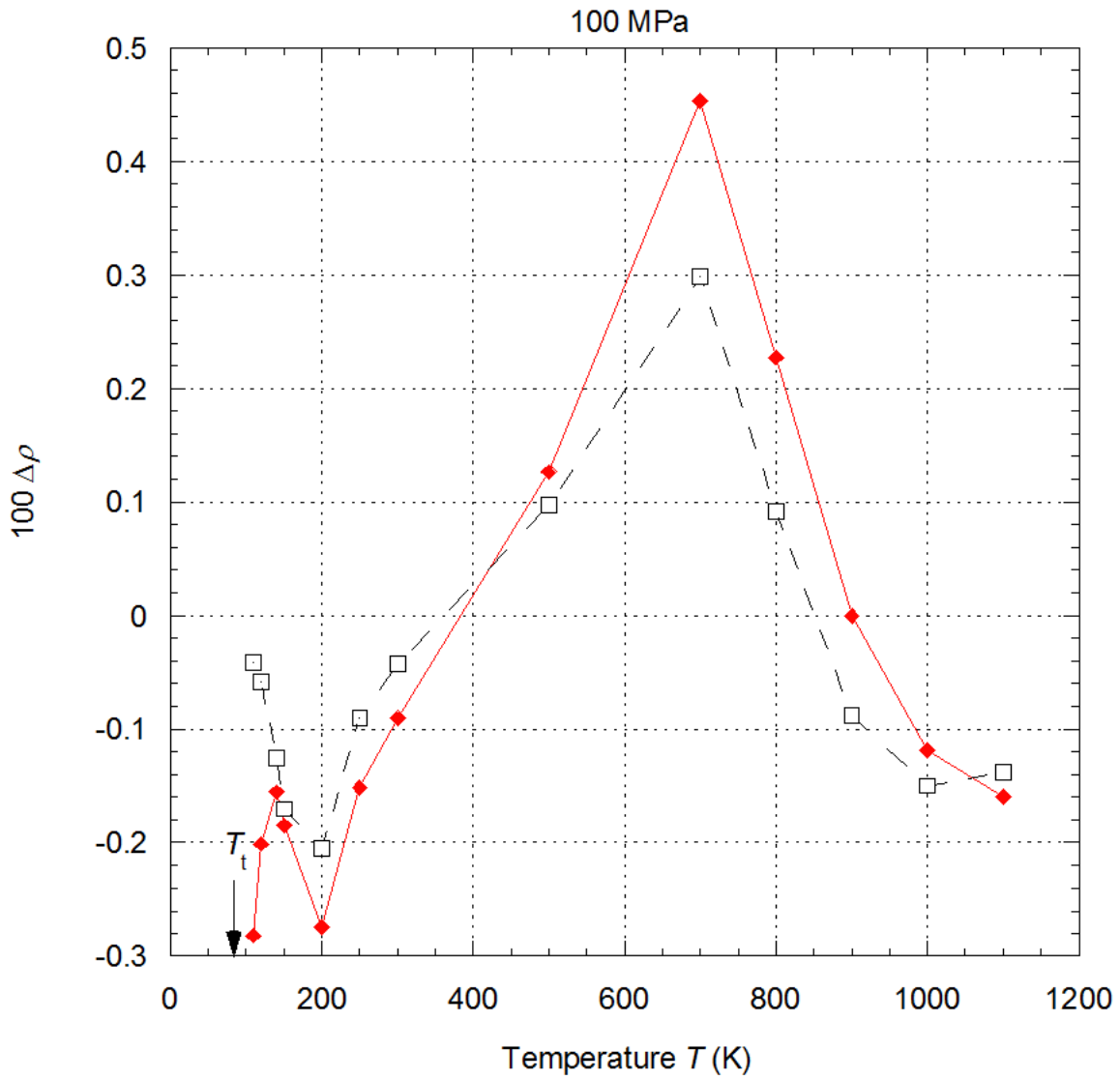


Figure 18



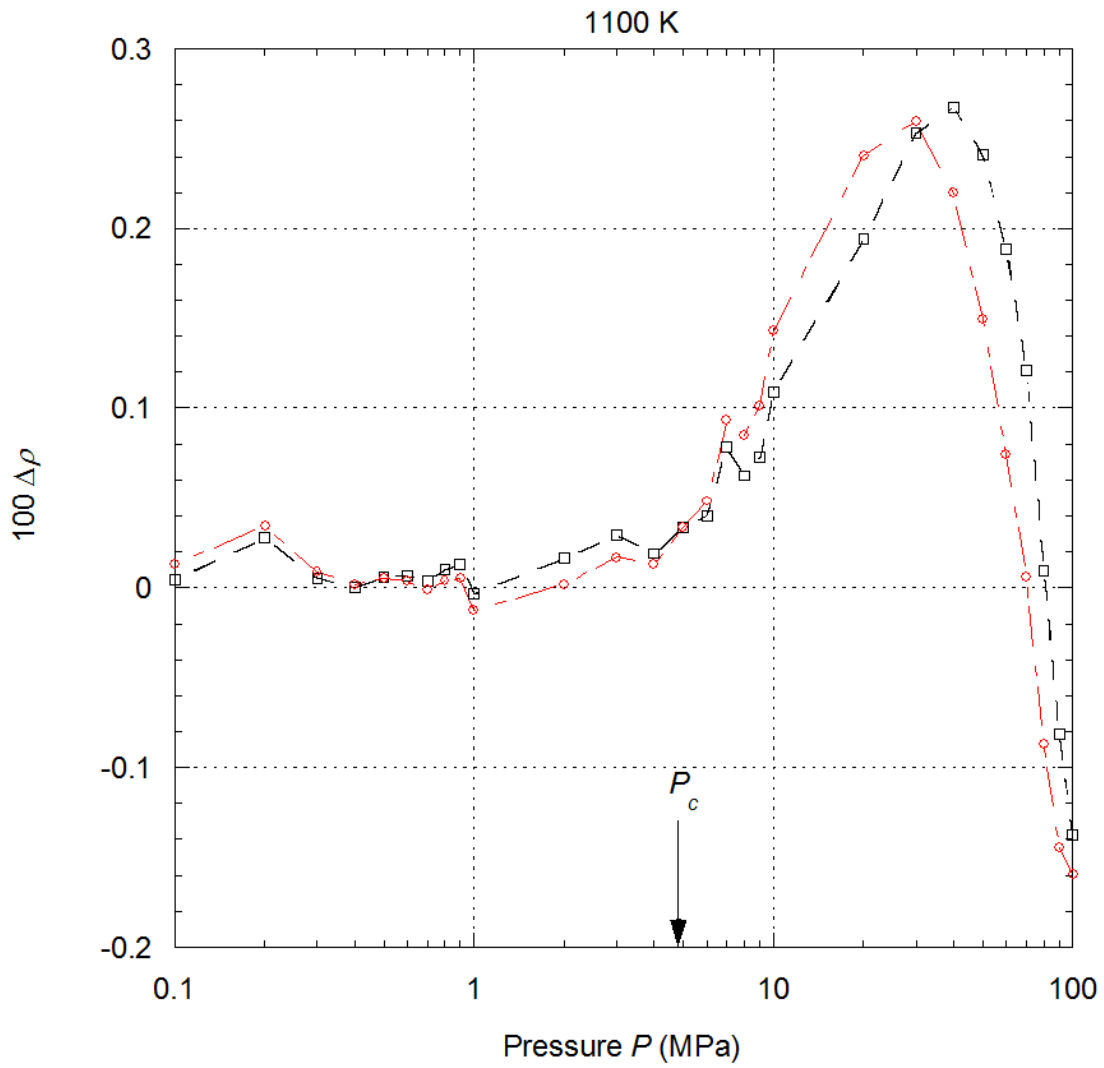
—◆— From inversion of Eq. (45) non-ext. -□- Tegeler *et al.* (1999)

Figure 19



—◆— From inversion of Eq. (45) non-ext. -□- Tegeler *et al.* (1999)

Figure 20



—□— Tegeler *et al.* (1999)

—○— From inversion of Eq. (45) non-ext.

Figure 21

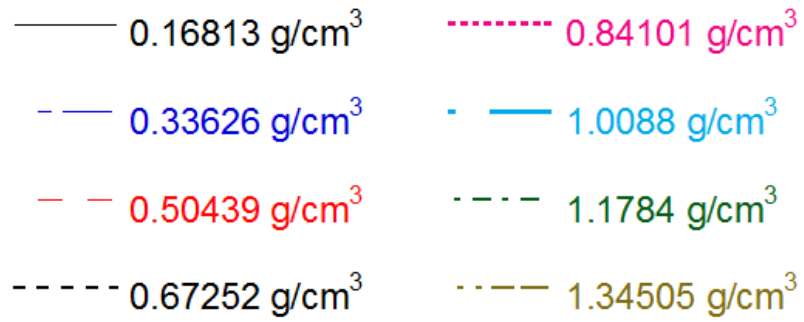
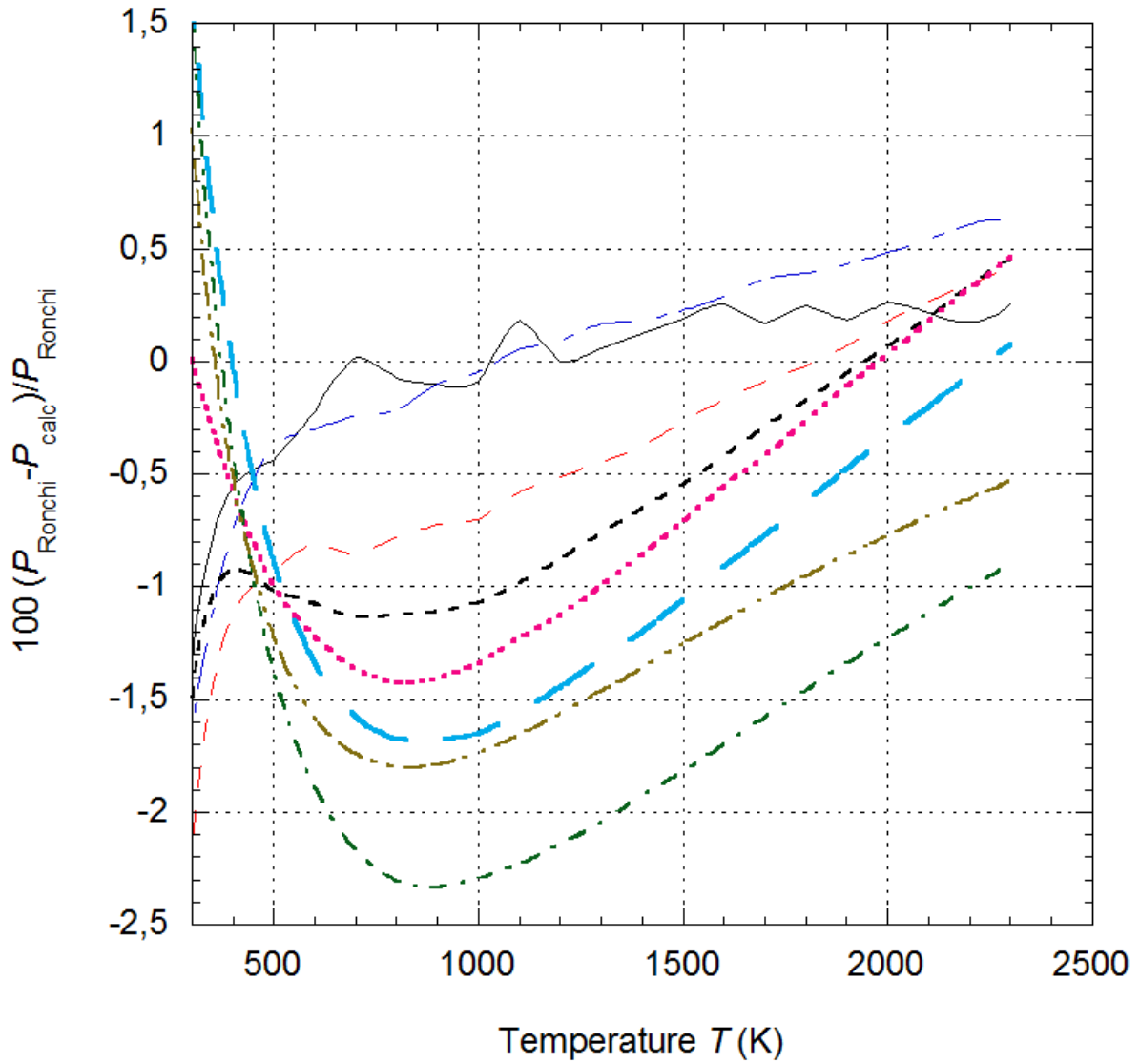


Figure 22

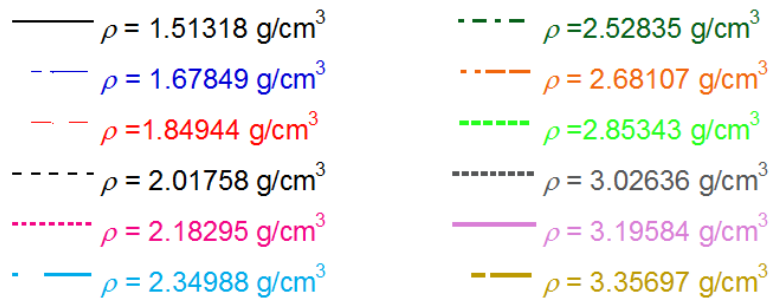
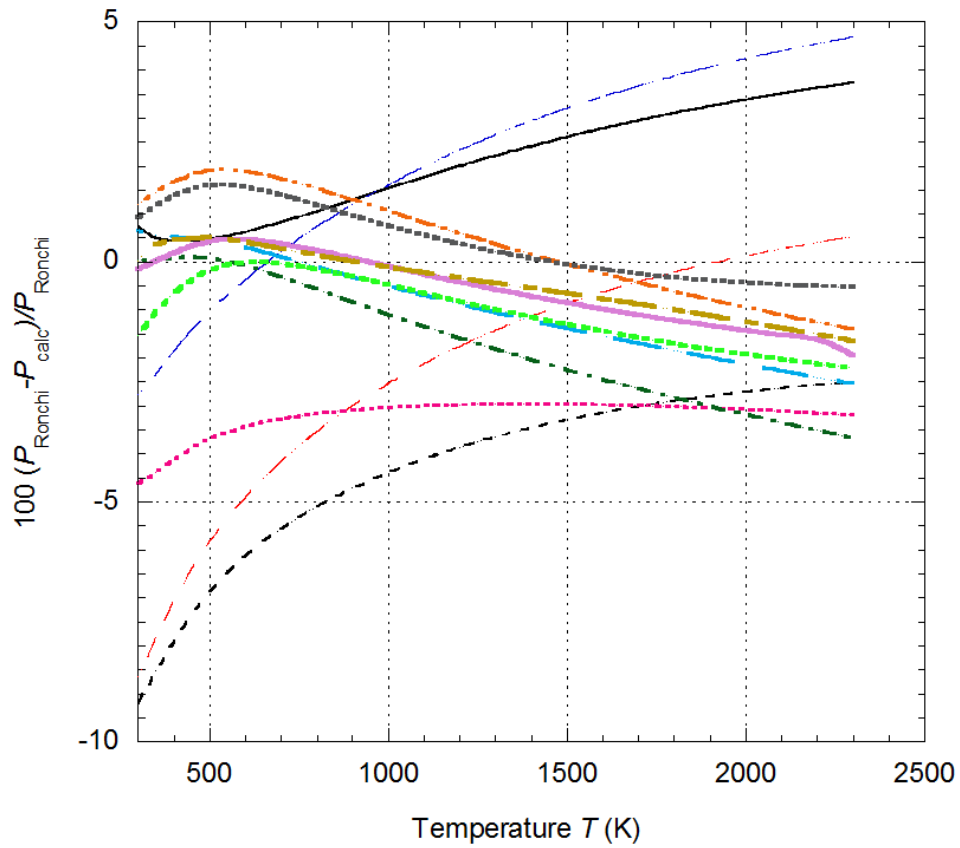


Figure 23

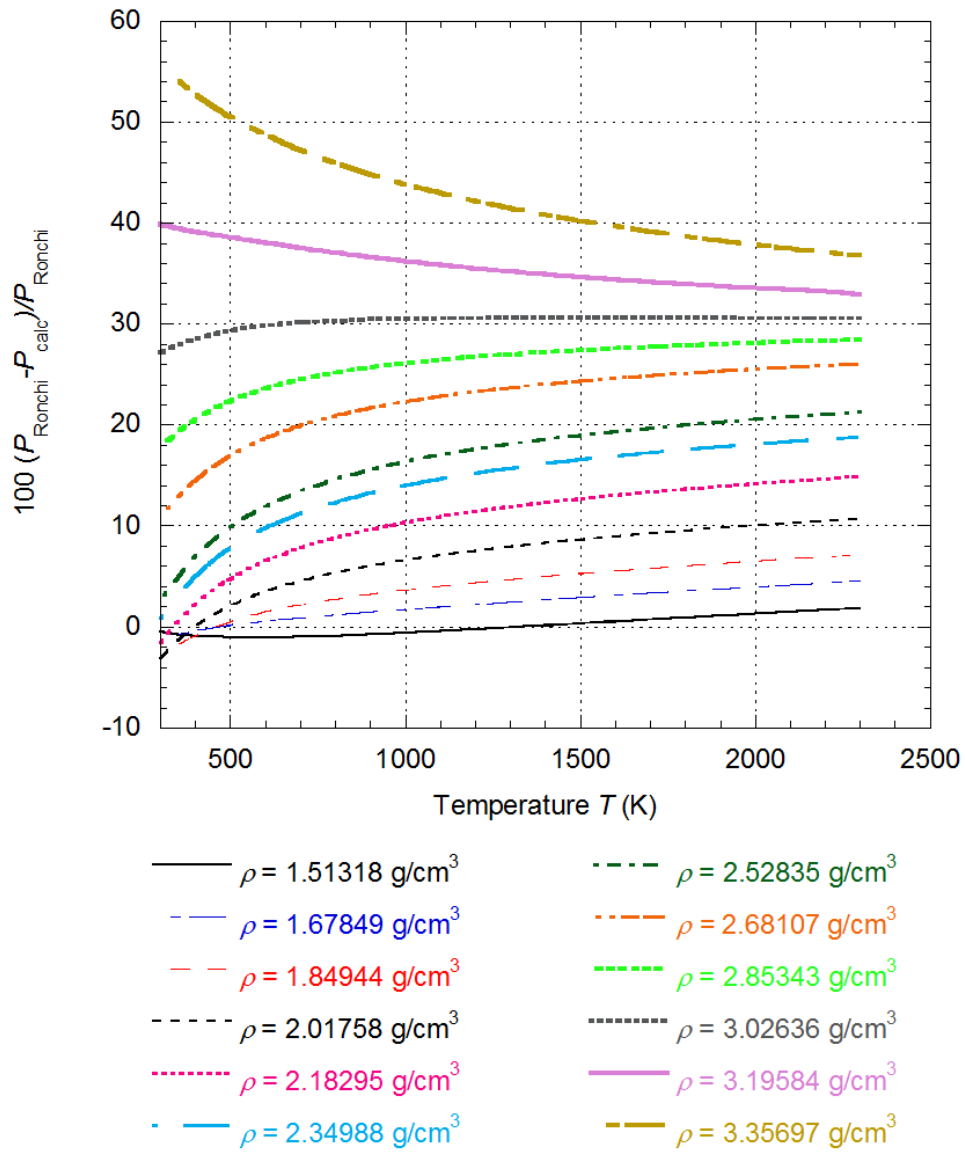


Figure 24

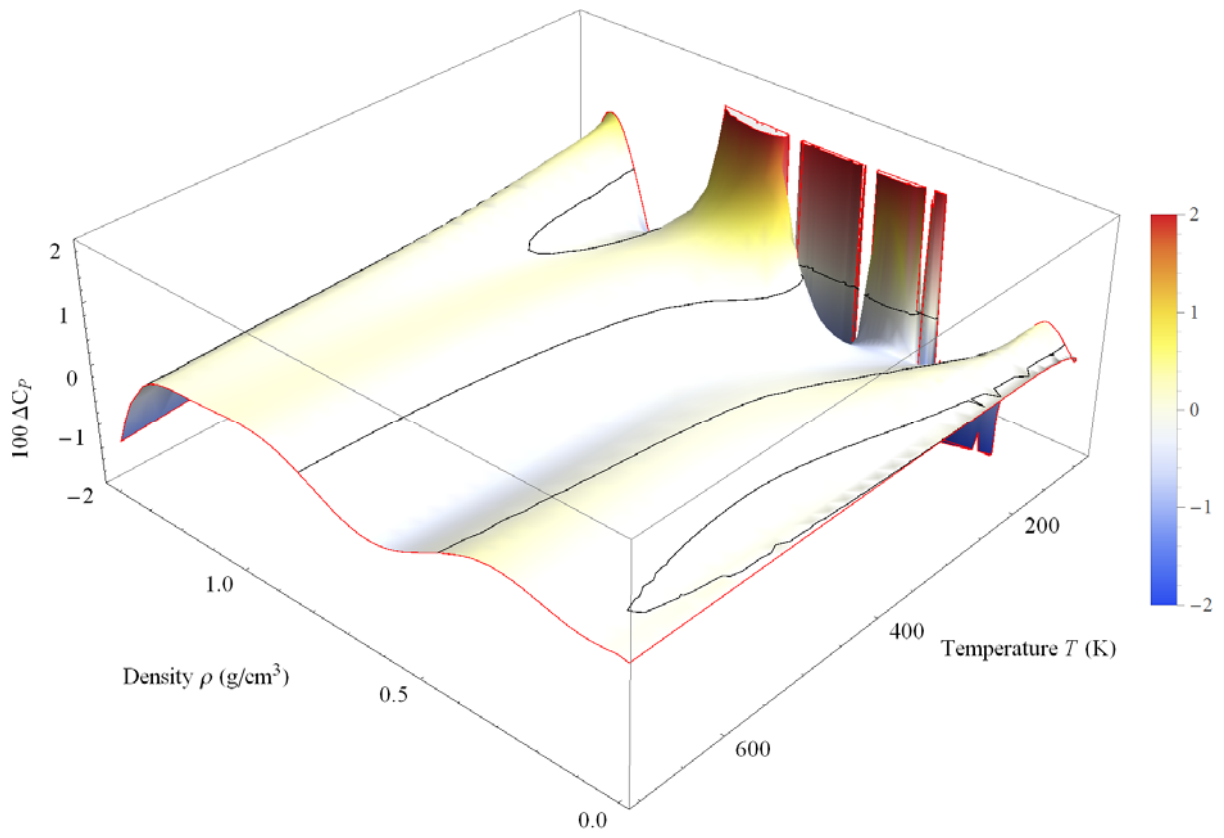


Figure 25

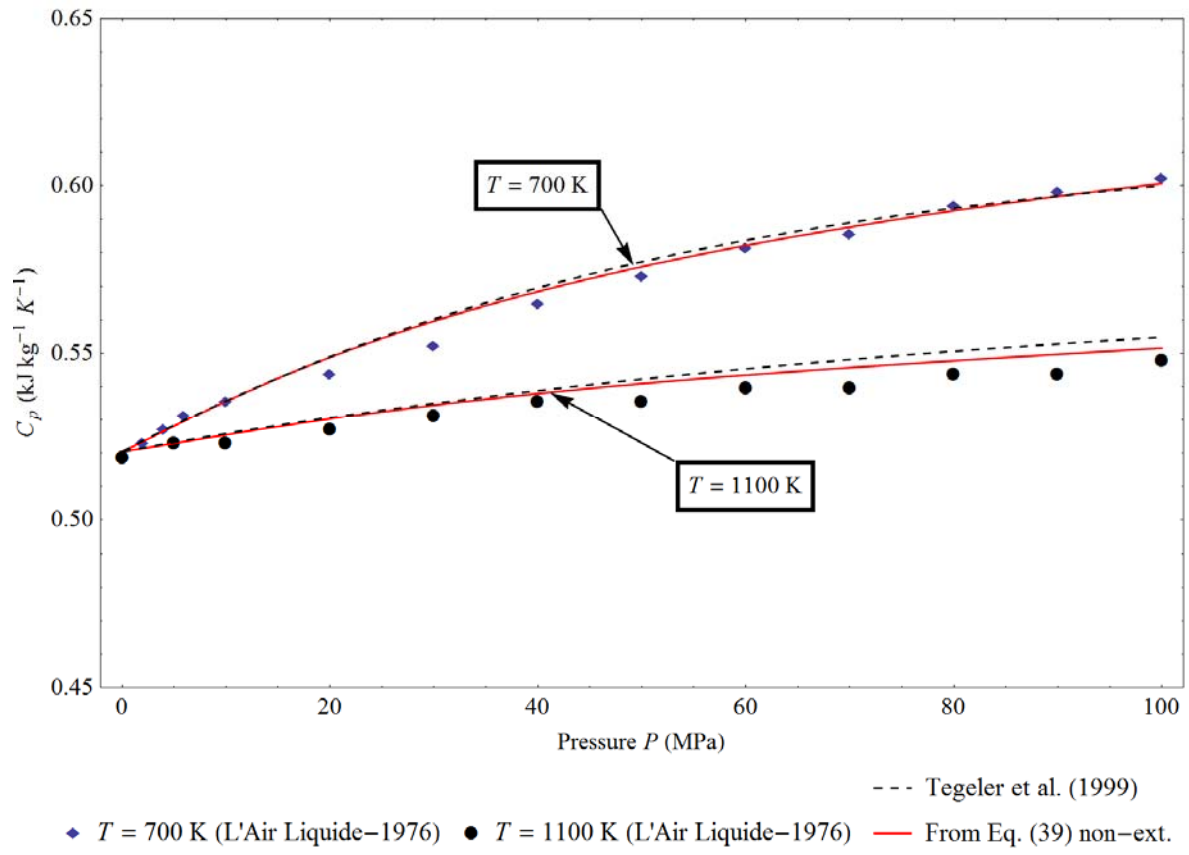


Figure 26

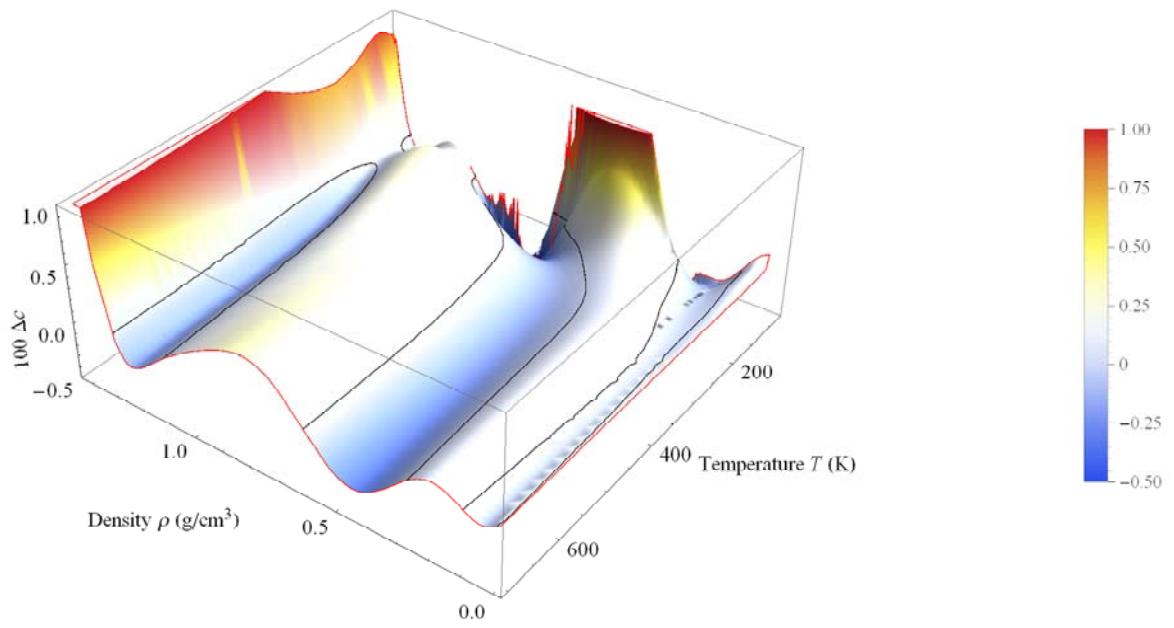


Figure 27

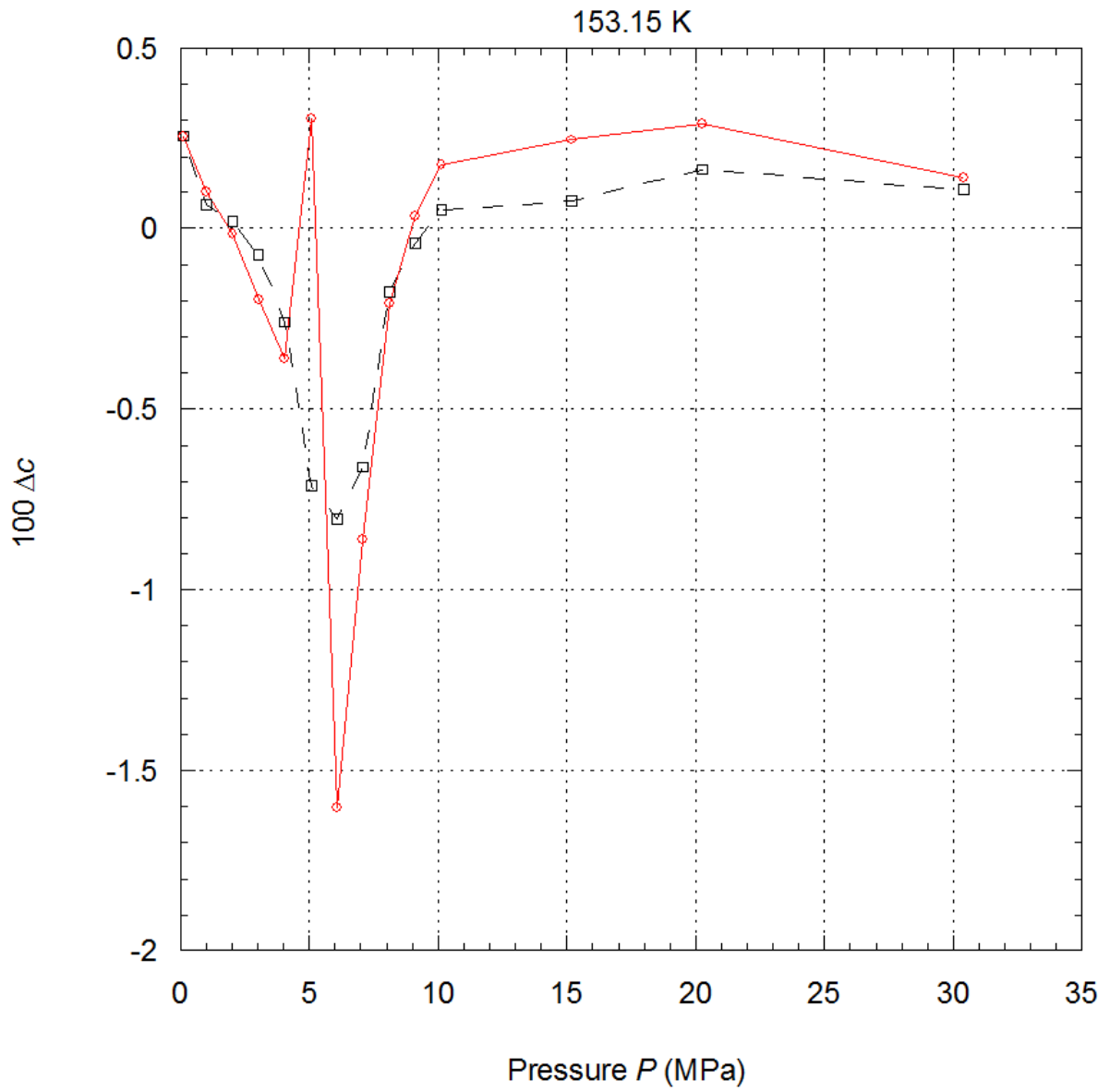


Figure 28

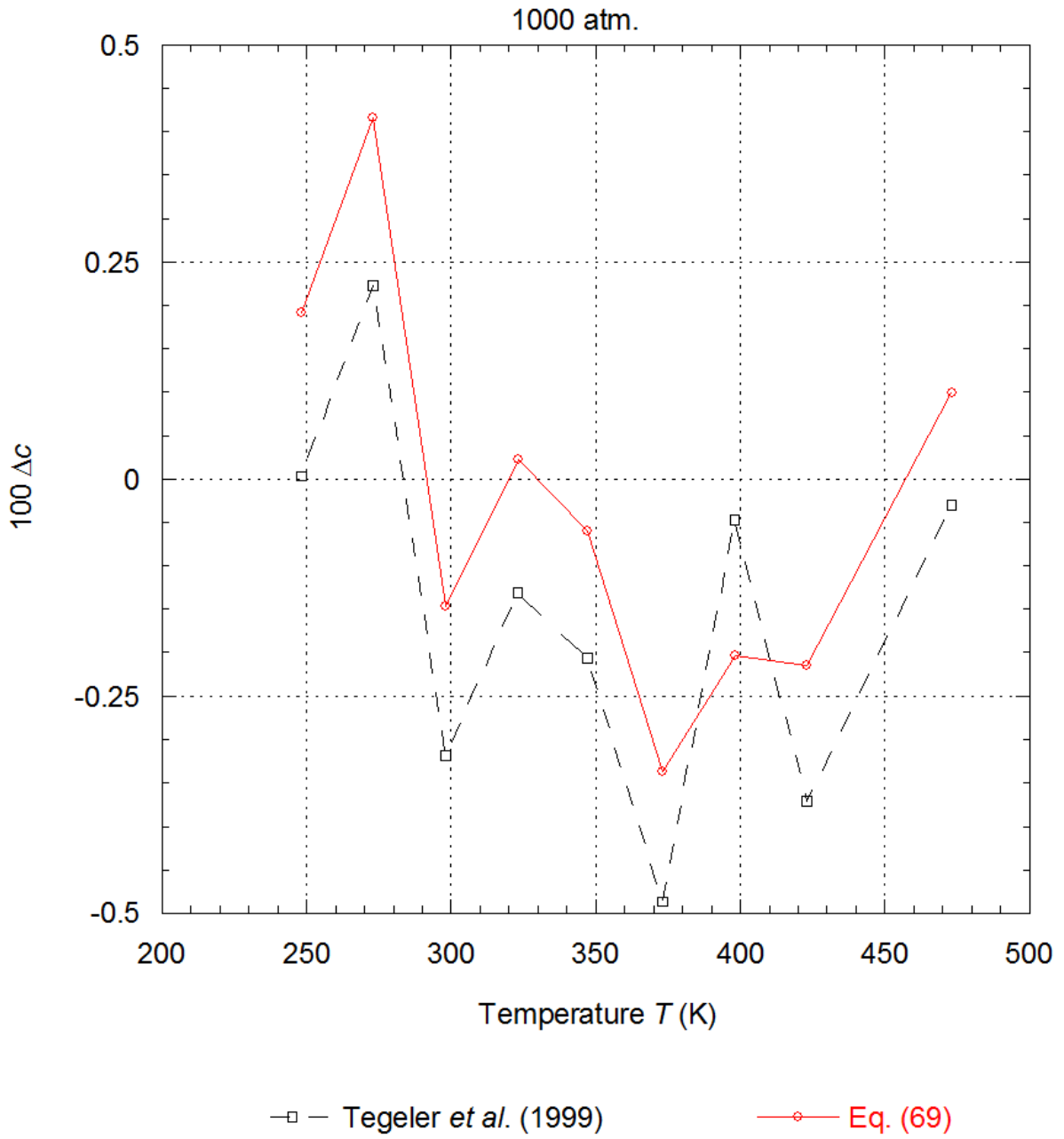


Figure 29

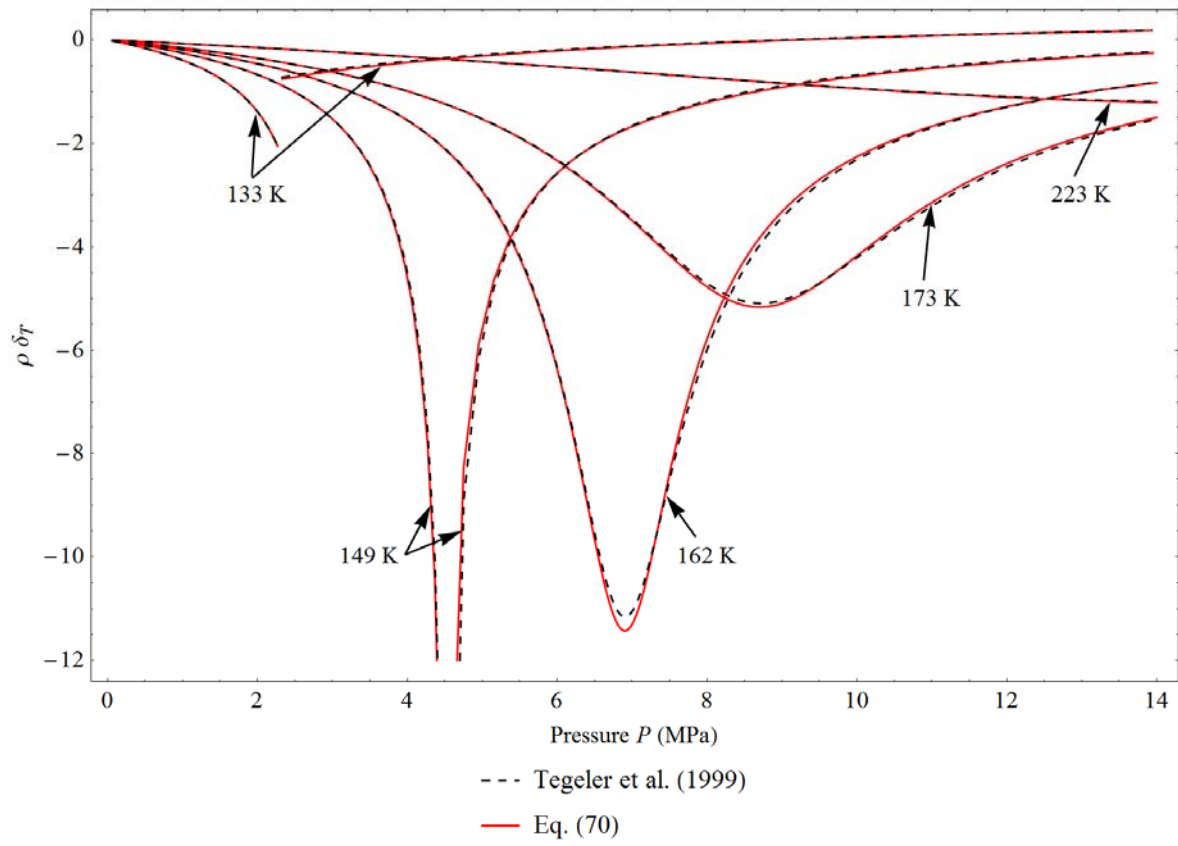
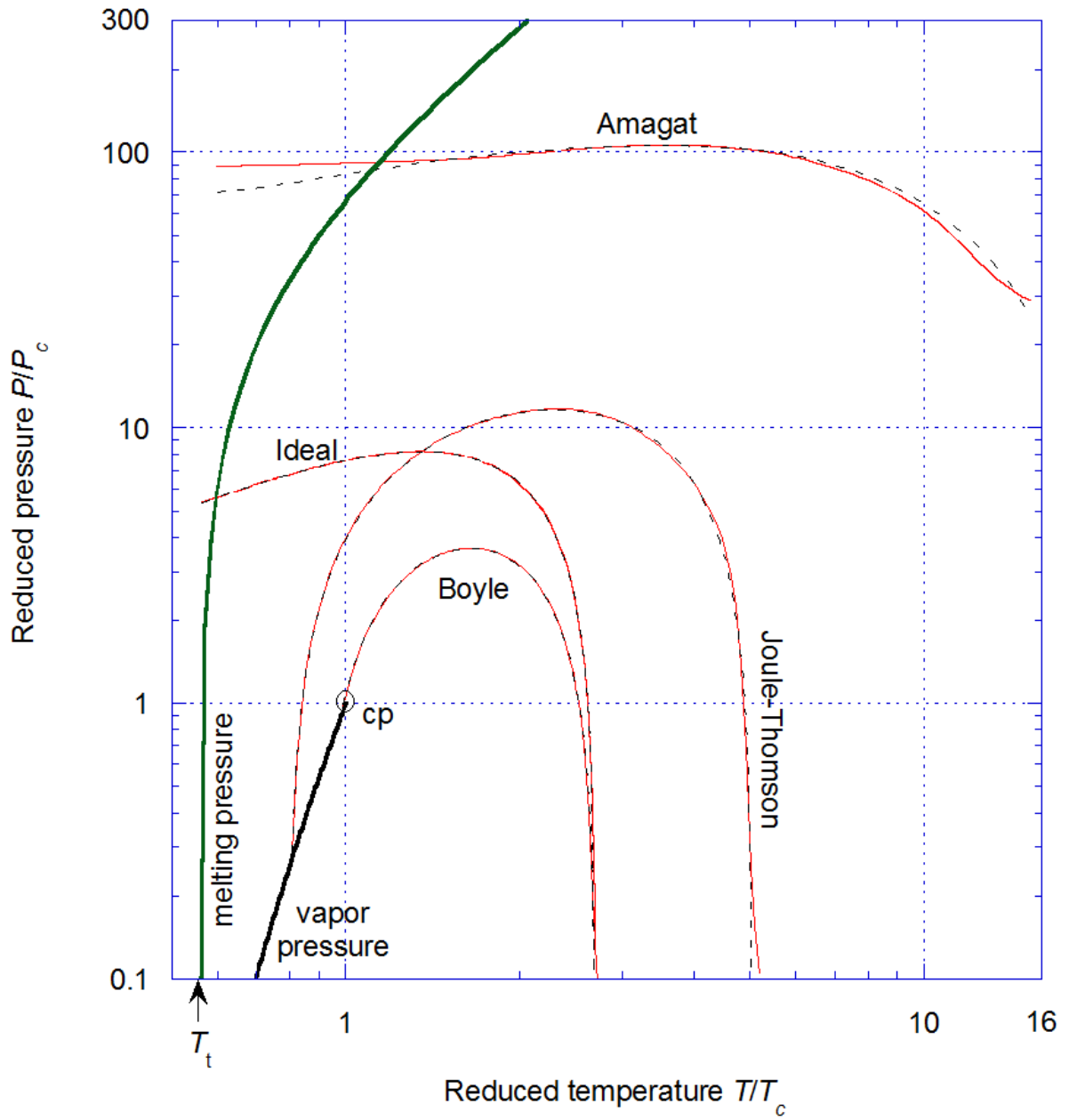


Figure 30



— Eq. (39) non-ext.

- - - Tegeler *et al.* (1999)

Figure 31

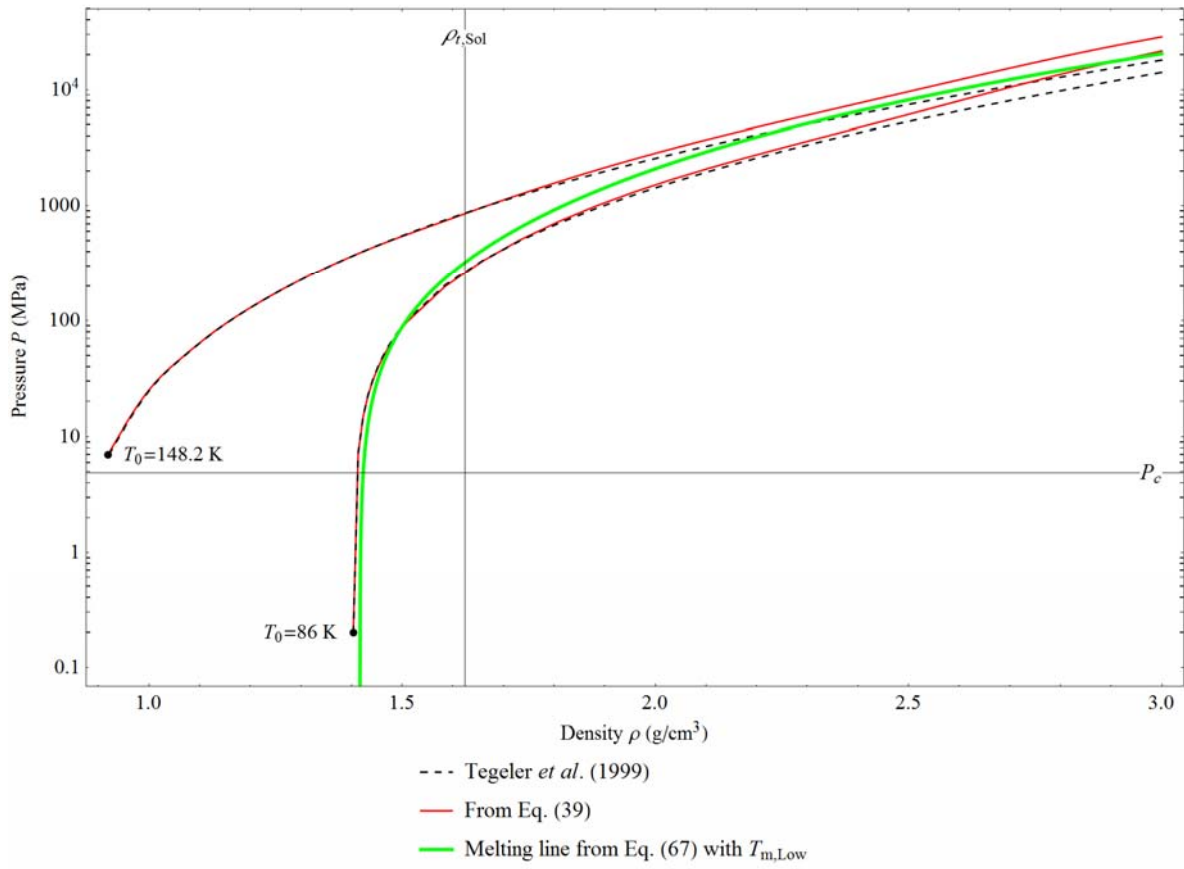
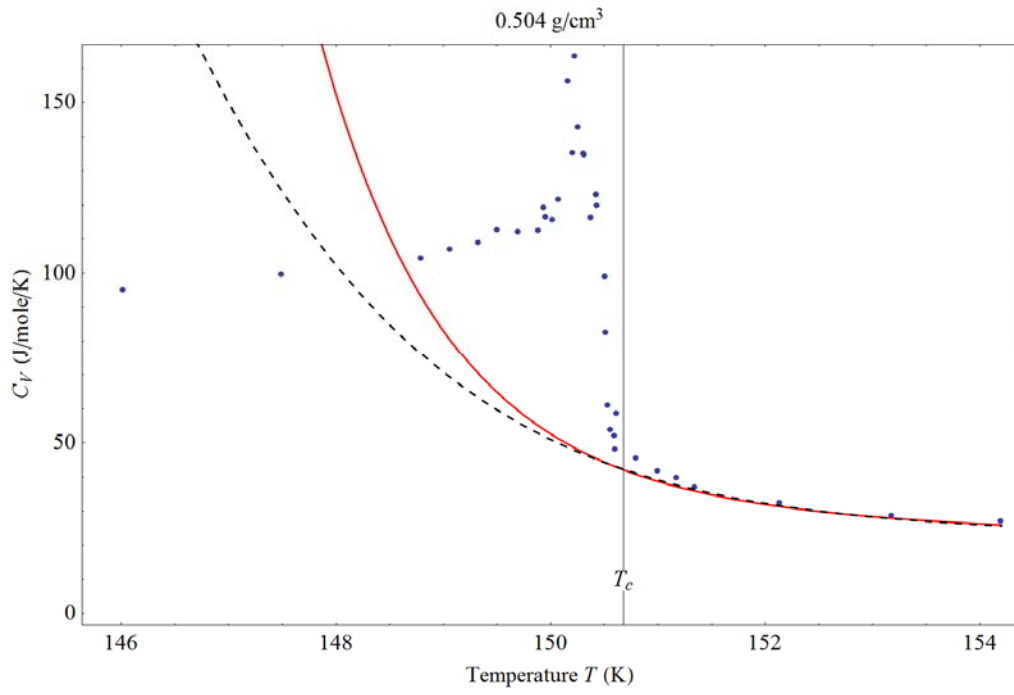
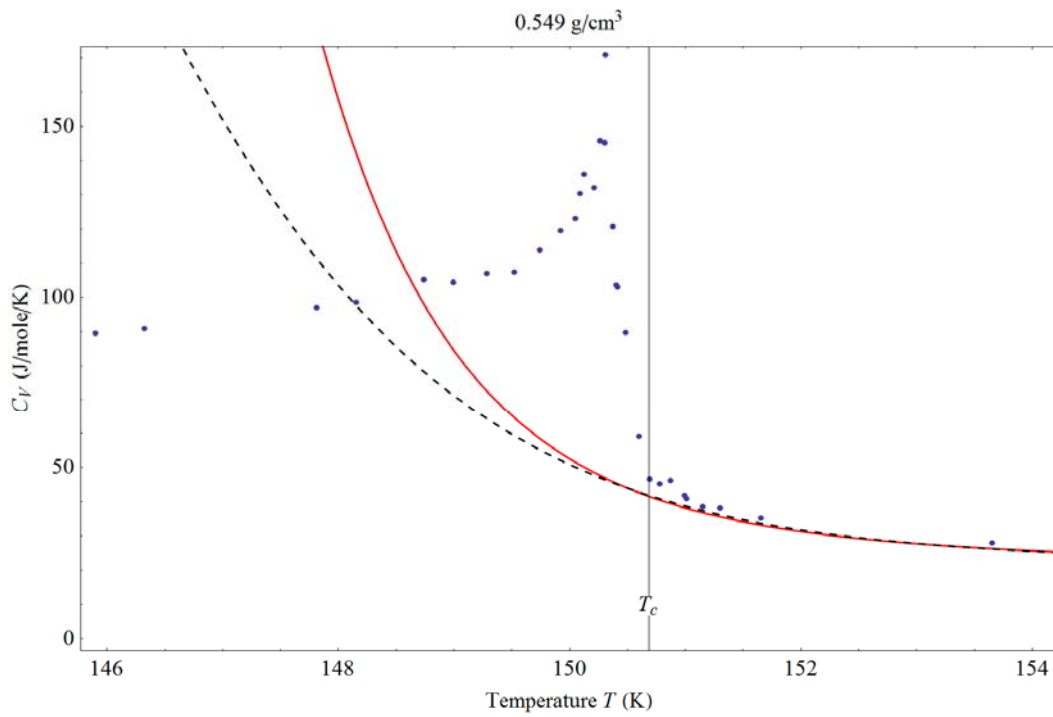


Figure 32

(a)

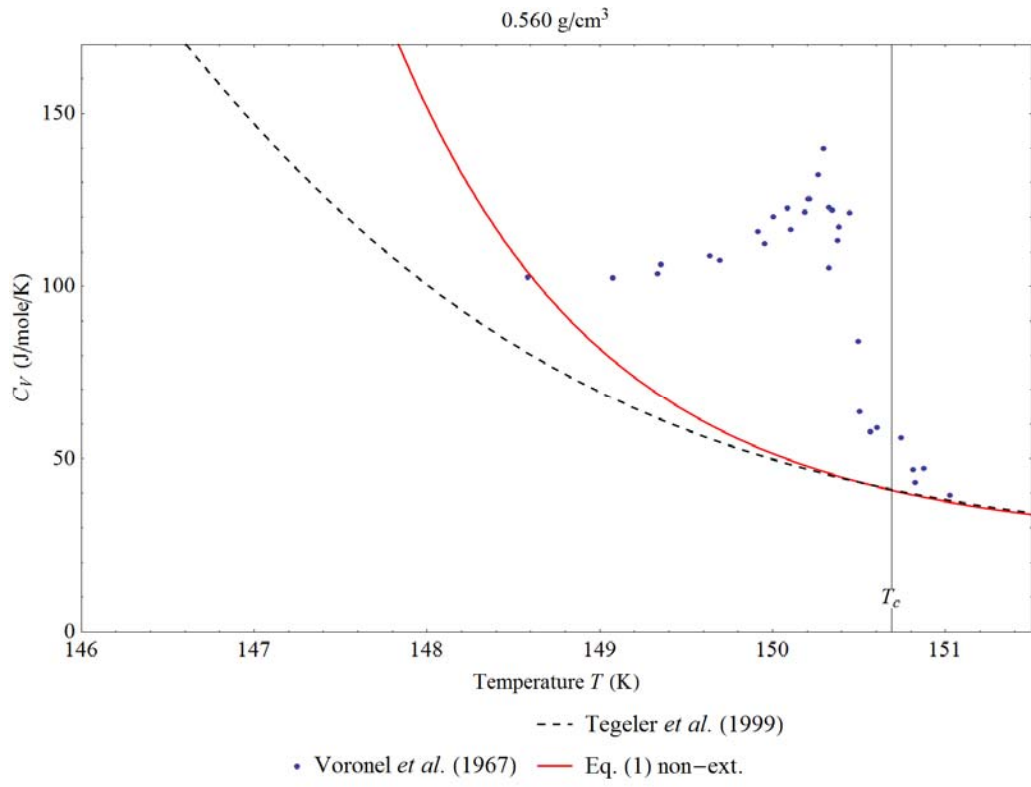


(b)



--- Tegeler *et al.* (1999)
• Voronel *et al.* (1967) — Eq. (1) non-ext.

(c)



(d)

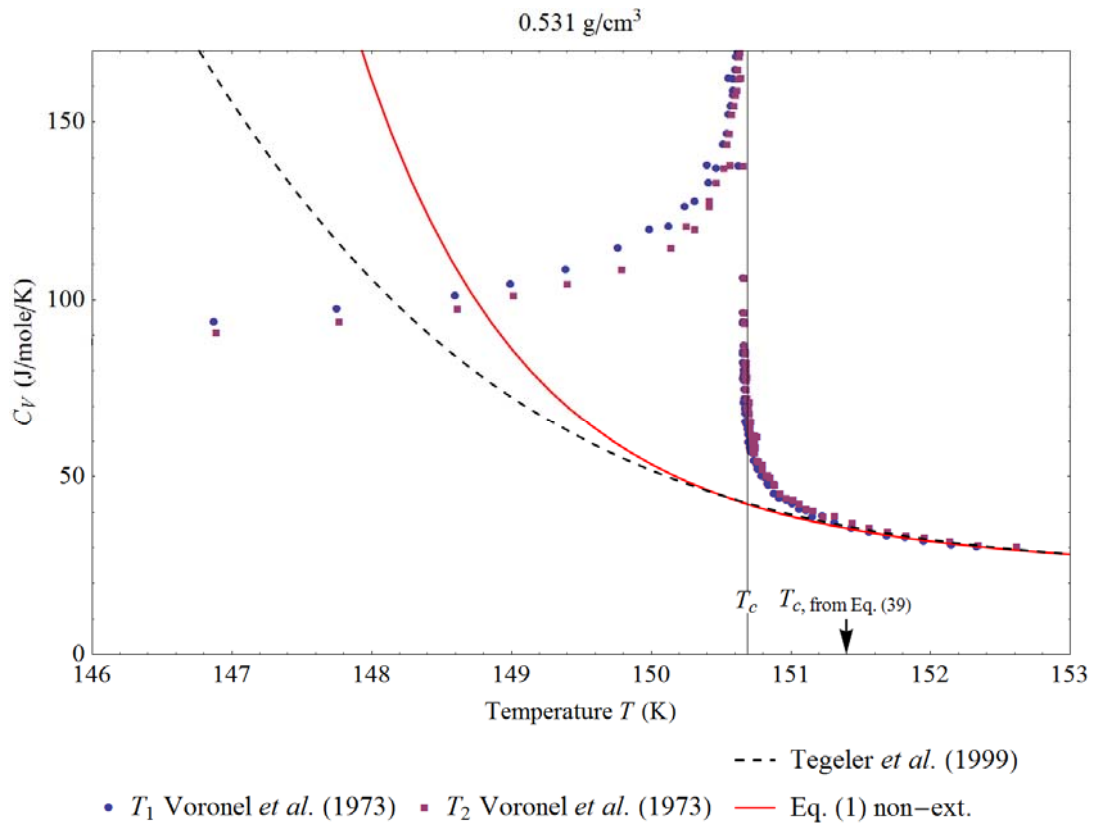


Figure 33

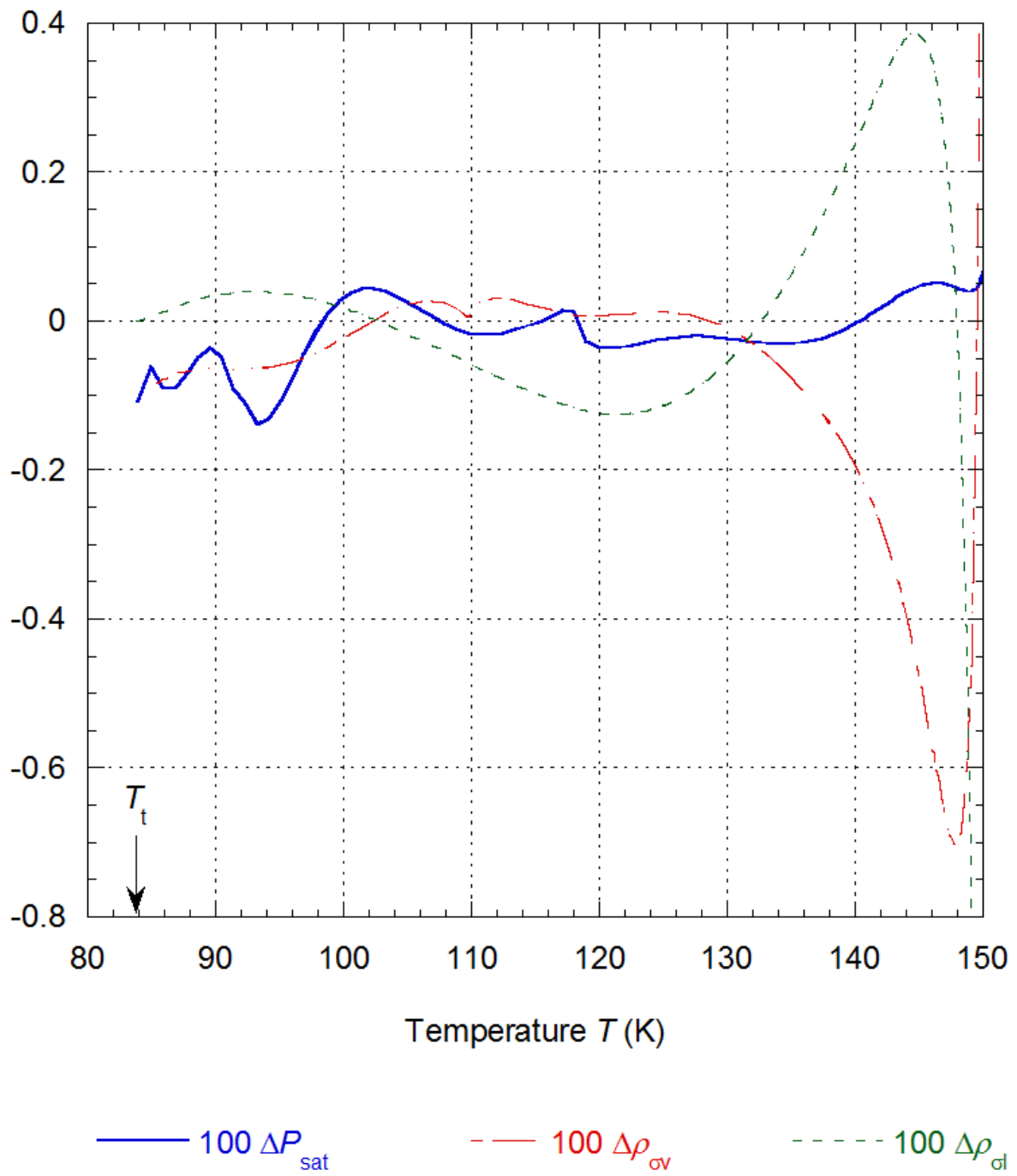


Figure 34

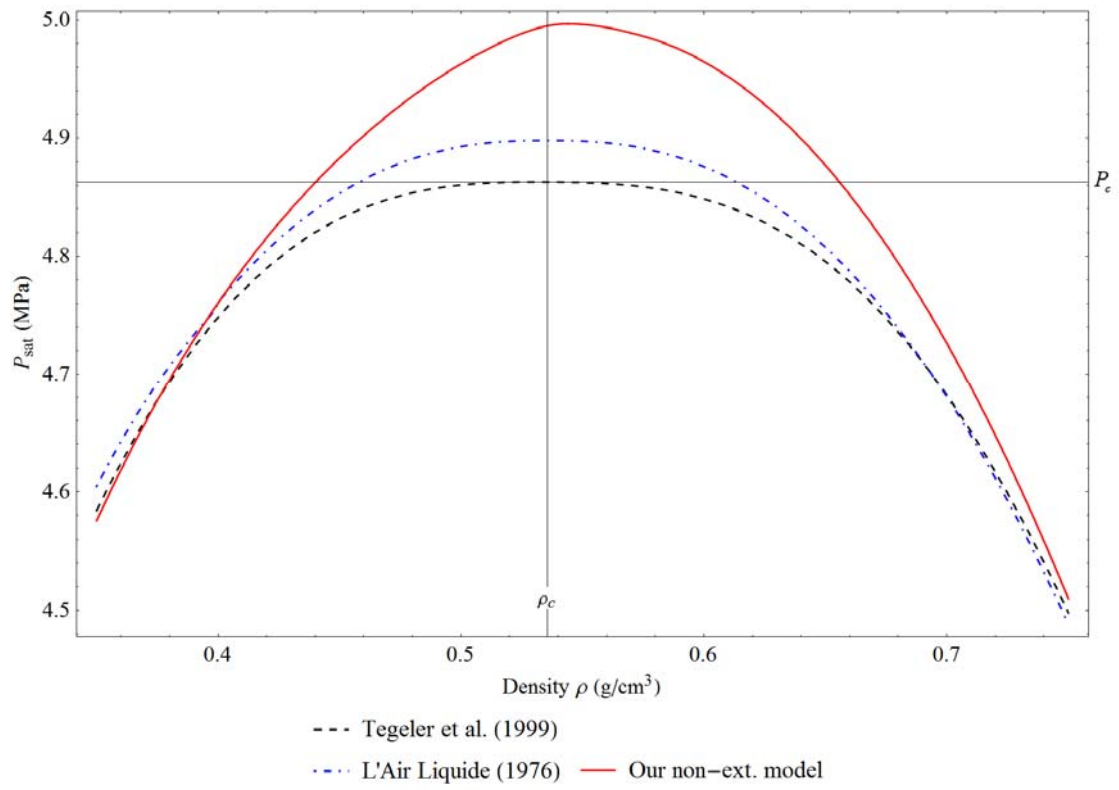


Figure 35

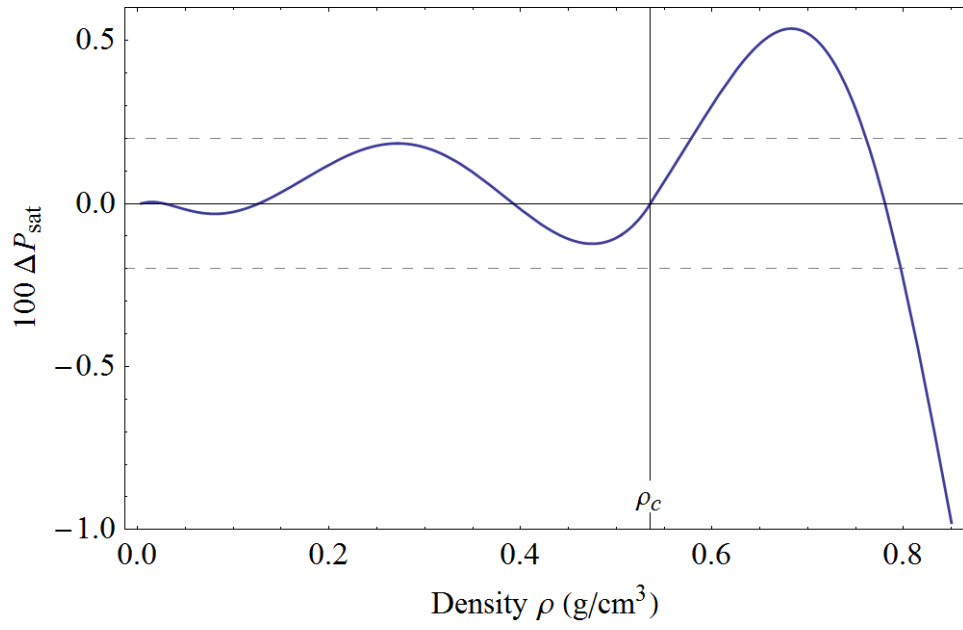


Figure 36

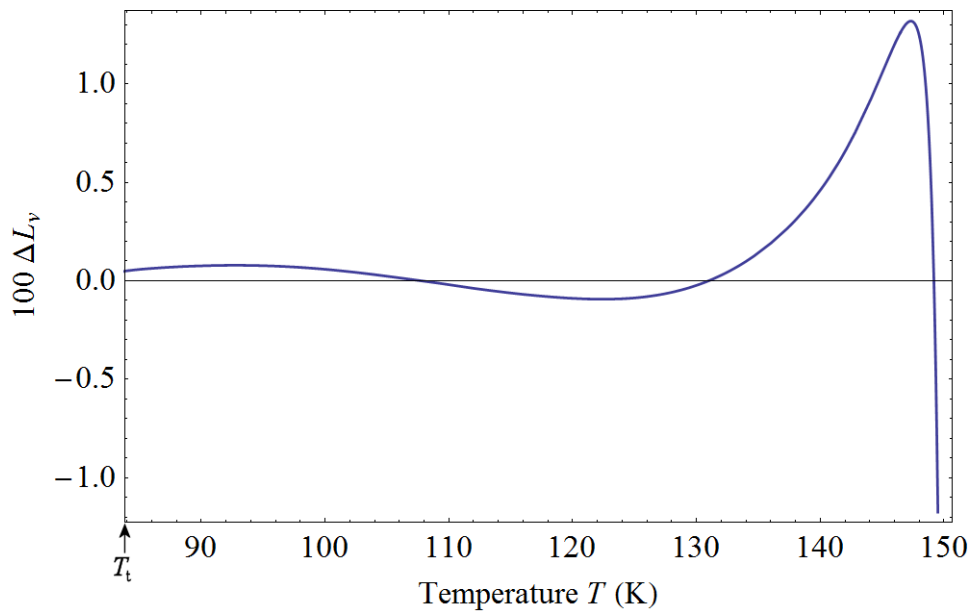
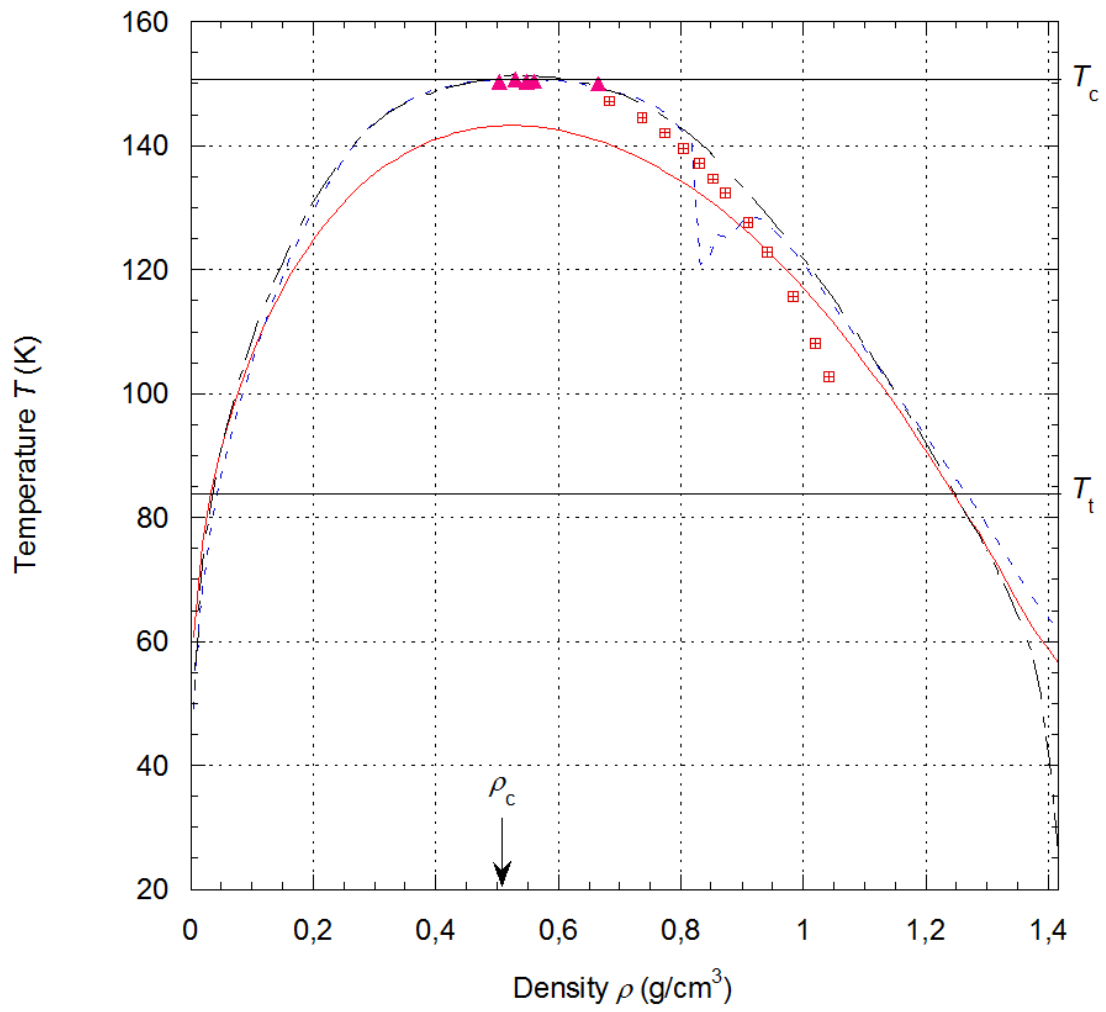


Figure 37



— T_{div}
 - - - T_{sp} using derivatives of Eq. (45)
 - - - - T_{sp} from Tegeler et al. (1999)

▲ Voronel et al. (1967,1973)
 ■ Baidakov et al. (1975)

Figure 38

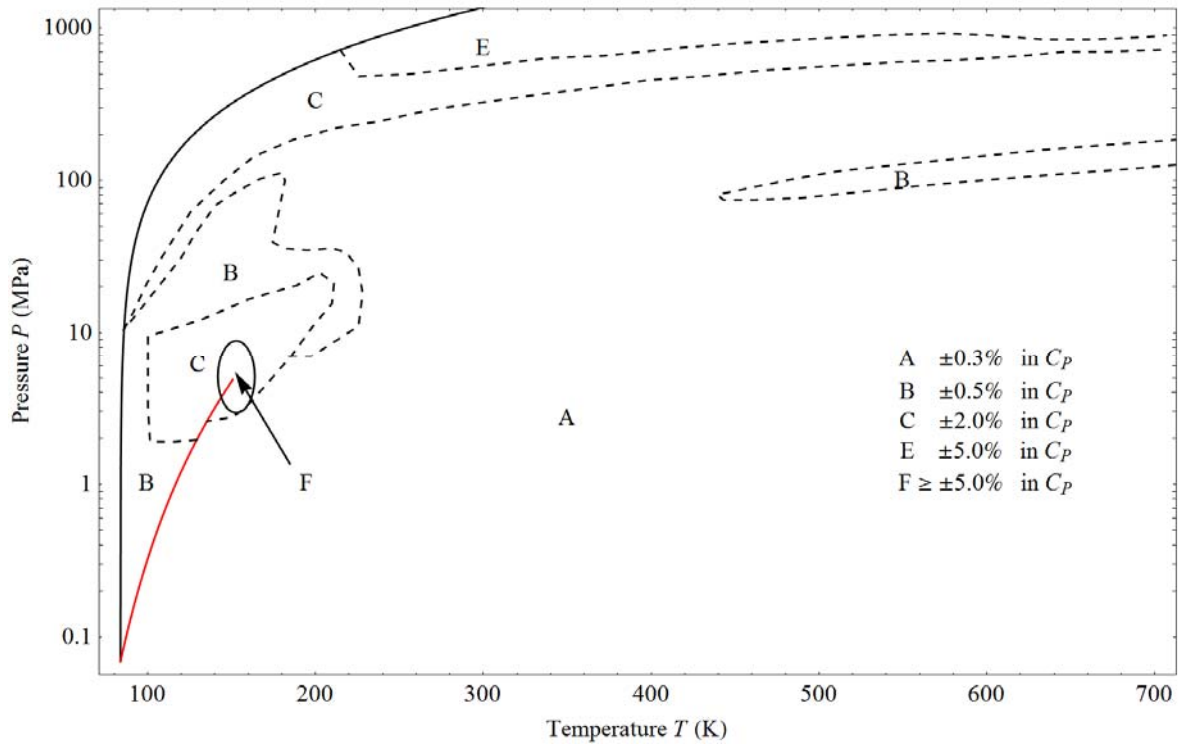


Figure 39

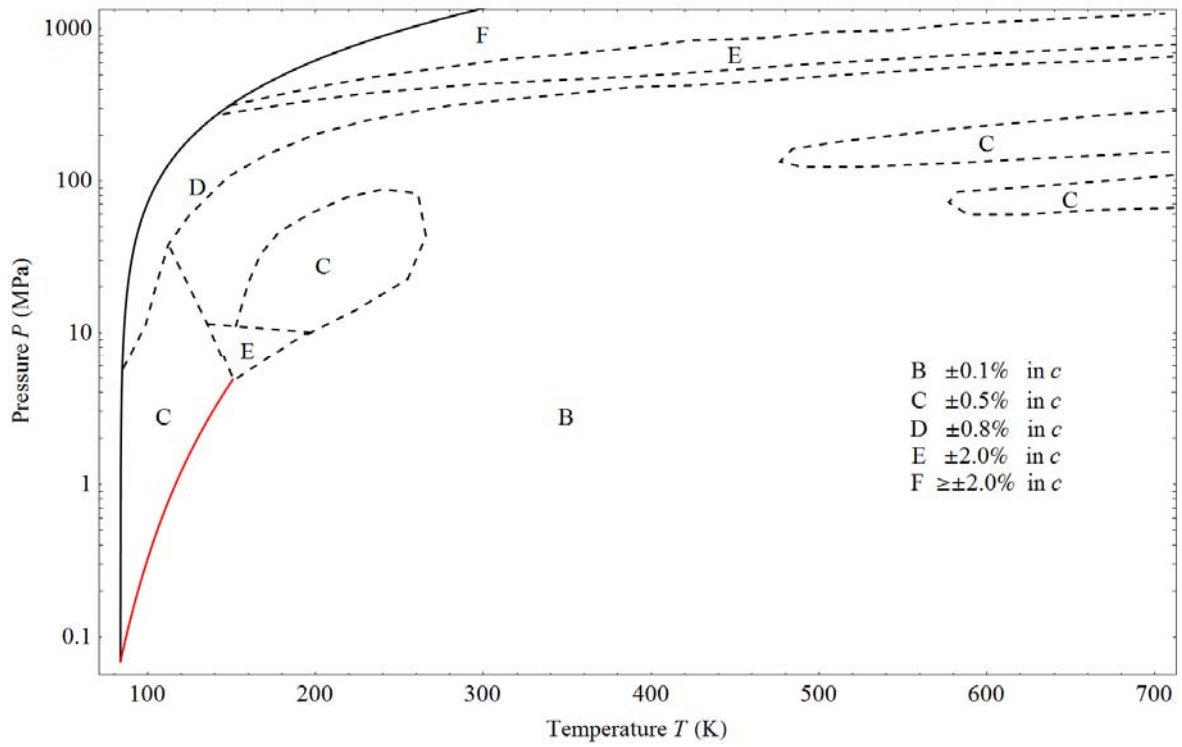


Figure 40

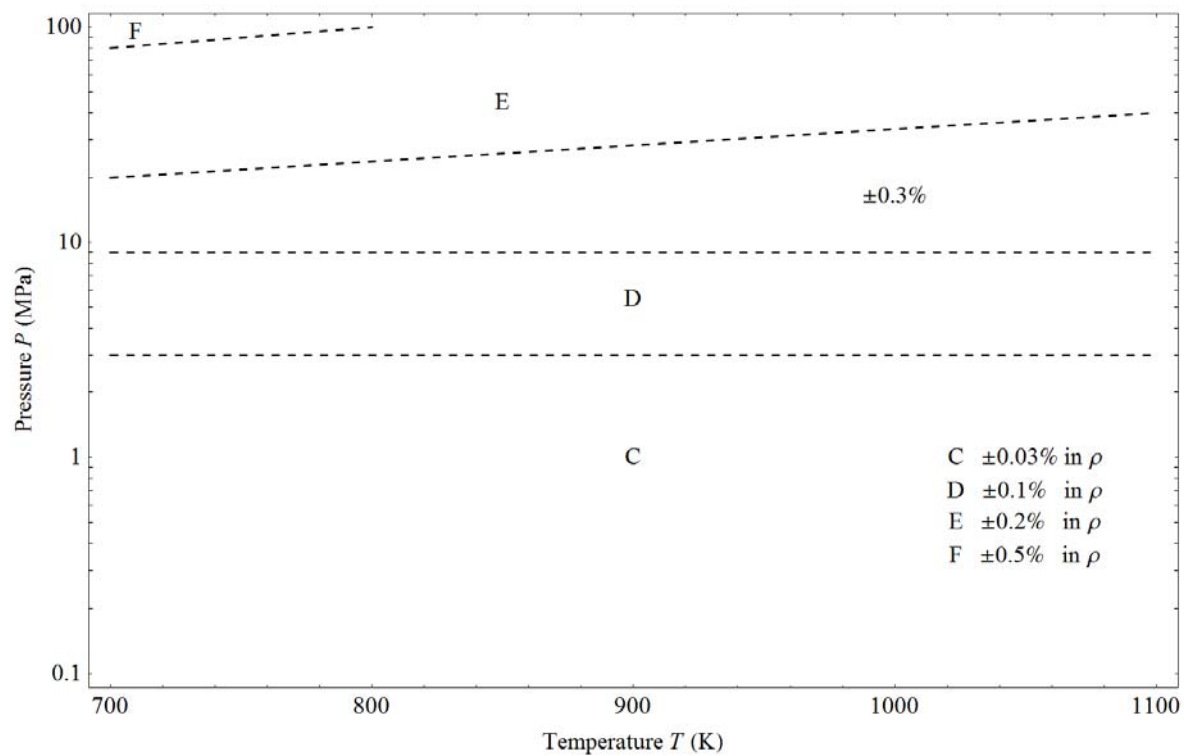


Figure 41

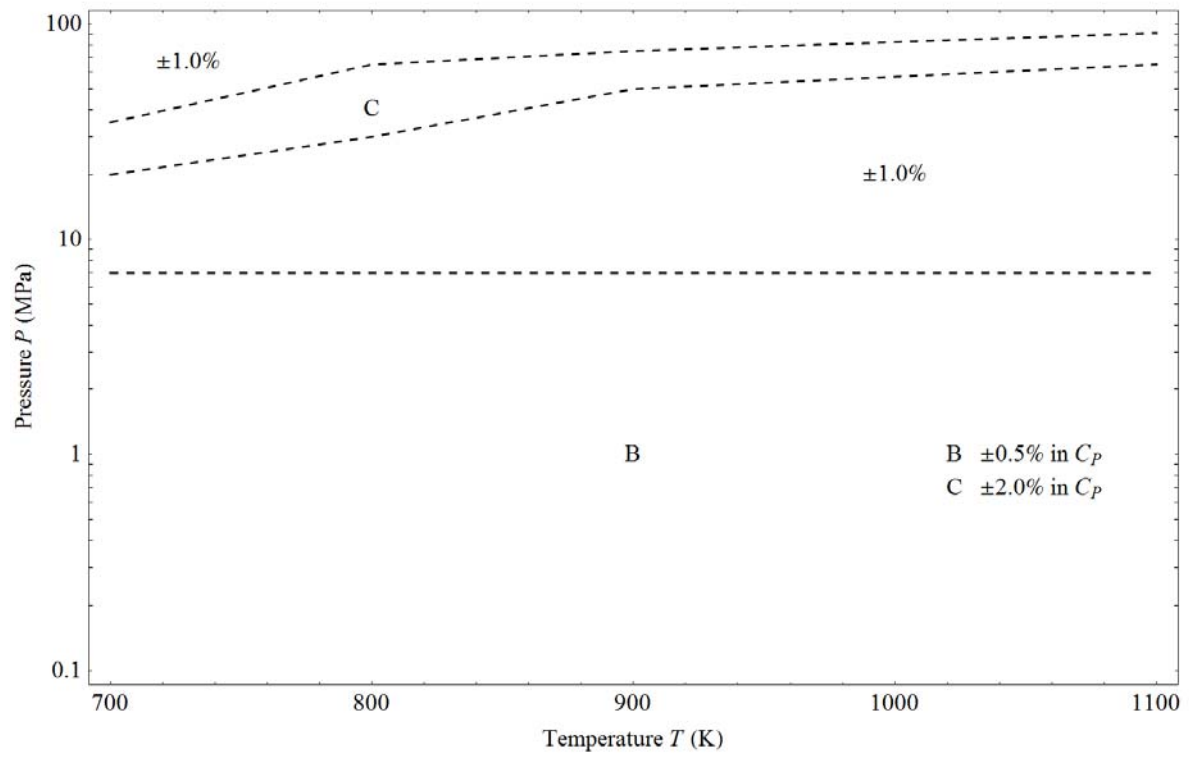


Figure 42

